

(NASA-CR-123645) STUDY OF AERODYNAMIC
SURFACE CONTROL OF SPACE SHUTTLE BOOST AND
REENTRY, VOLUME 2 Final Report, Apr. 1971
C.J. Chang, et al (Lockheed Missiles and
Space Co.) Mar. 1972 118 p

N72-25844

Unclas
CSCL 22C G3/31 15439



Lockheed

HUNTSVILLE RESEARCH & ENGINEERING CENTER

LOCKHEED MISSILES & SPACE COMPANY, INC.
A SUBSIDIARY OF LOCKHEED AIRCRAFT CORPORATION

HUNTSVILLE, ALABAMA

LOCKHEED MISSILES & SPACE COMPANY
HUNTSVILLE RESEARCH & ENGINEERING CENTER
HUNTSVILLE RESEARCH PARK
4800 BRADFORD DRIVE, HUNTSVILLE, ALABAMA

STUDY OF AERODYNAMIC SURFACE
CONTROL OF SPACE SHUTTLE
BOOST AND REENTRY

VOLUME II
FINAL REPORT

March 1972
CR-193645

Contract NAS8-26772

by

C. J. Chang
C. L. Connor
G. P. Gill

APPROVED:

U. Trautwein
W. Trautwein, Supervisor
Vehicle Dynamics & Control Section

T.R. Beal
T. R. Beal, Manager
Dynamics & Guidance Department

George D. Farrior
J. S. Farrior
Resident Director

PRECEDING PAGE BLANK NOT FILMED

FOREWORD

This report presents the work performed during the period of April 1971 to March 1972 by Lockheed's Huntsville Research & Engineering Center while under contract to the National Aeronautics and Space Administration for the Aero-Astroynamics Laboratory of Marshall Space Flight Center (MSFC), Contract NAS8-26772.

Mr. J.M. Livingston of NASA-MSFC, Aero-Astroynamics Laboratory, S&E-AERO-DF, was the MSFC Contracting Officer's Representative for the ascent portion of this study. Mr. R. C. Lewis of NASA-MSFC, Aero-Astroynamics Laboratory, S&E-AERO-DOA, was the Contracting Officer's Representative for the reentry portion of the study. Mr. G. P. Gill was the project engineer at Lockheed. Major contributors were Dr. C. J. Chang, Dr. W. Trautwein and Mr. C. L. Connor. The hybrid programming was performed by Mr. D. C. Cruze and Mr. A. M. Hansing. Mr. K. R. Leimbach, Mr. W. G. Green, Mr. P. O. McCormick and Mr. J. B. Baker provided assistance in establishing payload sensitivities.

This report is divided into two volumes. Volume I presents the optimization technique, the problem formulation and the results obtained. Volume II presents all the Appendices which describe derivations of mathematical models and all peripheral studies related to contract performance.

PRECEDING PAGE BLANK NOT FILMED

CONTENTS

Appendix		Page
A	DERIVATION OF THE PERTURBATION EQUATIONS OF MOTION FOR SHUTTLE REENTRY STUDIES	A-1
	A.1 Six-Degree-of-Freedom Equations of Motion for Reentry Vehicle	A-1
	A.2 Perturbation Equations of Motion	A-2
	A.3 Perturbation Forces and Moments	A-6
	A.4 6-D Perturbation Equations of Motion for Reentry Vehicles	A-10
B	REDUCTION OF LOCKHEED'S 6-D PERTURBATION EOM TO CONVENTIONAL AIRFRAME 6-D PERTURBATION EOM	B-1
C	ANALYSIS OF HYDRAULIC SYSTEM COMPONENT WEIGHTS	C-1
	C.1 Horsepower	C-1
	C.2 Actuators	C-1
	C.3 Transmission Lines	C-2
	C.4 Pumps	C-2
	C.5 Accessory Power Unit (APU)	C-3
	C.6 Propellants	C-3
D	COMPUTATION OF HINGE MOMENTS IN THE ABSENCE OF HINGE MOMENT COEFFICIENTS	D-1
E	PHASE PLANE DESIGN OF APS CONTROLLER	E-1
	E.1 Assumptions	E-1
	E.2 Order-of-Magnitude Analysis	E-2
	E.3 Phase Plane Analysis	E-3
	E.4 Optimum Switching	E-4
	E.5 Optimum Switching in the Presence of Time Delay, Hysteresis and Contact Space	E-6

CONTENTS (Continued)

Appendix		Page
E.6	The Effect of Time Delay on the Optimum Switching Line of a Simple Pure Inertia Load Servo	E-7
E.7	Optimum Commanded Switching Line in the Presence of a Constant Time Delay	E-10
E.8	Implementation of the Programmed Controllers	E-11
E.9	Raw Control Law	E-13
E.10	Fine Control Law	E-16
F	TIME-VARYING COEFFICIENTS GENERATED BY DATA PREPROCESSOR PROGRAMS	F-1
G	SHUTTLE REENTRY CONTROL GAINS SYNTHESIS PROGRAM AND SOME REPRESENTATIVE RESULTS	G-1
H	SHUTTLE REENTRY SIMULATION PROGRAM AND SOME REPRESENTATIVE RESULTS	H-1
I	SCOPE OF WORK	I-1

Appendix A

**DERIVATION OF THE PERTURBATION EQUATIONS OF MOTION
FOR SHUTTLE REENTRY STUDIES**

Appendix A

A.1 SIX-DEGREE-OF-FREEDOM EQUATIONS OF MOTION FOR REENTRY VEHICLE

The translational equations of motion can be written in wind axes as:

$$\dot{\hat{V}} = \hat{F}_{xw} / m \quad (A-1)$$

$$\dot{\hat{\alpha}} = \hat{Q} - (P \cos \hat{\alpha} + R \sin \hat{\alpha}) \tan \hat{\beta} + \hat{F}_{zw} / m V \cos \hat{\beta} \quad (A-2)$$

$$\dot{\hat{\beta}} = \hat{P} \sin \hat{\alpha} - \hat{R} \cos \hat{\alpha} + \hat{F}_{yw} / m V \quad (A-3)$$

The rotational equations of motion for vehicles symmetric with respect to $X_b - Z_b$ plane, and with constant moment and product moment of inertia can be written in the body axis system coordinates as

$$\dot{\hat{P}} = \left[\frac{I_z(I_y - I_z) - I_{xz}^2}{I_x I_z - I_{xz}^2} \right] \hat{Q} \hat{R} + \left[\frac{I_{xz}(I_x - I_y + I_z)}{I_x I_z - I_{xz}^2} \right] \hat{P} \hat{Q} + \left[\frac{I_z \hat{L} + I_{xz} \hat{N}}{I_x I_z - I_{xz}^2} \right] \quad (A-4)$$

$$\dot{\hat{Q}} = \left[\frac{I_z - I_x}{I_y} \right] \hat{P} \hat{R} + \left[\frac{I_{xz}}{I_y} \right] (R^2 - P^2) + \left[\frac{\hat{M}}{I_y} \right] \quad (A-5)$$

$$\dot{\hat{R}} = \left[\frac{I_x(I_x - I_y) + I_{xz}^2}{I_x I_z - I_{xz}^2} \right] \hat{P} \hat{Q} + \left[\frac{I_{xz}(-I_x + I_y - I_z)}{I_x I_z - I_{xz}^2} \right] \hat{Q} \hat{R} + \left[\frac{I_{xz} \hat{L} + I_x \hat{N}}{I_x I_z - I_{xz}^2} \right] \quad (A-6)$$

The orientation of reentry vehicles is given by a series of three consecutive rotations. By following 1-2-3 sequence of rotations (bank an angle $\hat{\phi}$ about relative velocity vector, pitch an angle $\hat{\theta}$, and yaw an

angle $\hat{\psi}$) the orientational equations can approximately be written as

$$\dot{\hat{\phi}} = \frac{\hat{P} \cos\hat{\psi} - \hat{Q} \sin\hat{\psi}}{\cos\hat{\theta}} / \cos\hat{\theta} \quad (\text{A-7})$$

$$\dot{\hat{\theta}} = \frac{\hat{P} \sin\hat{\psi} + \hat{Q} \cos\hat{\psi}}{\cos\hat{\theta}} \quad (\text{A-8})$$

$$\dot{\hat{\psi}} = \frac{\hat{R} - (\hat{P} \cos\hat{\psi} - \hat{Q} \sin\hat{\psi}) \tan\hat{\theta}}{\cos\hat{\theta}} \quad (\text{A-9})$$

A.2 PERTURBATION EQUATIONS OF MOTION

It is assumed that the motion of the reentry vehicle consists of small deviation from a reference condition of flight. The reference values of all variables are denoted by a subscript zero, and the small perturbations are indicated as follows:

$$V = V_0 + v, \quad \hat{\alpha} = \alpha_0 + \alpha, \quad \hat{\beta} = \beta_0 + \beta, \quad \hat{\gamma} = \gamma_0 + \gamma$$

$$\hat{P} = P_0 + p, \quad \hat{Q} = Q_0 + q, \quad \hat{R} = R_0 + r$$

$$\hat{\phi} = \phi_0 + \phi, \quad \hat{\theta} = \theta_0 + \theta, \quad \hat{\psi} = \psi_0 + \psi$$

$$\hat{F}_{xw} = F_{xwo} + f_{xw}, \quad \hat{F}_{yw} = F_{ywo} + f_{yw}, \quad \hat{F}_{zw} = F_{zwo} + f_{zw}$$

$$\hat{L} = L_0 + M_x, \quad \hat{M} = M_0 + M_y, \quad \hat{N} = N_0 + M_z$$

$$f_{xw} = f_{xw(p)} + f_{xw(A)} + f_{xw(g)}, \quad f_{yw} = f_{yw(p)} + f_{yw(A)} + f_{yw(g)}$$

$$f_{zw} = f_{zw(p)} + f_{zw(A)} + f_{zw(g)}$$

$$M_x = M_{x(p)} + M_{x(a)}, \quad M_y = M_{y(p)} + M_{y(a)}, \quad M_z = M_{z(p)} + M_{z(a)}$$

$$F_{xwo(p)} = F_{xwo(p)} + F_{xwo(a)} + F_{xwo(g)}, \quad F_{ywo(p)} = F_{ywo(p)} + F_{ywo(a)} + F_{ywo(g)},$$

$$F_{zwo(p)} = F_{zwo(p)} + F_{zwo(a)} + F_{zwo(g)}$$

where subscripts (p), (a), (g) represent propulsive, aerodynamic, and gravitational contributions, respectively.

The translational equations of motion can be rewritten as

$$(\dot{V}_o + \dot{v}) = (F_{xwo} + f_{xw}) / m \quad (A-9)$$

$$(\dot{\beta}_o + \dot{\beta}) = [(P_o + p) \sin(\alpha_o + \alpha) - (R_o + r) \cos(\alpha_o + \alpha)] + [(F_{ywo} + f_{yw}) / m(V_o + v)] \quad (A-10)$$

$$\begin{aligned} (\dot{\alpha}_o + \dot{\alpha}) &= (Q_o + q) - [(P_o + p) \cos(\alpha_o + \alpha) + (R_o + r) \sin(\alpha_o + \alpha)] \tan(\beta_o + \beta) \\ &\quad + [(F_{zwo} + f_{zw}) / m(V_o + v)] / \cos(\beta_o + \beta) \end{aligned} \quad (A-11)$$

Along any reference trajectory the translational equations of motion are

$$\dot{V}_o = F_{xwo} / m \quad (A-12)$$

$$\dot{\beta}_o = P_o \sin \alpha_o - R_o \cos \alpha_o + F_{ywo} / m V_o \quad (A-13)$$

$$\dot{\alpha}_o = Q_o - (P_o \cos \alpha_o + R_o \sin \alpha_o) \tan \beta_o + (F_{zwo} / m V_o) / \cos \beta_o \quad (A-14)$$

Subtracting Eqs. (A-12), (A-13) and (A-14) from Eqs. (A-9), (A-10) and (A-11), respectively, then, by neglecting products of disturbance quantities, the following linear equations are obtained

$$\dot{v} = f_{xw} / m \quad (A-15)$$

$$\begin{aligned}\dot{\beta} = & (P_o \cos\alpha_o + R_o \sin\alpha_o) \alpha + (\sin\alpha_o) p + (-\cos\alpha_o) r \\ & + \left(\frac{1}{mV_o} \right) f_{yw} + \left(-\frac{F_{ywo}}{m V_o^2} \right) v \end{aligned} \quad (A-16)$$

$$\begin{aligned}\dot{\alpha} = & \left[-(P_o \cos\alpha_o + R_o \sin\alpha_o) \frac{1}{\cos^2 \beta_o} \right] \beta + \left[-(-P_o \sin\alpha_o + R_o \cos\alpha_o) \tan\beta_o \right] \alpha + q \\ & + \left[-\cos\alpha_o \tan\beta_o \right] p + \left[-\sin\alpha_o \tan\beta_o \right] r + \left[\frac{F_{zwo} \tan\beta_o}{m V_o \cos\beta_o} \right] \beta \\ & + \left[\frac{1}{m V_o \cos\beta_o} \right] f_{zw} + \left[-\frac{F_{zwo}}{m V_o^2 \cos\beta_o} \right] v \end{aligned} \quad (A-17)$$

In most flight conditions, it can be assumed that $\beta_o = 0$, $v = 0$. Then, Eqs. (A-15), (A-16) and (A-17) can be written as

$$f_{xw} = 0 \quad (A-18)$$

$$\dot{\beta} = \left[P_o \cos\alpha_o + R_o \sin\alpha_o \right] \alpha + \left[\sin\alpha_o \right] p + \left[-\cos\alpha_o \right] r + \left[\frac{1}{m V_o} \right] f_{yw} \quad (A-19)$$

$$\dot{\alpha} = \left[-(P_o \cos\alpha_o + R_o \sin\alpha_o) \right] \beta + q + \left[\frac{1}{m V_o} \right] f_{zw} \quad (A-20)$$

Following the same procedure as shown above, the rotational and orientational perturbation equations of motion can be written as:

$$\dot{p} = \left[\frac{I_{xz}(I_x - I_y - I_z)}{I_x I_z - I_{xz}^2} Q_o \right] p + \left[\frac{I_{xz}(I_x - I_y + I_z) P_o + (I_z(I_y - I_z) - I_{xz}^2) R_o}{I_x I_z - I_{xz}^2} \right] q$$

$$+ \left[\frac{(I_z(I_y - I_z) - I_{xz}^2) Q_o}{I_x I_z - I_{xz}^2} \right] r + \frac{I_z M_x + I_{xz} M_z}{I_x I_z - I_{xz}^2} \quad (A-21)$$

$$\dot{q} = \left[\frac{(I_z - I_x) R_o - 2 I_{xz} P_o}{I_y} \right] p + \left[\frac{(I_z - I_x) P_o + 2 I_{xz} R_o}{I_y} \right] r + \frac{M_y}{I_y} \quad (A-22)$$

$$\dot{r} = \left[\frac{(I_x(I_x - I_y) + I_{xz}^2) Q_o}{I_x I_z - I_{xz}^2} \right] p + \left[\frac{(I_x(I_x - I_y) + I_{xz}^2) P_o + I_{xz}(-I_x + I_y - I_z) R_o}{I_x I_z - I_{xz}^2} \right] q$$

$$+ \left[\frac{I_{xz}(-I_x + I_y - I_z) Q_o}{I_x I_z - I_{xz}^2} \right] r + \frac{I_{xz} M_x + I_x M_z}{I_x I_z - I_{xz}^2} \quad (A-23)$$

$$\dot{\phi} = \left[\frac{\cos\psi_o}{\cos\theta_o} \right] p + \left[-\frac{\sin\psi_o}{\cos\theta_o} \right] q + \left[\frac{(P_o \cos\psi_o - Q_o \sin\psi_o) \tan\theta_o}{\cos\theta_o} \right] \theta$$

$$+ \left[\frac{-P_o \sin\psi_o - Q_o \cos\psi_o}{\cos\theta_o} \right] \psi \quad (A-24)$$

$$\dot{\theta} = \left[\sin\psi_o \right] p + \left[\cos\psi_o \right] q + \left[P_o \cos\psi_o - Q_o \sin\psi_o \right] \psi \quad (A-25)$$

$$\dot{\psi} = \left[-\cos\psi_o \tan\theta_o \right] p + \left[\sin\psi_o \tan\theta_o \right] q + \left[-(P_o \cos\psi_o - Q_o \sin\psi_o) / \cos^2\theta_o \right] \theta$$

$$+ \left[(P_o \sin\psi_o + Q_o \cos\psi_o) \tan\theta_o \right] \psi \quad (A-26)$$

In most flight conditions it can be assumed that $\psi_o = 0$; then, Eqs. (A-24), (A-25), and (A-26) can be rewritten as

$$\dot{\phi} = \left[\frac{1}{\cos \theta_o} \right] p + \left[\frac{P_o \tan \theta_o}{\cos \theta_o} \right] \theta + \left[\frac{-Q_o}{\cos \theta_o} \right] \psi \quad (A-27)$$

$$\dot{\theta} = q + [P_o] \psi \quad (A-28)$$

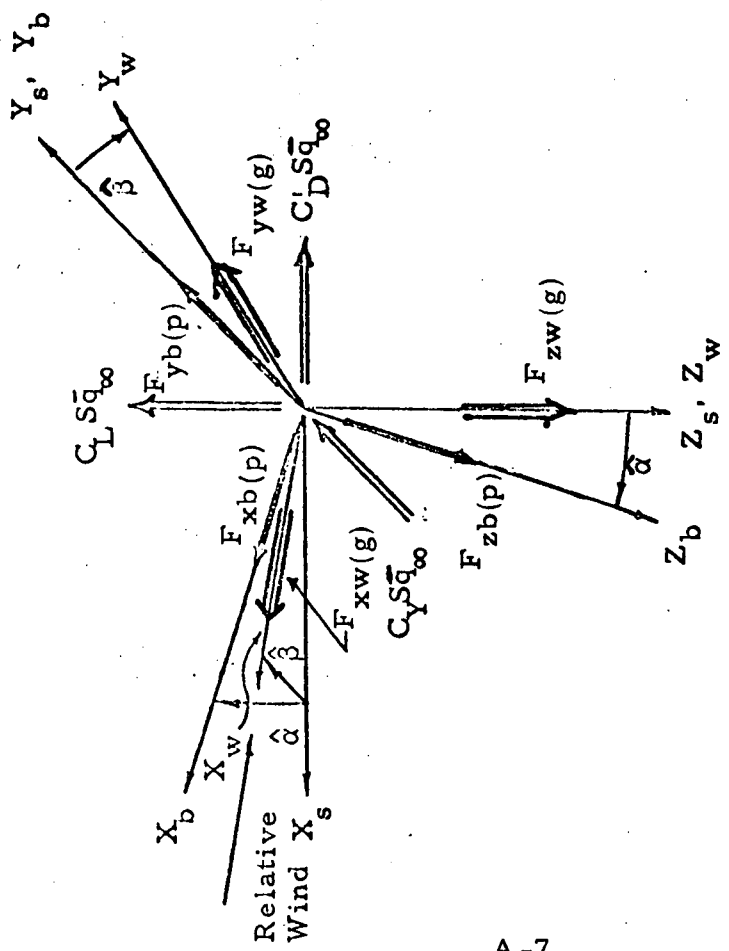
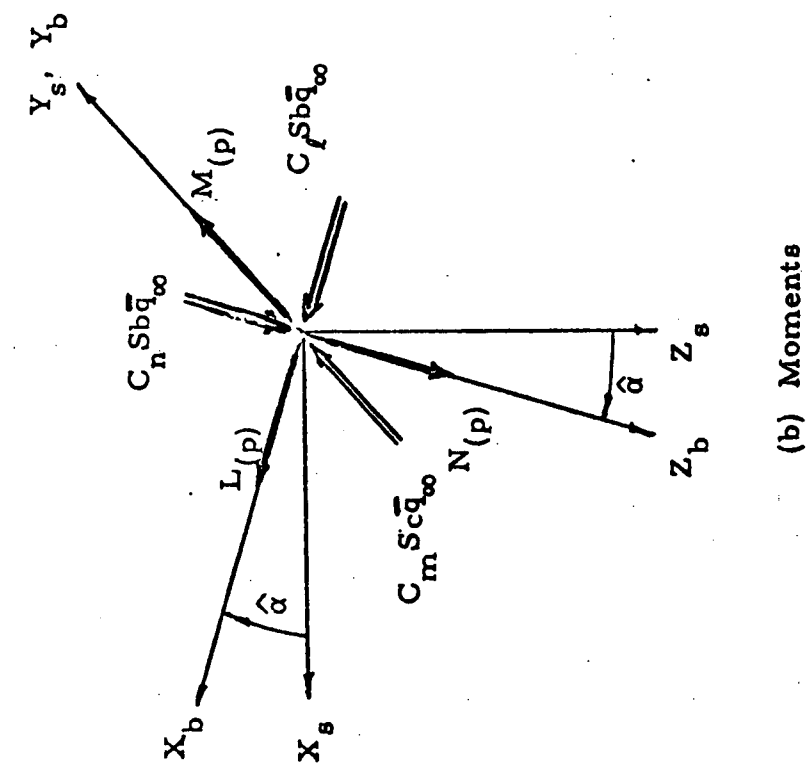
$$\dot{\psi} = [-\tan \theta_o] p + r + \left[-\frac{P_o}{\cos^2 \theta_o} \right] \theta + [Q_o \tan \theta_o] \psi \quad (A-29)$$

A.3 PERTURBATION FORCES AND MOMENTS

The aerodynamic forces are most frequently expressed in stability axis system coordinates, and the propulsive forces are most conveniently expressed in body axis system coordinates (as shown in Fig. A-1). Then, the external force components expressed in wind axis system coordinates can be written as

$$\begin{aligned} \hat{F}_{xw} &= \hat{F}_{xs(a)} \cos \hat{\beta} + \hat{F}_{ys(a)} \sin \hat{\beta} + \hat{F}_{xw(g)} + \left[\hat{F}_{xb(p)} \cos \hat{\alpha} + \hat{F}_{zb(p)} \sin \hat{\alpha} \right] \cos \hat{\beta} \\ &\quad + \hat{F}_{yb(p)} \sin \hat{\beta} \end{aligned} \quad (A-30)$$

$$\begin{aligned} \hat{F}_{yw} &= -\hat{F}_{ys(a)} \sin \hat{\beta} + \hat{F}_{ys(a)} \cos \hat{\beta} + \hat{F}_{yw(g)} - \left[\hat{F}_{xb(p)} \cos \hat{\alpha} + \hat{F}_{zb(p)} \sin \hat{\alpha} \right] \sin \hat{\beta} \\ &\quad + \hat{F}_{yb(p)} \cos \hat{\beta} \end{aligned} \quad (A-31)$$



\bar{q} = Dynamic pressure

Fig. A-1 - External Forces and Moments

$$\hat{F}_{zw} = \hat{F}_{zs(a)} + \hat{F}_{zw(g)} + \left[-\hat{F}_{xb(p)} \sin\alpha + \hat{F}_{zb(p)} \cos\alpha \right] \quad (A-32)$$

The perturbation force components in wind axis system coordinates can be expressed as

$$\begin{aligned} f_{xw} &= f_{xs(a)} \cos\beta_o + f_{ys(a)} \sin\beta_o + f_{yw(g)} + \left[f_{xb(p)} \cos\alpha_o + f_{zb(p)} \sin\alpha_o \right] \cos\beta_o \\ &\quad + f_{yb(p)} \sin\beta_o + \left[(-F_{xs(a)o} \sin\beta_o + F_{ys(a)o} \cos\beta_o) \right. \\ &\quad \left. + (-F_{xb(p)o} \cos\alpha_o - F_{zb(p)o} \sin\alpha_o) \sin\beta_o + F_{yb(p)o} \cos\beta_o \right] \beta \\ &\quad + \left[(-F_{xb(p)o} \sin\alpha_o + F_{zb(p)o} \cos\alpha_o) \cos\beta_o \right] \alpha \end{aligned} \quad (A-33)$$

$$\begin{aligned} f_{yw} &= -f_{xs(a)} \sin\beta_o + f_{ys(a)} \cos\beta_o + f_{yw(g)} - \left[f_{xb(p)} \cos\alpha_o + f_{xb(p)} \sin\alpha_o \right] \sin\beta_o \\ &\quad + f_{yb(p)} \cos\beta_o + \left[(-F_{xs(a)o} \cos\beta_o - F_{ys(a)o} \sin\beta_o) \right. \\ &\quad \left. - (F_{yb(p)o} \cos\alpha_o + F_{zb(p)o} \sin\alpha_o) \cos\beta_o - F_{yb(p)o} \sin\beta_o \right] \beta \\ &\quad + \left[(F_{xb(p)o} \sin\alpha_o - F_{zb(p)o} \cos\alpha_o) \sin\beta_o \right] \alpha \end{aligned} \quad (A-34)$$

$$\begin{aligned} f_{zw} &= f_{zs(a)} + f_{zw(g)} + \left[-f_{xb(p)} \sin\alpha_o + f_{zb(p)} \cos\alpha_o \right] \\ &\quad + \left[-F_{xb(p)o} \cos\alpha_o - F_{zb(p)o} \sin\alpha_o \right] \alpha \end{aligned} \quad (A-35)$$

where

$$F_{xs(a)o} = - \left[C'_D + C'_{D_\alpha} \alpha_o + C'_{D_q} Q_o \frac{c}{2V_o} + C'_{D_{\delta_e}} \delta_{e_o} \right] \bar{q} s = -C'_{D_o} \bar{q} s$$

$$F_{ys(a)o} = \left[C_{y_o} \right] \bar{q} s$$

$$F_{zs(a)o} = - \left[C_L + C_{L_\alpha} \alpha_o + C_{L_q} \left(\frac{Q_o c}{2V_o} \right) + C_{L_{\delta_e}} \delta_{e_o} \right] \bar{q} s = -C_{L_o} \bar{q} s$$

$$f_{xs(a)} \cong - \left[C'_{D_\alpha} \alpha + C'_{D_q} \frac{c}{2V_o} q + C'_{D_{\delta_e}} \delta_{e} \right] \bar{q} s$$

$$\begin{aligned} f_{ys(a)} = & \left[C_{y_p} \frac{b}{2V_o} p + C_{y_r} \frac{b}{2V_o} r + C_{y_\beta} \beta + C_{y_{\dot{\beta}}} \frac{b}{2V_o} \dot{\beta} \right. \\ & \left. + C_{y_{\delta_a}} \delta_a + C_{y_{\delta_r}} \delta_r \right] \bar{q} s \end{aligned}$$

$$f_{zs(a)} = - \left[C_{L_\alpha} \alpha + C_{L_{\dot{\alpha}}} \frac{c}{2V_o} \dot{\alpha} + C_{L_q} \frac{c}{2V_o} q + C_{L_{\delta_e}} \delta_e \right] \bar{q} s$$

$$F_{xw(g)o} = -mg \sin \gamma_o \quad F_{yw(g)o} = mg \cos \gamma_o \sin \phi_o$$

$$F_{zw(g)o} = mg \cos \gamma_o \cos \phi_o$$

$$f_{xw(g)} = (-mg \cos \gamma_o) \gamma$$

$$f_{yw(g)} = \left[-mg \sin \gamma_o \sin \phi_o \right] \gamma + \left[mg \cos \gamma_o \cos \phi_o \right] \phi$$

$$f_{zw(g)} = \left[-mg \sin \gamma_o \cos \phi_o \right] \gamma + \left[-mg \cos \gamma_o \sin \phi_o \right] \phi$$

where \bar{q} is the dynamic pressure, s is the reference area, and b and c are the reference lengths. The external moment components expressed in body axis system coordinates can be written as

$$\hat{L} = L_o + M_x \quad M_x = M_{x(p)} + M_{x(a)} \quad (A-36)$$

$$\hat{M} = M_o + M_y \quad M_y = M_{y(p)} + M_{y(a)} \quad (A-37)$$

$$\hat{N} = N_o + M_z \quad M_z = M_{z(p)} + M_{z(a)} \quad (A-38)$$

Since the aerodynamic moments are most conveniently expressed in body axis system coordinates, then

$$M_{x(a)} = \bar{q} sb \left\{ C_{\ell p} \frac{bp}{2V_o} + C_{\ell r} \frac{br}{2V_o} + C_{\ell \beta} \beta + C_{\ell \dot{\beta}} \frac{b\dot{\beta}}{2V_o} + C_{\ell \delta_a} \delta_a + C_{\ell \delta_r} \delta_r \right\}$$

$$M_{y(a)} = \bar{q} sc \left\{ C_{mq} \frac{cq}{2V_o} + C_{mu} \frac{u}{V_o} + C_{m\dot{\alpha}} \frac{c\dot{\alpha}}{2V_o} + C_{m\delta_e} \delta_e \right\}$$

$$M_{z(a)} = \bar{q} sb \left\{ C_{np} \frac{bp}{2V_o} + C_{nr} \frac{br}{2V_o} + C_{n\beta} \beta + C_{n\dot{\beta}} \frac{b\dot{\beta}}{2V_o} + C_{n\delta_a} \delta_a + C_{n\delta_r} \delta_r \right\}$$

A.4 6-D PERTURBATION EQUATIONS OF MOTION FOR REENTRY VEHICLES

Substituting Eqs. (A-33), (A-34) and (A-35) into Eqs. (A-18), (A-19) and (A-20), assuming $\beta_o = 0$ and neglecting higher order aerodynamic effects, there results

$$\begin{aligned} \gamma = & \frac{1}{mg \cos \gamma_o} \left\{ \left[-F_{xb(p)o} \sin \alpha_o + F_{zb(p)o} \cos \alpha_o - C'_{D_\alpha} s\bar{q} \right] \alpha \right. \\ & + \left[C_{yo} s\bar{q} + F_{yb(p)o} \right] \beta + \left[-C'_{D_q} s\bar{q} \frac{c}{2V_o} \right] q + \left[\cos \alpha_o \right] f_{xb(p)} \\ & \left. + \left[\sin \alpha_o \right] f_{zb(p)} + \left[-C'_{D_{\delta_e}} s\bar{q} \right] \delta_e \right\} \quad (A-39) \end{aligned}$$

$$\begin{aligned}
\dot{\beta} = & \left[-C_{y\beta} \frac{bs\bar{q}}{2mV_o^2} + 1 \right]^{-1} \left\{ \left[C_{y\beta} \frac{s\bar{q}}{mV_o} + \frac{1}{mV_o} (-F_{xb(p)o} \cos\alpha_o - F_{zb(p)o} \sin\alpha_o \right. \right. \\
& + C'_{D_o} s\bar{q}) \Big] \beta + \left[P_o \cos\alpha_o + R_o \sin\alpha_o \right] \alpha \\
& + \left[\sin\alpha_o + C_{yp} \frac{bs\bar{q}}{2mV_o^2} \right] p + \left[-\cos\alpha_o + C_{yr} \frac{bs\bar{q}}{2mV_o^2} \right] r \\
& + \left[\frac{1}{mV_o} \right] f_{yb(p)} + \left[C_{y\delta_a} \frac{s\bar{q}}{mV_o} \right] \delta_a + \left[C_{y\delta_r} \frac{s\bar{q}}{mV_o} \right] \delta_r \\
& \left. \left. + \left[-\frac{g}{V_o} \sin\gamma_o \sin\phi_o \right] \gamma + \left[\frac{g}{V_o} \cos\gamma_o \cos\phi_o \right] \phi \right\} \quad (A-40)
\end{aligned}$$

$$\begin{aligned}
\dot{\alpha} = & \left[1 + C_{L\alpha} \frac{cs\bar{q}}{2mV_o^2} \right]^{-1} \left\{ \left[-(P_o \cos\alpha_o + R_o \sin\alpha_o) \right] \beta \right. \\
& + \left[\left(\frac{-F_{xb(p)o} \cos\alpha_o - F_{zb(p)o} \sin\alpha_o}{mV_o} \right) - C_{L\alpha} \frac{s\bar{q}}{mV_o} \right] \alpha \\
& + \left[1 - C_{Lq} \frac{cs\bar{q}}{2mV_o^2} \right] q + \left[-\frac{\sin\alpha_o}{mV_o} \right] f_{xp(p)} \\
& + \left[\frac{\cos\alpha_o}{mV_o} \right] f_{zb(p)} + \left[-C_{L\delta_e} \frac{s\bar{q}}{mV_o} \right] \delta_e \\
& \left. + \left[-\frac{g}{V_o} \sin\gamma_o \cos\phi_o \right] \gamma + \left[-\frac{g}{V_o} \cos\gamma_o \sin\phi_o \right] \phi \right\} \quad (A-41)
\end{aligned}$$

Substituting Eq. (A-39) into Eqs. (A-40) and (A-41), and assuming $F_{xb(p)o}$, $F_{yb(p)o}$, $F_{zb(p)o}$ zero, the translational perturbation equations become

$$\begin{aligned}
 \dot{\alpha} = & \left[1 + C_{L\alpha} \frac{c s \bar{q}}{2 m V_o^2} \right]^{-1} \left\{ \left[-(P_o \cos \alpha_o + R_o \sin \alpha_o) - \frac{\tan \gamma_o \cos \phi_o}{m V_o} C_{y_o} \bar{q} s \right] \beta \right. \\
 & + \left[-C_{L\alpha} \frac{\bar{q} s}{m V_o} + \frac{\tan \gamma_o \cos \phi_o}{m V_o} C'_{D\alpha} \bar{q} s \right] \alpha \\
 & + \left[1 - C_{Lq} \frac{\bar{q} s c}{2 m V_o^2} + \tan \gamma_o \cos \phi_o s q \frac{c}{2 m V_o} C'_{Dq} \right] q \\
 & + \left[-\frac{g}{V_o} \cos \gamma_o \sin \phi_o \right] \phi \\
 & + \left[-C_{L\delta_e} \frac{\bar{q} s}{m V_o} + \frac{\tan \gamma_o \cos \phi_o}{m V_o} C'_{D\delta_e} \bar{q} s \right] \delta_e \\
 & + \left[-\frac{\sin \gamma_o}{m V_o} - \frac{\tan \gamma_o \cos \phi_o}{m V_o} \cos \alpha_o \right] f_{xb(p)} \\
 & \left. + \left[\frac{\cos \alpha_o}{m V_o} - \frac{\tan \gamma_o \cos \phi_o}{m V_o} \sin \alpha_o \right] f_{zb(p)} \right\} \quad (A-42)
 \end{aligned}$$

$$\begin{aligned}
\dot{\beta} = & \left[1 - C_{y\beta} \frac{\bar{q}_{sb}}{2mV_o^2} \right]^{-1} \left\{ \left[C_{y\beta} \frac{\bar{q}_s}{mV_o} + C'_{D_o} \frac{\bar{q}_s}{mV_o} - \tan \gamma_o \sin \phi_o C_{y_o} \frac{\bar{q}_s}{mV_o} \right] \beta \right. \\
& + \left[P_o \cos \alpha_o + R_o \sin \alpha_o + \frac{\tan \gamma_o \sin \phi_o}{mV_o} C'_{D_\alpha} \bar{q}_s \right] \alpha \\
& + \left[\sin \alpha_o + C_{y_p} \frac{\bar{q}_{sb}}{2mV_o^2} \right] p + \left[-\cos \alpha_o + C_{y_r} \frac{\bar{q}_{sb}}{2mV_o^2} \right] r \\
& + \left[\frac{g}{V_o} \cos \gamma_o \cos \phi_o \right] \phi + \left[C_{y_{\delta_a}} \frac{\bar{q}_s}{mV_o} \right] \delta_a \\
& + \left[\frac{\tan \gamma_o \sin \phi_o}{mV_o} C'_{D_{\delta_e}} \bar{q}_s \right] \delta_e + \left[C_{y_{\delta_r}} \frac{\bar{q}_s}{mV_o} \right] \delta_r \\
& + \left[\frac{c}{2mV_o^2} \tan \gamma_o \sin \phi_o C'_{D_q} s\bar{q} \right] q \\
& + \left[\frac{1}{mV_o} f_{yb(p)} \right] + \left[-\frac{\tan \gamma_o}{mV_o} \cos \alpha_o \right] f_{xb(p)} \\
& \left. + \left[-\frac{\tan \gamma_o \sin \phi_o}{mV_o} \sin \alpha_o \right] f_{zb(p)} \right\} \quad (A-43)
\end{aligned}$$

Similarly, the rotational perturbation equations of motion can be obtained by substituting Eqs. (A-36), (A-37) and (A-38) into Eqs. (A-21), (A-22) and (A-23).

$$\begin{aligned}
p &= \left[\frac{\bar{q}_s b}{I_x I_z - I_{xz}^2} \right] \left\{ \left[I_z C_{\ell_\beta} + I_{xz} C_{n_\beta} \right] \dot{\beta} + \left[(I_z C_{\ell_\beta} + I_{xz} C_{n_\beta}) \frac{b}{2V_o} \right] \ddot{\beta} \right. \\
&\quad + \left[I_z C_{\ell_{\delta_a}} + I_{xz} C_{n_{\delta_a}} \right] \dot{\delta_a} + \left[I_z C_{\ell_{\delta_r}} + I_{xz} C_{n_{\delta_r}} \right] \dot{\delta_r} \Big\} \\
&\quad + \left[\frac{1}{I_x I_z - I_{xz}^2} \right] \left\{ \left[I_{xz} (I_x - I_y + I_z) Q_o + \bar{q}_s \frac{b^2}{2V_o} (I_z C_{\ell_p} + I_{xz} C_{n_p}) \right] p \right. \\
&\quad + \left[I_{xz} (I_x - I_y + I_z) P_o + I_z (I_y - I_z) - I_{xz}^2 R_o \right] q \\
&\quad + \left. \left[(I_z (I_y - I_z) - I_{xz}^2) Q_o + \bar{q}_s \frac{b^2}{2V_o} (I_z C_{\ell_r} + I_{xz} C_{n_r}) \right] r \right. \\
&\quad + \left. \left[I_z \right] M_{x(p)} + \left[I_{xz} \right] M_{z(p)} \right\} \tag{A-44}
\end{aligned}$$

$$\begin{aligned}
\dot{q} &= \left[\frac{\bar{q}_s c}{I_y} \right] \left\{ \left[C_{m_\alpha} \right] \alpha + \left[\frac{c}{2V_o} C_{m_\dot{\alpha}} \right] \dot{\alpha} + \left[C_{m_{\delta_e}} \right] \dot{\delta_e} + \left[\frac{c}{2V_o} C_{m_q} \right] q \right\} \\
&\quad + \left[\frac{I_z - I_x}{I_y} R_o - \frac{2I_{xz}}{I_y} P_o \right] p \\
&\quad + \left[\frac{I_z - I_x}{I_y} P_o + \frac{2I_{xz}}{I_y} R_o \right] r + \left[\frac{1}{I_y} \right] M_{y(p)} \tag{A-45}
\end{aligned}$$

$$\begin{aligned}
\dot{r} = & \left[\frac{q_s b}{I_x I_z - I_{xz}^2} \right] \left\{ \left[(I_{xz} C_{l_\beta} + I_x C_{n_\beta}) \beta + \left[(I_{xz} C_{l_\beta} + I_x C_{n_\beta}) \frac{b}{2V_o} \right] \dot{\beta} \right. \right. \\
& + \left[I_{xz} C_{l_{\delta_a}} + I_x C_{n_{\delta_a}} \right] \delta_a + \left[I_{xz} C_{l_{\delta_r}} + I_x C_{n_{\delta_r}} \right] \delta_r \Big\} \\
& + \left[\frac{1}{I_x I_z - I_{xz}^2} \right] \left\{ \left[(I_x (I_x - I_y) + I_{xz}^2) Q_o \right. \right. \\
& + \left. \left. \bar{q}_s \frac{b^2}{2V_o} (I_{xz} C_{l_p} + I_x C_{n_p}) \right] p + \left[(I_x (I_x - I_y) + I_{xz}^2) P_o \right. \right. \\
& + \left. \left. I_{xz} (-I_x + I_y - I_z) R_o \right] q + \left[I_{xz} (-I_x + I_y - I_z) Q_o \right. \right. \\
& + \left. \left. \bar{q}_s \frac{b^2}{2V_o} (I_{xz} C_{l_r} + I_x C_{n_r}) \right] r + \left[I_{xz} \right] M_x(p) + \left[I_x \right] M_z(p) \right\} \quad (A-46)
\end{aligned}$$

Define

$$\begin{aligned}
K_1 &= \left[1 + C_{L_\alpha} \frac{\bar{q}_s c}{2mV_o^2} \right]^{-1} \left[-(P_o \cos \alpha_o + R_o \sin \alpha_o) - \frac{\tan \gamma_o \cos \phi_o}{mV_o} C_{y_o} \bar{q}_s \right] \\
K_2 &= \left[1 + C_{L_\alpha} \frac{\bar{q}_s c}{2mV_o^2} \right]^{-1} \left[-C_{L_\alpha} \frac{\bar{q}_s}{mV_o} + \frac{\tan \gamma_o \cos \phi_o}{mV_o} C_{D_\alpha} \bar{q}_s \right] \\
K_3 &= \left[1 + C_{L_\alpha} \frac{\bar{q}_s c}{2mV_o^2} \right]^{-1} \left[1 - C_{L_q} \frac{\bar{q}_s c}{2mV_o^2} \right] \\
K_4 &= \left[1 + C_{L_\alpha} \frac{\bar{q}_s c}{2mV_o^2} \right]^{-1} \left[-\frac{g}{V_o} \cos \gamma_o \sin \phi_o \right]
\end{aligned}$$

$$\begin{aligned}
K_5 &= \left[1 + C_{L_\alpha} \frac{\bar{q}_{sc}}{2mV_o^2} \right]^{-1} \left[-C_{L_{\delta_e}} \frac{\bar{q}_s}{mV_o} + \frac{\tan \gamma_o \cos \phi_o}{mV_o} C'_{D_{\delta_e}} \bar{q}_s \right] \\
K_6 &= \left[1 + C_{L_\alpha} \frac{\bar{q}_{sc}}{2mV_o^2} \right]^{-1} \left[-\frac{\sin \alpha_o}{mV_o} - \frac{\tan \gamma_o \cos \phi_o}{mV_o} \cos \alpha_o \right] \\
K_7 &= \left[1 + C_{L_\alpha} \frac{\bar{q}_{sc}}{2mV_o^2} \right]^{-1} \left[\frac{\cos \alpha_o}{mV_o} - \frac{\tan \gamma_o \cos \phi_o}{mV_o} \sin \alpha_o \right] \\
K_8 &= \left[1 - C_{y_\beta} \frac{\bar{q}_{sb}}{2mV_o^2} \right]^{-1} \left[C_{y_\beta} \frac{\bar{q}_s}{mV_o} + C'_{D_o} \frac{\bar{q}_s}{mV_o} - \tan \gamma_o \sin \phi_o C_{y_o} \frac{\bar{q}_s}{mV_o} \right] \\
K_9 &= \left[1 - C_{y_\beta} \frac{\bar{q}_{sb}}{2mV_o^2} \right]^{-1} \left[P_o \cos \alpha_o + R_o \sin \alpha_o + \frac{\tan \gamma_o \sin \phi_o}{mV_o} C'_{D_\alpha} \bar{q}_s \right] \\
K_{10} &= \left[1 - C_{y_\beta} \frac{\bar{q}_{sb}}{2mV_o^2} \right]^{-1} \left[\sin \alpha_o + C_{y_p} \frac{\bar{q}_{sb}}{2mV_o^2} \right] \\
K_{11} &= \left[1 - C_{y_\beta} \frac{\bar{q}_{sb}}{2mV_o^2} \right]^{-1} \left[\frac{c}{2mV_o^2} \tan \gamma_o \sin \phi_o C'_{D_q} s \bar{q} \right] \\
K_{12} &= \left[1 - C_{y_\beta} \frac{\bar{q}_{sb}}{2mV_o^2} \right]^{-1} \left[-\cos \alpha_o + C_{y_r} \frac{\bar{q}_{sb}}{2mV_o^2} \right] \\
K_{13} &= \left[1 - C_{y_\beta} \frac{\bar{q}_{sb}}{2mV_o^2} \right]^{-1} \left[\frac{q}{V_o} \cos \gamma_o \cos \phi_o \right] \\
K_{14} &= \left[1 - C_{y_\beta} \frac{\bar{q}_{sb}}{2mV_o^2} \right]^{-1} \left[C_{y_{\delta_a}} \frac{\bar{q}_s}{mV_o} \right] \\
K_{15} &= \left[1 - C_{y_\beta} \frac{\bar{q}_{sb}}{2mV_o^2} \right]^{-1} \left[\frac{\tan \gamma_o \sin \phi_o}{mV_o} C'_{D_{\delta_e}} \bar{q}_s \right]
\end{aligned}$$

$$K_{16} = \left[1 - C_{y\beta} \frac{\bar{q}_{sb}}{2mV_o^2} \right]^{-1} \begin{bmatrix} C_{y\delta_r} & \frac{\bar{q}_s}{mV_o} \end{bmatrix}$$

$$K_{17} = \left[1 - C_{y\beta} \frac{\bar{q}_{sb}}{2mV_o^2} \right]^{-1} \begin{bmatrix} -\frac{\tan\gamma_o}{mV_o} \cos\alpha_o \\ \end{bmatrix}$$

$$K_{18} = \left[1 - C_{y\beta} \frac{\bar{q}_{sb}}{2mV_o^2} \right]^{-1} \begin{bmatrix} \frac{1}{mV_o} \end{bmatrix}$$

$$K_{19} = \left[1 - C_{y\beta} \frac{\bar{q}_{sb}}{2mV_o^2} \right]^{-1} \begin{bmatrix} -\frac{\tan\gamma_o \sin\phi_o}{mV_o} \sin\alpha_o \end{bmatrix}$$

Let

$$I_D = \left[\frac{\bar{q}_{sb}}{I_x I_z - I_{xz}^2} \right], \quad I_{DD} = \left[\frac{1}{I_x I_z - I_{xz}^2} \right]$$

Then

$$K_{20} = I_D (I_z C_{\ell\beta} + I_{xz} C_{n\beta})$$

$$K_{21} = I_D (I_z C_{\ell\beta} + I_{xz} C_{n\beta}) \frac{b}{2V_o}$$

$$K_{22} = I_D (I_z C_{\ell_{\delta_a}} + I_{xz} C_{n_{\delta_a}})$$

$$K_{23} = (I_z C_{\ell_{\delta_r}} + I_{xz} C_{n_{\delta_r}}) I_D$$

$$K_{24} = I_{DD} \left[I_{xz} (I_x - I_y + I_z) Q_o + \bar{q}_s \frac{b^2}{2V_o} (I_z C_{\ell_p} + I_{xz} C_{n_p}) \right]$$

$$K_{25} = I_{DD} \left[I_{xz} (I_x - I_y + I_z) P_o + \left(I_z (I_y - I_z) - I_{xz}^2 \right) R_o \right]$$

$$K_{26} = I_{DD} \left[\left(I_z (I_y - I_z) - I_{xz}^2 \right) Q_o + \bar{q}_s \frac{b^2}{2V_o} (I_2 C_{\ell_r} + I_{xz} C_{n_r}) \right]$$

$$K_{27} = I_{DD} I_z$$

$$K_{28} = I_{DD} I_{xz}$$

$$K_{29} = \left[\frac{\bar{q}_{sc}}{I_y} C_{m_\alpha} \right]$$

$$K_{30} = \left[\frac{\bar{q}_{sc}}{I_y} \frac{C}{2V_o} C_{m_\alpha} \right]$$

$$K_{31} = \left[\frac{\bar{q}_{sc}}{I_y} C_{m_{\delta_e}} \right]$$

$$K_{32} = \left[\frac{\bar{q}_{sc}}{I_y} \frac{C}{2V_o} C_{m_q} \right]$$

$$K_{33} = \left[\frac{I_z - I_x}{I_y} R_o - \frac{2I_{xz}}{I_y} P_o \right]$$

$$K_{34} = \left[\frac{I_z - I_x}{I_y} P_o + \frac{2I_{xz}}{I_y} R_o \right]$$

$$K_{35} = \left[\frac{1}{I_y} \right]$$

$$K_{36} = \left[I_D (I_{xz} C_{\ell_\beta} + I_x C_{n_\beta}) \right]$$

$$K_{37} = I_D \left[I_{xz} C_{\ell_\beta} + I_x C_{n_\beta} \right] \frac{b}{2V_o}$$

$$K_{38} = I_D \left[I_{xz} C_{\ell_{\delta_a}} + I_x C_{n_{\delta_a}} \right]$$

$$K_{39} = I_D \left[I_{xz} C_{\ell_{\delta_r}} + I_x C_{n_{\delta_r}} \right]$$

$$K_{40} = I_{DD} \left[I_x (I_x - I_y) + I_{xz}^2 \right] + I_{DD} \left[\bar{q}s \frac{b^2}{2V_o} (I_{xz} C_{\ell_p} + I_x C_{n_p}) \right]$$

$$K_{41} = I_{DD} \left[I_x (I_x - I_y) + I_{xz}^2 \right] P_o + I_{DD} I_{xz} (-I_x + I_y - I_z) R_o$$

$$K_{42} = I_{DD} \left[(-I_x + I_y - I_z) Q_o I_{xz} + \bar{q}s \frac{b^2}{2V_o} (I_{xz} C_{\ell_r} + I_x C_{n_r}) \right]$$

$$K_{43} = I_{DD} I_x$$

$$K_{44} = \left[\frac{1}{\cos \alpha_o} \right]$$

$$K_{45} = \left[\frac{P_o \tan \alpha_o}{\cos \alpha_o} \right]$$

$$K_{46} = \left[- \frac{Q_o}{\cos \alpha_o} \right]$$

$$K_{47} = \left[P_o \right]$$

$$K_{48} = \left[- \tan \alpha_o \right]$$

$$K_{49} = \left[-\frac{P_o}{\cos^2 \alpha_o} \right]$$

$$K_{50} = \left[Q_o \tan \alpha_o \right]$$

Then the perturbation equations of motion for shuttle reentry can be written as

$$\dot{\alpha} = K_1 \beta + K_2 \alpha + K_3 q + K_4 \phi + K_5 \delta_e + K_6 f_{x(p)} + K_7 f_{z(p)}$$

$$\begin{aligned} \dot{\beta} = & K_8 \beta + K_9 \alpha + K_{10} p + K_{11} q + K_{12} r + K_{13} \phi + K_{14} \delta_a + K_{15} \delta_e + K_{16} \delta_r \\ & + K_{17} f_{x(p)} + K_{18} f_{y(p)} + K_{19} f_{z(p)} \end{aligned}$$

$$\dot{p} = K_{20} \beta + K_{21} \dot{\beta} + K_{22} \delta_a + K_{23} \delta_r + K_{24} p + K_{25} q + K_{26} r + K_{27} M_{x(p)} + K_{28} M_{z(p)}$$

$$\dot{q} = K_{29} \alpha + K_{30} \dot{\alpha} + K_{31} \delta_e + K_{32} q + K_{33} p + K_{34} r + K_{35} M_{y(p)}$$

$$\dot{r} = K_{36} \beta + K_{37} \dot{\beta} + K_{38} \delta_a + K_{39} \delta_r + K_{40} p + K_{41} q + K_{42} r + K_{28} M_{x(p)} + K_{43} M_{z(p)}$$

$$\dot{\phi} = K_{44} p + K_{45} \theta + K_{46} \psi$$

$$\dot{\theta} = q + K_{47} \psi$$

$$\dot{\psi} = K_{48} p + r + K_{49} \theta + K_{50} \psi$$

Appendix B

**REDUCTION OF LOCKHEED'S 6-D PERTURBATION EOM
TO CONVENTIONAL AIRFRAME 6-D PERTURBATION EOM**

Appendix B

The assumptions used in the derivation of conventional airframe perturbation EOM are:

1. The airframe is assumed to be a rigid body.
2. The earth is assumed to be fixed in space, and the earth's atmosphere is assumed to be fixed with respect to the earth.
3. The mass of the airplane is assumed to remain constant for the duration of any particular dynamic analysis.
4. The airframe XZ plane is assumed to be a plane of symmetry.
5. The disturbances from the steady flight condition are assumed to be small enough so that second-order changes in velocity are negligible compared to the changes themselves. Also, the disturbance angles are assumed to be small enough so that the sines of these angles may be set equal to the angle and the cosines set equal to unity.
6. During the steady flight condition, the airframe is assumed to be flying with wings level, and along a straight flight path at constant linear velocity and zero angular velocity.

The differences between the above assumptions and the ones used in the derivation of the shuttle reentry perturbation equations of motion (see Section 4) are:

1. The steady flight condition that it must fly with wings level and along a straight flight path at constant linear velocity and zero angular velocity is disregarded. The vehicle may fly any given reference flight condition.
2. The small angle assumption is valid only for the derivation of conventional airframe perturbation EOM and is invalid for the shuttle reentry perturbation EOM.

Furthermore, the orientation of the conventional airframe is expressed in 3-2-1 sequence of rotation (yaw an angle $\hat{\psi}$, pitch an angle $\hat{\theta}$, and roll an angle $\hat{\phi}$). However, for the shuttle reentry study, the sequence of rotation is 1-2-3. The rate of change of the Eulerian angles for the 3-2-1 sequence of rotation can be expressed as functions of the instantaneous angular velocities (\hat{P} , \hat{Q} , \hat{R}).

$$\dot{\hat{\theta}} = \hat{Q} \cos \hat{\phi} - \hat{R} \sin \hat{\phi} \quad (B-1)$$

$$\dot{\hat{\phi}} = \hat{P} + \hat{Q} \sin \hat{\phi} \tan \hat{\theta} + \hat{R} \cos \hat{\phi} \tan \hat{\theta} \quad (B-2)$$

$$\dot{\hat{\psi}} = (\hat{Q} \sin \hat{\phi} + \hat{R} \cos \hat{\phi}) \sec \hat{\theta} \quad (B-3)$$

The components of the weight in the direction of the body axes which are used in the derivation of conventional equations of motion are found to be:

$$\hat{F}_{xb(g)} = -mg \sin \hat{\theta} \quad (B-4)$$

$$\hat{F}_{yb(g)} = mg \cos \hat{\theta} \sin \hat{\phi} \quad (B-5)$$

$$\hat{F}_{zb(g)} = mg \cos \hat{\theta} \cos \hat{\phi} \quad (B-6)$$

The components of the weight in the direction of the wind axes can be expressed as:

$$\hat{F}_{xw(g)} = \hat{F}_{xb(g)} \cos \alpha \cos \beta - \hat{F}_{yb(g)} \sin \beta + \hat{F}_{zb(g)} \sin \alpha \cos \beta \quad (B-7)$$

$$\hat{F}_{yw(g)} = -\hat{F}_{xb(g)} \cos \alpha \sin \beta + \hat{F}_{yb} \cos \beta - \hat{F}_{zb} \sin \alpha \sin \beta \quad (B-8)$$

$$\hat{F}_{zw(g)} = \hat{F}_{xb(g)} \sin \alpha + \hat{F}_{zb} \cos \alpha \quad (B-9)$$

$$\hat{F}_{xw(g)} = mg [\sin(\theta - \alpha)] \cos\beta \cos\phi + mg(1 - \cos\phi) \sin\theta \cos\alpha \quad (B-10)$$

$$\hat{F}_{yw(g)} = -mg [\sin(\theta - \alpha)] \sin\beta + mg \cos\theta \sin\phi \cos\beta \quad (B-11)$$

$$\hat{F}_{zw(g)} = mg [\cos(\theta - \alpha)] \cos\phi \quad (B-12)$$

where $(\hat{\cdot})$ is the sum of the steady state value and a small deviation from the steady state value.

Obviously, the shuttle reentry perturbation EOM are less restrictive in comparison with the conventional airframe perturbation EOM. The former set of equations should be able to reduce to the latter set of equations by assuming

$$P_o = Q_o = R_o = \phi_o = \psi_o = \beta_o \approx 0 \quad \beta \approx -\psi \quad (B-13)$$

and $V_o = \text{constant} \quad \frac{v}{mV_o^2} \approx 0$

In the derivation of translational perturbation EOM, the shuttle study uses flight path axes whereas the conventional airframe uses body axes. By using the above listed additional assumptions, the translational perturbation EOM in the flight path axes can be reduced to:

$$\dot{v} = f_{xw}/m \quad (B-14)$$

$$\dot{\beta} = -r + \frac{1}{mV_o} f_{yw} \quad (B-15)$$

$$\dot{\alpha} = q + \frac{1}{mV_o} f_{zw} \quad (B-16)$$

where

$$f_{xw} = f_{xw(g)} + f_{xw(a)} + f_{xw(p)}$$

$$f_{yw} = f_{yw(g)} + f_{yw(a)} + f_{yw(p)}$$

$$f_{zw} = f_{zw(g)} + f_{zw(a)} + f_{zw(p)}$$

and

$$f_{xw(a)} \approx - \left[C_{D_\alpha} \alpha + C_{D_q} \frac{c}{2V_o} q + C_{D_{\delta_e}} \delta_e + C_{D_v} v \right] s \bar{q}$$

$$f_{yw(a)} \approx - \left[C_{y_p} \frac{b}{2V_o} p + C_{y_r} \frac{b}{2V_o} r + C_{y_\beta} \beta + C_{y_{\dot{\beta}}} \frac{b}{2V_o} \dot{\beta} + C_{y_{\delta_a}} \delta_a + C_{y_{\delta_r}} \delta_r \right] \bar{q} s$$

$$f_{zw(a)} \approx - \left[C_{L_\alpha} \alpha + C_{L_{\dot{\alpha}}} \frac{c}{2V_o} \dot{\alpha} + C_{L_q} \frac{c}{2V_o} q + C_{L_{\delta_e}} \delta_e \right] \bar{q} s$$

$$f_{xw(g)} \approx - (mg \sin \gamma_o) \alpha$$

$$f_{yw(g)} \approx (mg \sin \gamma_o) \psi + (mg \cos \gamma_o) \phi$$

$$f_{zw(g)} \approx -(mg \sin \gamma_o) \alpha$$

here $\gamma_o = \theta_o - \alpha_o$ and $\psi \approx -\beta$ are used. The translational perturbation equations of motion can be written as

$$\begin{aligned} m \dot{v} &= (-mg \sin \gamma_o) \alpha + f_{xw(p)} + \left[-C_{D_\alpha} s \bar{q} \right] \alpha + \left[-C_{D_q} \frac{c}{2V_o} s \bar{q} \right] q \\ &\quad + \left[-C_{D_v} s \bar{q} \right] v + \left[-C_{D_{\delta_e}} s \bar{q} \right] \delta_e \end{aligned} \quad (B-17)$$

$$\begin{aligned} m V_o \dot{\beta} &= [mg \sin \gamma_o] \psi + [mg \cos \gamma_o] \phi + f_{xw(p)} + [-m V_o] r + \left[C_{y_p} \frac{b}{2V_o} \bar{q} s \right] p \\ &\quad + \left[C_{y_r} \frac{b}{2V_o} \bar{q} s \right] r + \left[C_{y_\beta} \bar{q} s \right] \beta + \left[C_{y_{\dot{\beta}}} \frac{b}{2V_o} \bar{q} s \right] \dot{\beta} \\ &\quad + \left[C_{y_{\delta_a}} \bar{q} s \right] \delta_a + \left[C_{y_{\delta_r}} \bar{q} s \right] \delta_r \end{aligned} \quad (B-18)$$

$$\begin{aligned}
 mV_o \alpha = & [-mg \sin \gamma_o] \alpha + f_{xw(p)} + [mv_o] q + \left[-C_{L\alpha} \bar{q} \quad s \right] \alpha \\
 & + \left[-C_{L\alpha} \frac{c}{2V_o} \bar{q} \quad s \right] \dot{\alpha} + \left[-C_{Lq} \frac{c}{2V_o} \bar{q} \quad s \right] q \\
 & + \left[-C_{L\delta_e} \bar{q} \quad s \right] \delta_e
 \end{aligned} \tag{B-19}$$

Since both sets of rotational perturbation EOM utilize body axes, the rotational perturbation EOM for the conventional airframe can easily be obtained by applying the assumptions given in Eq. (B-13) to Eqs. (A-44), (A-45) and (A-46).

$$\begin{aligned}
 p = & \left[\frac{\bar{q} sb}{I_x I_z - I_{xz}^2} \right] \left\{ \left[I_z C_{l\beta} + I_{xz} C_{n\beta} \right] \beta + \left[(I_z C_{l\dot{\beta}} + I_{xz} C_{n\dot{\beta}}) \frac{b}{2V_o} \right] \dot{\beta} \right. \\
 & + \left[I_z C_{l\delta_a} + I_{xz} C_{n\delta_a} \right] \delta_a + \left[I_z C_{l\delta_r} + I_{xz} C_{n\delta_r} \right] \delta_r \Big\} \\
 & + \left[\frac{1}{I_x I_z - I_{xz}^2} \right] \left\{ \left[\bar{q} s \frac{b^2}{2V_o} (I_z C_{l_p} + I_{xz} C_{n_p}) \right] p \right. \\
 & + \left[\bar{q} s \frac{b^2}{2V_o} (I_z C_{l_r} + I_{xz} C_{n_r}) \right] r \\
 & \left. \left. + \left[I_z \right] M_{x(p)} + \left[I_{xz} \right] M_{z(p)} \right\}
 \right. \tag{B-20}
 \end{aligned}$$

$$\dot{q} = \left[\frac{\bar{q} sc}{I_y} \right] \left\{ \left[C_{m\alpha} \right] \alpha + \left[\frac{c}{2V_o} C_{m\dot{\alpha}} \right] \dot{\alpha} + \left[C_{m\delta_e} \right] \delta_e + \left[\frac{c}{2V_o} C_{m_q} \right] q \right\} \tag{B-21}$$

$$\begin{aligned}
 \dot{r} = & \left[\frac{\bar{q}_s b}{I_x I_z - I_{xz}^2} \right] \left\{ \left[I_{xz} C_{\ell_\beta} + I_x C_{n_\beta} \right] \beta + \left[(I_{xz} C_{\ell_\beta} + I_x C_{n_\beta}) \frac{b}{2V_o} \right] \dot{\beta} \right. \\
 & + \left[I_{xz} C_{\ell_{\delta_a}} + I_x C_{n_{\delta_a}} \right] \delta_a + \left[I_{xz} C_{\ell_{\delta_r}} + I_x C_{n_{\delta_r}} \right] \delta_r \Big\} \\
 & + \left[\frac{1}{I_x I_z - I_{xz}^2} \right] \left\{ \left[+ \bar{q}_s \frac{b^2}{2V_o} (I_{xz} C_{\ell_p} + I_x C_{n_p}) \right] p \right. \\
 & \left. + \left[\bar{q}_s \frac{b^2}{2V_o} (I_{xz} C_{\ell_r} + I_x C_{n_r}) \right] r + \left[I_{xz} \right] M_{x(p)} + \left[I_x \right] M_{z(p)} \right\} \quad (B-22)
 \end{aligned}$$

The orientational perturbation equations in 3-2-1 sequence of rotation can be derived from Eqs. (B-1), (B-2) and (B-3) by using the assumptions given in Eq. (B-13).

$$\dot{\theta} = q \quad (B-23)$$

$$\dot{\phi} = p + r \tan \theta_0 \quad (B-24)$$

$$\dot{\psi} = r \sec \theta_0 \quad (B-25)$$

Appendix C

ANALYSIS OF HYDRAULIC SYSTEM COMPONENT WEIGHTS

Appendix C

In the analysis of hydraulic system component weights, efforts are placed on the determination of the empirical formulae relating both the power requirements and each component weight to the hinge moment.

C.1 HORSEPOWER

The horsepower required at the central surface hydraulic actuator was determined from the aerodynamic control surface hinge moment (H_m), the deflection rate ($\dot{\delta}$), angular acceleration ($\ddot{\delta}$), and the control surface inertia (I) as follows:

$$\text{HORSEPOWER} = [H_m + I\ddot{\delta}] \dot{\delta}$$

The horsepower required for control surface angular acceleration is small compared to the horsepower required for hinge moment and was neglected in determining horsepower requirements for the rudder.

C.2 ACTUATORS

The size of the actuator piston was determined from the applied hinge moment and actuator moment arm. From Ref. C-1, it was determined that the GDC/B-9U booster elevons are segmented into three surfaces per side and the rudder is segmented into two surfaces. Each surface is powered by two tandem power actuators accepting all four hydraulic circuits. Each power piston contributes 50% of the required hinge moment for each surface. Thus, the hinge moment carried by a single elevon actuator piston is 1/12 of the total elevon hinge moment. Similarly, the hinge moment carried by a single rudder actuator piston is 1/4 of the total rudder hinge moment.

The piston area was determined as follows.

$$\text{Area Piston} = \frac{\text{Hinge Moment}}{\text{Working Pressure} \times \text{Moment Arm}}$$

The working pressure is 67% of the total system pressure or 2000 psi.

Actuator weight was determined from a plot of weight versus work capability given in Ref. C-2. Work capability is based on full cutoff pressure of 3000 psi.

$$\text{Work Capability} = \text{Area Piston} \times \text{Cutoff Pressure} \times \text{Stroke}$$

The stroke necessary for elevon deflection angle travel was determined from a kinematic diagram of the actuator moment arm.

The weight of fluid in the actuator was determined as follows:

$$\text{Fluid Weight} = \text{Area Piston} \times \text{Stroke} \times \text{Fluid Specific Weight}$$

C.3 TRANSMISSION LINES

Hydraulic line lengths were estimated using the hydraulic system general arrangement given in Ref. C-1 and a schematic diagram of the GDC/B-9U hydraulic system. Transmission line weights, including the weight of fittings, brackets, fluid, and reservoirs, were determined using a plot of specific weight versus fluid power delivered given in Ref. C-3 and the relationship

$$\text{Line Weight} = \text{Specific Weight} \times \text{Horsepower Delivered} \times \text{Distance}$$

C.4 PUMPS

The required flow rate into each actuator in gal. per minute (GPM) was determined from the following equation taken from Ref. C-2.

$$GPM = \frac{1714 \times \text{Horsepower}}{\text{Pressure Differential}}$$

The local pressure differential is 67% of system total pressure or 2000 psi. A factor of 0.36 pounds per GPM was used to determine pump weight.

C.5 ACCESSORY POWER UNIT (APU)

The APU is made up primarily of a turbine and an O₂/H₂ energy source. The weight of the turbine was determined from a plot of turbine weight per horsepower versus horsepower given in Ref. C-2. To determine the turbine horsepower, the following efficiencies were assumed:

- Overall hydraulic pump efficiency, E_p, 40%
- Fluid transmission efficiency, E_t, 70%

The turbine output horsepower was then determined as follows:

$$\text{Turbine Horsepower} = \frac{\text{Horsepower Delivered}}{E_p \times E_t}$$

The O₂/H₂ energy source horsepower was determined assuming a turbine efficiency of 64% and

$$\text{Energy Source Horsepower} = \frac{\text{Turbine Output}}{\text{Turbine Efficiency}}$$

The weight of the energy source was determined from a conversion factor used on the weight of a 100 horsepower O₂/H₂ energy source system given in Ref. C-2. This conversion factor was presented in Ref. C-2 to obtain weights for energy source systems less than 100 horsepower because of the lack of a better method of determining energy source weight.

C.6 PROPELLANTS

The time/power relationship for the GDC/B-9U booster was determined from the Hydraulic System Duty Cycle given in Ref. C-4. Assuming

a propellant consumption rate of 1.36 pounds per horsepower-hour, the weight of propellants was determined as follows:

$$\text{Propellant Weight} = 1.36 \times \text{Time} \times \text{Energy Source Horsepower}$$

REFERENCES

- C-1. "Phase B Final Report, Volume II, Book 3, Booster Vehicle Definition," Report Number SD 71-114-2, Space Division North American Rockwell, 26 March 1971.
- C-2. Cannon, C. H., "Study of Criteria for Hydraulic and Pneumatic Systems for Space Vehicles, Part I," WADC TR 59-217, April 1959.
- C-3. "Hydraulic Transmission Line Optimization Study," Vickeus, Inc., 1957.
- C-4. "Flow Demand Analysis for Space Shuttle Booster Hydraulic System," Report Number 76-549-1-050, Convair Aerospace Division of General Dynamics, May 1971.

Appendix D

**COMPUTATION OF HINGE MOMENTS
IN THE ABSENCE OF HINGE MOMENT COEFFICIENTS**

Appendix D

In the determination of control surface weight penalties, it has been found that the structural and hydraulic system component weight are functions of hinge moments. However, the hinge moment coefficient data are usually not available until the final phase of test and design. A method to approximate the hinge moments by using available aerodynamic force coefficient data is derived as follows:

Define

- S_{ref} = reference area of the vehicle
- S_w = planform area of the wing
- $S_e (S_r)$ = planform area of the elevon (rudder)
- $\ell_e (\ell_r)$ = average chord of the elevon (rudder)
- $\bar{X} (\bar{Y})$ = distance from the elevon (rudder) hinge line to center-of-pressure location
- $\delta_e (\delta_r)$ = angle of deflection of elevon (rudder)
- q_∞ = dynamic pressure of free stream
- $C_N (C_Y)$ = normal (side) force coefficient

In general, the normal aerodynamic force, N , acting on the vehicle can be regarded as the sum of the normal aerodynamic force components caused by body ($N_{(b)}$), wind ($N_{(w)}$), and control surfaces ($N_{(\delta)}$)

$$N = N_{(b)} + N_{(w)} + N_{(\delta)}$$

The variation in normal force, ΔN , due to variation in control surface deflection angle, $\Delta \delta$, can be written as

$$\Delta N = \frac{\partial N}{\partial \delta} \Delta \delta \approx \left(\frac{\partial N_{(b)}}{\partial \delta} + \frac{\partial N_{(w)}}{\partial \delta} + \frac{\partial N_{(\delta)}}{\partial \delta} \right) \Delta \delta \quad (D-1)$$

Since $\partial N_{(b)} / \partial \delta$ and $\partial N_{(w)} / \partial \delta$ are usually negligible, then

$$\Delta N = \frac{\partial N}{\partial \delta} \Delta \delta \approx \frac{\partial N_{(\delta)}}{\partial \delta} \Delta \delta = C_{N_\delta} S_{ref} q_\infty \underline{\Delta \delta} \quad (D-2)$$

where $\Delta \delta$ is the variation in control surface deflection. This component of variation in normal force is acting on the center of pressure of the control surface and produce a variation in aerodynamic moment, which is acting on the hinge of the control surface. This variation in hinge moment, H_m , can be written as

$$\Delta H_m = \Delta N * \bar{X} \quad (D-3)$$

It can be assumed that ΔH_m is fairly close to the total variation in hinge moment. Then

$$\Delta H_m \approx C_{h_\delta} S_e q_\infty \Delta \delta l_e \approx C_{N_\delta} S_{ref} q_\infty \Delta \delta \bar{X} \quad (D-4)$$

or

$$C_{h_\delta} = C_{N_\delta} \frac{S_{ref} \bar{X}}{S_e l_e} \quad (D-5)$$

Therefore, the variation in elevon hinge moment, $\Delta H_{m_{\delta_e}}$, can be written as

$$\Delta H_{m_{\delta_e}} = C_{h_{\delta_e}} q_\infty S_e l_e \approx C_{N_{\delta_e}} q_\infty S_{ref} \bar{X} \quad (D-6)$$

Similarly, the variation in rudder hinge moment, $\Delta H_{m_{\delta_r}}$, can be written as

$$\Delta H_{m_{\delta_r}} = C_{h_{\delta_r}} q_\infty S_r l_r \approx C_{y_{\delta_r}} q_\infty S_{ref} \bar{Y} \quad (D-7)$$

Appendix E

PHASE PLANE DESIGN OF APS CONTROLLER

Appendix E

E.1 ASSUMPTIONS

The following assumptions are made:

1. Rotational and translational demand are determined separately.
2. Products of inertia are small in comparison with the moments of inertia.
3. Maximum preferred angular rates exist along each of the body axes.
4. Each of the body axes is basically controlled separately with no controller time delay but are relaxed at a later stage.
5. The minimum impulse bit and the thrust levels for attitude hold and maneuvering are given.

E.2 ORDER-OF-MAGNITUDE ANALYSIS

The rotational equations of motion for the reentry vehicle are:

$$\begin{aligned}
 \dot{\hat{I}_x P} &= (\hat{I}_y - \hat{I}_z) \hat{Q} \hat{R} + \hat{I}_{xz} (\hat{R} + \hat{P} \hat{Q}) + \hat{L} \\
 \dot{\hat{I}_y Q} &= (\hat{I}_z - \hat{I}_x) \hat{R} \hat{P} + \hat{I}_{xz} (\hat{R}^2 - \hat{P}^2) + \hat{M} \\
 \dot{\hat{I}_z R} &= (\hat{I}_x - \hat{I}_y) \hat{P} \hat{Q} + \hat{I}_{xz} (\hat{P} - \hat{Q} \hat{R}) + \hat{N}.
 \end{aligned} \tag{E-1}$$

For a typical booster, such as the GDC-B9U booster configuration, the following data are available.

$$I_x = 8.782 * 10^6, \quad I_y = 102.00 * 10^6, \quad I_z = 102.70 * 10^6, \quad I_{xz} = -1.38 * 10^{6*}$$

i.e., $\frac{I_y - I_z}{I_x} \sim O(10^{-1}), \quad \frac{I_z - I_x}{I_y} \sim O(10^0), \quad \frac{I_x - I_y}{I_z} \sim O(10^0)$

$$\frac{I_{xz}}{I_x} \sim O(10^{-1}), \quad \frac{I_{xz}}{I_y} \sim O(10^{-2}), \quad \frac{I_{xz}}{I_z} \sim O(10^{-2}).$$

The preferred angular rates are 2 to 5 deg/sec (0.35 0.0875 rad/sec), i.e., $O(10^{-2})$. The angular accelerations are in the neighborhood of 0.5 deg/sec² (0.009 rad/sec²); i.e., $O(10^{-2})$. The aerodynamic disturbance torques are negligibly small. Based on these given data, an order-of-magnitude analysis of the rotational equations of motion is performed:

$$\dot{P} - \left[\left(\frac{I_{xz}}{I_x} \right) (Q) \right] P = \left[\left(\frac{I_y - I_z}{I_x} \right) (Q) (R) \right] + \left[\left(\frac{I_{xz}}{I_x} \right) (\dot{R}) \right] + \frac{\hat{L}(p)}{I_x}$$

or $O(10^{-2}) \quad O(10^{-1-2-2}) \quad O(10^{-1-2-2}) \quad O(10^{-1-2}) \quad O(10^{-2})$

$$O(10^{-2}) \quad O(10^{-5}) \quad O(10^{-5}) \quad O(10^{-3}) \quad O(10^{-2})$$

$$\dot{Q} = \left[\left(\frac{I_z - I_x}{I_y} \right) (R)(P) \right] + \left[\left(\frac{I_{xz}}{I_y} \right) (R^2 - P^2) \right] + \frac{\hat{M}(p)}{I_y}$$

$$O(10^{-2}) \quad O(10^{0-2-2}) \quad O(10^{-2-4}) \quad O(10^{-2})$$

or $O(10^{-2}) \quad O(10^{-4}) \quad O(10^{-6}) \quad O(10^{-2})$

* slug/ft².

$$\dot{\hat{R}} + \left[\left(\frac{I_{xz}}{I_z} \right) (\hat{Q}) \right] \hat{R} = \left[\left(\frac{I_x - I_y}{I_z} \right) (\hat{P}) (\hat{Q}) \right] + \left[\left(\frac{I_{xz}}{I_z} \right) (\hat{P}) \right] + \frac{\dot{\hat{N}}(p)}{I_z}$$

$$O(10^{-2}) \quad O(10^{-2-2-2}) \quad O(10^{0-2-2}) \quad O(10^{-2-2}) \quad O(10^{-2})$$

or

$$O(10^{-2}) \quad O(10^{-6}) \quad O(10^{-4}) \quad O(10^{-4}) \quad O(10^{-2})$$

It is clearly seen that, by neglecting the higher order terms, the rotational equations of motion reduce to:

$$\dot{\hat{P}} = \frac{\dot{\hat{L}}(p)}{I_x}, \quad \dot{\hat{Q}} = \frac{\dot{\hat{M}}(p)}{I_y}, \quad \dot{\hat{R}} = \frac{\dot{\hat{N}}(p)}{I_z} \quad (E-2)$$

E.3 PHASE PLANE ANALYSIS

All three equations have similar form. Therefore, only one of the equations needs analyzing. Let $P = \theta$ and $\dot{P} = \ddot{\theta}$, and the command is the constant angular displacement, θ_c , only. Then the error and error rates in angle can be written as

$$\epsilon_1 = \theta_c - \theta, \quad \epsilon_2 = -\dot{\theta}.$$

The rotational equation of motion for the x-body axis can be rewritten as:

$$\left\{ \begin{array}{l} \dot{\epsilon}_1 = \epsilon_2 \\ \dot{\epsilon}_2 = \pm \left| \frac{L}{I_x} \right| \end{array} \right\} \quad (E-3)$$

where L is defined as the multi-level control moment produced by firing various total number of roll APS thrusters.

The $\epsilon_1 - \epsilon_2$ phase plane solution for constant I_x/L is

$$\epsilon_1 = \pm \left| \frac{I_x}{L} \right| \frac{\epsilon_2^2}{2} + \epsilon_1(0) \mp \left| \frac{I_x}{L} \right| \frac{\epsilon_2^2(0)}{2} \quad (\text{E-4})$$

where $\epsilon_1(0)$ and $\epsilon_2(0)$ are the initial conditions in error and error rates. The trajectories for various L levels and with apex at origin are given in Fig. 4.2-3.

E.4 OPTIMUM SWITCHING

The problem of Eq. (E-3) for multi-level L is essentially a digitized relay-servo problem. It is known that the location of the switching line is critical in determining the nature of the system response. In order to develop the concept of nonlinear optimization by means of switching line location, a phase plane trajectory analysis is needed. Let the constraints be: (1) limited torque; and (2) optimum in the sense of bringing the system to rest (zero error and error rate) at the origin in the minimum period of time and with no unduly high angular velocity (i.e., no acceleration beyond the preferred upper limit angular rate). This will involve two or more instants when the torque is reversed, changed in torque level, or removed. In general, the system is initially accelerated toward some point, at this point the torque is reversed to decelerate the system and bring it to rest, and finally, the decelerating torque is removed when the system reaches equilibrium. For a single level L , the zero trajectories, which go through the origin in the phase plane, are seen to correspond to the "optimum" torque reversal or switching lines as shown in Fig. E-1. It is evident that the system is not accelerated for angular rates beyond certain preferred limits.

To achieve any of these optimum responses, a controller is required which detects the state of the system relative to zero trajectory and maximum desired rate, and then switches when the two states coincide. The optimum switching curves are two segments of the parabolas given by

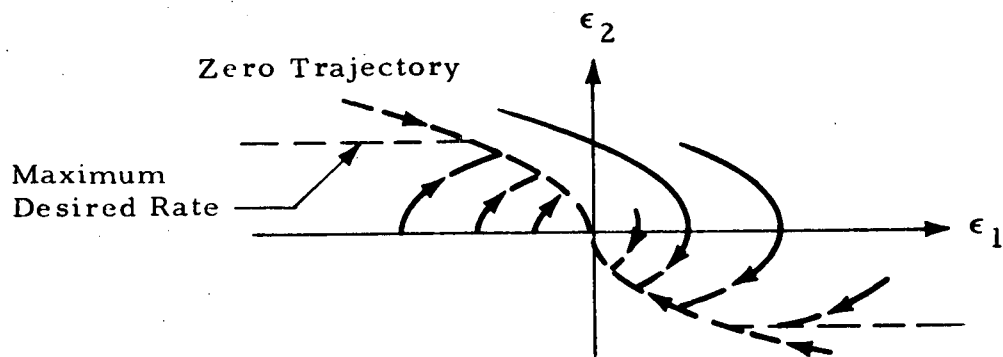


Fig. E-1 - Optimum Switching Criterion

$$\epsilon_1 = \pm \left| \frac{I_x}{2L} \right| \epsilon_2^2$$

and two segments of horizontal lines given by

$$\epsilon_2 = \epsilon_{2S} \quad \text{for} \quad \epsilon_1 \leq - \left| \frac{I_x}{2L} \right| \epsilon_{2S}^2$$

$$\epsilon_2 = -\epsilon_{2S} \quad \text{for} \quad \epsilon_1 \geq \left| \frac{I_x}{2L} \right| \epsilon_{2S}^2$$

where ϵ_{2S} is the maximum desired angular rate. Since the zero trajectories reach the origin only from the second and fourth quadrants, the switching lines are given by

$$\begin{aligned} \epsilon_1 &= - \left| \frac{I_x}{2L} \right| |\epsilon_2| \epsilon_2 \\ \epsilon_2 &= \epsilon_{2S} \quad \text{for} \quad \epsilon_1 \leq - \left| \frac{I_x}{2L} \right| \epsilon_{2S}^2 \\ \epsilon_2 &= -\epsilon_{2S} \quad \text{for} \quad \epsilon_1 \geq \left| \frac{I_x}{2L} \right| \epsilon_{2S}^2 \end{aligned} \tag{E-5}$$

The zero trajectories divide the phase plane into two sections. The control torque must be negative or zero above the boundary and positive or zero below it to ensure convergence of the error and error rate to zero. The analysis for a multi-level L controlled system is basically the same. An expansion to a two-level L controlled system is briefly presented in Section 4.

E.5 OPTIMUM SWITCHING IN THE PRESENCE OF TIME DELAY, HYSTERESIS AND CONTACT SPACE

The optimum response switching lines are valid for only a very restricted number of inputs. Two categories of imperfection may arise:

1. Errors, miscalibrations, and finite time delays in the computing elements required to generate the optimum switching line, sense the state of the system and switch the torque at the proper instant;
2. The effects of system operation for inputs or with loads other than those for which the optimum switching line was derived.

The slight nonoptimum switching may have the effect of permitting the state of the system to overtravel the switching line, reverse, overtravel again, etc. The state of the system then approaches equilibrium while executing a high frequency oscillation in the vicinity of the switching line. As an example, the effect of a time delay is shown in Fig. E-2. In this case, the actual switching line is a parabola of the same shape as the optimum switching line but displaced from it in both the ϵ_1 and ϵ_2 directions. From this example it may be seen that if the computer switches late, perhaps due to errors in the mechanization, the control system performs wasteful firings.

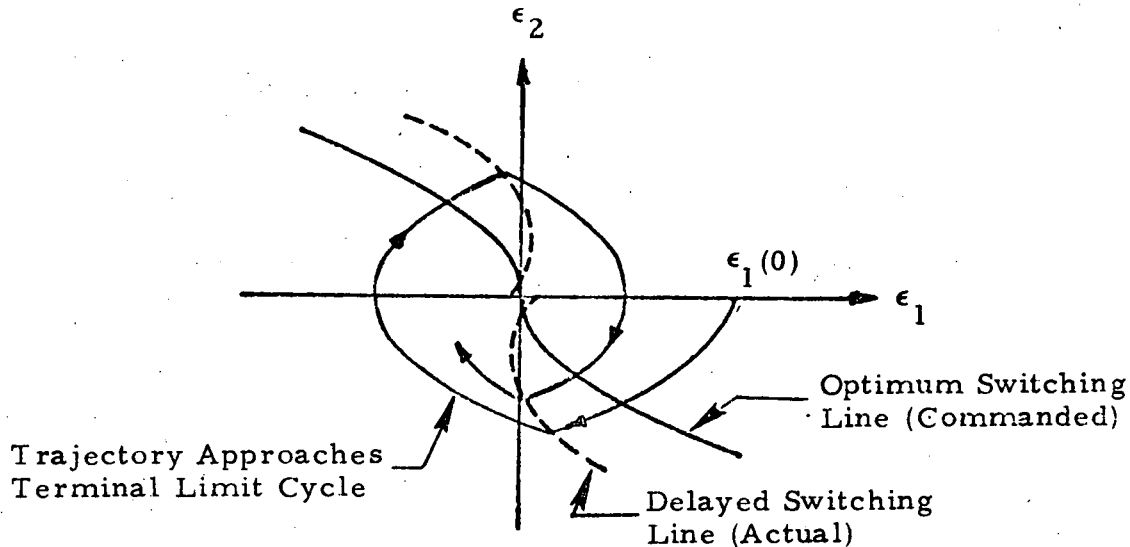


Fig. E-2 - Phase Plane Description of How System Time Delays Affect the Control Logic Switching

E.6 THE EFFECT OF TIME DELAY ON THE OPTIMUM SWITCHING LINE OF A SIMPLE PURE INERTIA LOAD SERVO

The equation of the parabolic trajectory in the lower half plane following a step input is

$$\epsilon_2^2 = -\frac{2L}{I} (\epsilon_1 - \epsilon_1(0))$$

In the phase plane, $\epsilon_2 = d\epsilon_1 / dt$ or $dt = d\epsilon_1 / \epsilon_2$. Therefore, in the lower half plane

$$t = \int_{\epsilon_1(0)}^{\epsilon_1} \frac{d\epsilon_1}{\epsilon_2} = \sqrt{-\frac{2I}{L} (\epsilon_1 - \epsilon_1(0))}$$

or

$$t^2 = -\frac{2I_x}{L} (\epsilon_1 - \epsilon_1(0))$$

rearranging:

$$\epsilon_1 = -\frac{Lt^2}{2I_x} + \epsilon_1(0) \quad \text{and} \quad \epsilon_2 = -\frac{Lt}{I}$$

Let $t = (t)_{sw}$, when $\epsilon_1 = (\epsilon_1)_{sw}$ and $\epsilon_2 = (\epsilon_2)_{sw}$, the switching line is

$$(\epsilon_1)_{sw} = \frac{I_x}{2L} (\epsilon_2)_{sw}^2 \quad (E-6)$$

then

$$(\epsilon_1)_{sw} = -\frac{L}{2I_x} (t)_{sw}^2 + \epsilon_1(0)$$

$$(\epsilon_2)_{sw} = -\frac{Lt_{sw}}{I_x}$$

Now the time, $(t')_{sw}$, at which the torque reversal actually takes place is delayed beyond the time $(t)_{sw}$, by the time delay, τ , so that the delayed switching line occurs at

$$(\epsilon'_2)_{sw} = -\frac{L(t')_{sw}}{I_x} = \epsilon_2_{sw} - \frac{L\tau}{I_x}$$

$$(\epsilon'_2)_{sw} = -\frac{L(t')_{sw}^2}{2I_x} + \epsilon_1(0) = (\epsilon_1)_{sw} + \left[(\epsilon_2)'_{sw} + \frac{L\tau^2}{2I_x} \right]$$

or

$$(\epsilon_2)_{sw} = \epsilon'_2_{sw} + \frac{L\tau}{I} \quad (E-7)$$

$$(\epsilon_1)_{sw} = \epsilon'_1_{sw} - \left[(\epsilon'_2)_{sw} + \frac{L\tau^2}{2I_x} \right] \quad (E-8)$$

Substituting into Eq. (E-6)

$$(\epsilon_1)'_{sw} - \left[(\epsilon'_2)_{sw} + \frac{L\tau^2}{I_x} \right] = \frac{I_x}{2L} \left[(\epsilon_2)'_{sw} + \frac{L\tau}{I_x} \right]$$

Substituting into Eq. (E-6)

$$(\epsilon_1'')_{sw} + \left[(\epsilon_2'')_{sw} \tau - \frac{L\tau^2}{2I_x} \right] = \frac{I_x}{2L} \left[(\epsilon_2'')_{sw} - \frac{L\tau}{I_x} \right]^2$$

rearranging

$$\left[(\epsilon_1'')_{sw} - \frac{L\tau^2}{I_x} \right] = \frac{I_x}{2L} \left[(\epsilon_2'')_{sw} - 2 \frac{L\tau}{I_x} \right]^2 \quad (E-9)$$

which is the trajectory of the lower advanced switching line with apex occurring at $(\epsilon_1'')_{sw} = -(L\tau^2/I)$ and $(\epsilon_2'')_{sw} = 2(L\tau/I)$. Similarly the trajectory of the upper advanced switching line is

$$\left[(\epsilon_1'')_{sw} - \frac{L\tau^2}{I} \right] = - \frac{I_x}{2L} \left[(\epsilon_2'')_{sw} + 2 \left(\frac{L\tau}{I} \right) \right]^2 \quad (E-10)$$

Its apex occurs at $(\epsilon_1'')_{sw} = -(L\tau^2/I)$ and $(\epsilon_2'')_{sw} = -2(L\tau/I)$. These advanced switching lines are in fact the commanded switching lines in the presence of a time delay, as shown in Fig. E-3.

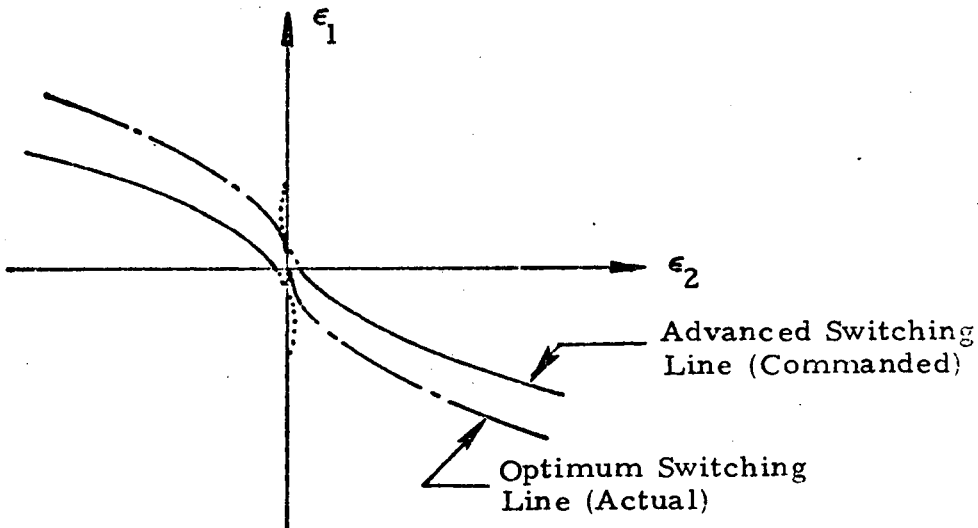


Fig. E-3 - Phase Plane Representation of Advanced Switching Lines to Compensate for Time Delays

rearranging

$$\left[(\epsilon'_1)_{sw} + \frac{L\tau^2}{I_x} \right] = \frac{I_x}{2L} \left[(\epsilon'_2)_{sw} + 2\left(\frac{L\tau}{I}\right) \right]^2$$

which is the trajectory of the lower delayed switching line with apex occurring at $(\epsilon'_1)_{sw} = - L\tau^2/I$ and $(\epsilon'_2)_{sw} = - 2(L\tau/I)$. Similarly the trajectory of the upper delayed switching line is

$$\left[(\epsilon'_1)_{sw} - \frac{L\tau^2}{I_x} \right] = - \frac{I_x}{2L} \left[(\epsilon'_2)_{sw} - 2\left(\frac{L\tau}{I_x}\right) \right]^2$$

Its apex occurs at $(\epsilon'_1)_{sw} = - L\tau^2/2$ and $(\epsilon'_2)_{sw} = 2(L\tau/I_x)$.

E.7 OPTIMUM COMMANDED SWITCHING LINE IN THE PRESENCE OF A CONSTANT TIME DELAY

In order that the effect of a constant time delay on the optimum switching line designed for zero time delay be compensated, it is necessary to advance the switching time by an amount exactly equal to the time delay. Let the time, $(t'')_{sw}$, at which the torque reversal actually takes place, be advanced ahead of the time $(t)_{sw}$ by the time, $-\tau$, then the advanced switching line occurs at

$$(\epsilon''_2)_{sw} = - \frac{L(t'')_{sw}}{I_x} = \epsilon_{2sw} + \frac{L\tau}{I_x}$$

$$(\epsilon''_1)_{sw} = - \frac{L(t'')_{sw}}{2I_x} + \epsilon_{1(0)} = (\epsilon'_1)_{sw} + \left[-(\epsilon''_2)_{sw} \tau + \frac{L\tau^2}{2I_x} \right]$$

or

$$(\epsilon_2)_{sw} = (\epsilon''_2)_{sw} - \frac{L\tau}{I_x}$$

$$(\epsilon_1)_{sw} = (\epsilon''_1)_{sw} + \left[(\epsilon''_2)_{sw} \tau - \frac{L\tau^2}{2I_x} \right]$$

E.8 IMPLEMENTATION OF THE PROGRAMMED CONTROLLERS

For the purpose of implementing the optimum switching, the phase plane is divided into three zones as shown in Fig. E-4.

1. A minimum impulse bit dead zone which is defined by the region that no combination of jet firing can provide worthwhile improvement.
2. Sampling period dead zone which is defined by the region that no combination of jet firings, each for a complete sampling period can provide worthwhile improvement; and
3. The remainder of the phase plane.

The tolerable dead zone for a shuttle reentry vehicle must be greater than minimum impulse bit dead zone and is, in general, much greater than the sample period dead zone.

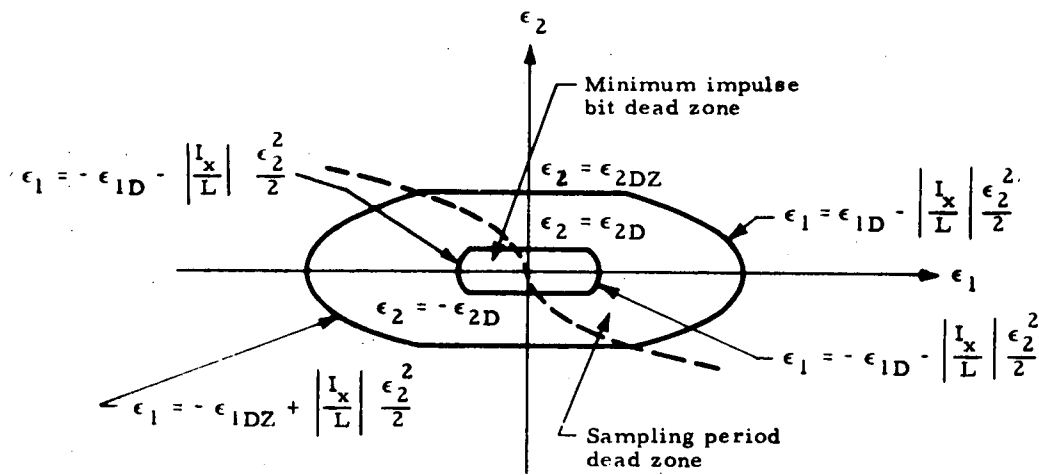


Fig. E-4 - Sampling Period and Minimum Impulse Bit Dead Zones

Let the minimum firing time be T_m , then the minimum impulse bit dead zone is confined by the following curves:

$$\epsilon_2 = \left| \frac{L}{I_x} \right| * T_m = \epsilon_{2D}$$

$$\epsilon_2 = - \left| \frac{L}{I_x} \right| * T_m = -\epsilon_{2D}$$

$$\epsilon_1 = \left| \frac{I_x}{L} \right| \frac{\epsilon_2^2}{2} - \left| \frac{L}{I_x} \right| * T_m * T_s = \left| \frac{I_x}{L} \right| \frac{\epsilon_2^2}{2} - \epsilon_{1D}$$

and

$$\epsilon_1 = - \left| \frac{I_x}{L} \right| \frac{\epsilon_2^2}{2} + \left| \frac{L}{I_x} \right| * T_m * T_s = - \left| \frac{I_x}{L} \right| \frac{\epsilon_2^2}{2} + \epsilon_{1D} \quad (E-11)$$

Let the sampling period time be T_s , then the sampling period dead zone is confined by the following curves:

$$\epsilon_2 = \left| \frac{L}{I_x} \right| * T_s = \epsilon_{2D}$$

$$\epsilon_2 = - \left| \frac{L}{I_x} \right| * T_s = -\epsilon_{2DZ} \quad (E-12)$$

$$\epsilon_1 = \left| \frac{I_x}{L} \right| \frac{\epsilon_2^2}{2} - \left| \frac{L}{I_x} \right| T_s^2 = \left| \frac{I_x}{L} \right| \frac{\epsilon_2^2}{2} - \epsilon_{1DZ}$$

$$\epsilon_1 = - \left| \frac{I_x}{L} \right| \frac{\epsilon_2^2}{2} + \left| \frac{L}{I_x} \right| T_s^2 = - \left| \frac{I_x}{L} \right| \frac{\epsilon_2^2}{2} + \epsilon_{1DZ}$$

Obviously the sampling period dead zone contains the minimum impulse bit dead zone. Two control laws are devised:

1. The raw control law is used to bring any point outside the sampling period dead zone on the phase plane into the sampling period dead zone in the minimum period of time. The jets are either firing for the complete sampling period or are not firing at all.

2. The fine control law is used to bring any point on the phase plane, which is inside the sampling period dead zone, into the minimum impulse bit dead zone in the suboptimal manner with the most efficient jet firing sequence.

An example for the implementation of single level control torque programmed controller is given here; however, it must be pointed out that the extension of the multi-level control torque case can be easily made.

E.9 RAW CONTROL LAW

Since the jets are either firing for the complete sample period or not firing at all, there exist switching zones, which will control the system in the optimum manner and guide the system to the sampling period dead zone. These zones as shown in Fig. E-5 are defined by the following curves:

For $\epsilon_2 \geq 0$, the zone confined by

$$\epsilon_1 = - \left| \frac{I_x}{L} \right| \frac{\epsilon_2^2}{2} - \epsilon_{1DZ} \quad \text{and} \quad \epsilon_1 = - \left| \frac{I_x}{L} \right| \frac{\epsilon_2^2}{2} \quad (\text{E-13})$$

and the zone confined by

$$\begin{cases} \epsilon_2 = \epsilon_{2S} - \epsilon_{2DZ} \\ \epsilon_1 \leq - \left| \frac{I_x}{L} \right| \frac{\epsilon_{2S}^2}{2} \end{cases} \quad \text{and} \quad \begin{cases} \epsilon_2 = \epsilon_{2S} \\ \epsilon_1 \leq - \left| \frac{I_x}{L} \right| \frac{\epsilon_{2S}^2}{2} \end{cases} \quad (\text{E-14})$$

For $\epsilon_2 \leq 0$, the zone confined by

$$\epsilon_1 = \left| \frac{I_x}{L} \right| \frac{\epsilon_2^2}{2} + \epsilon_{1DZ} \quad \text{and} \quad \epsilon_1 = \left| \frac{I_x}{L} \right| \frac{\epsilon_2^2}{2} \quad (\text{E-15})$$

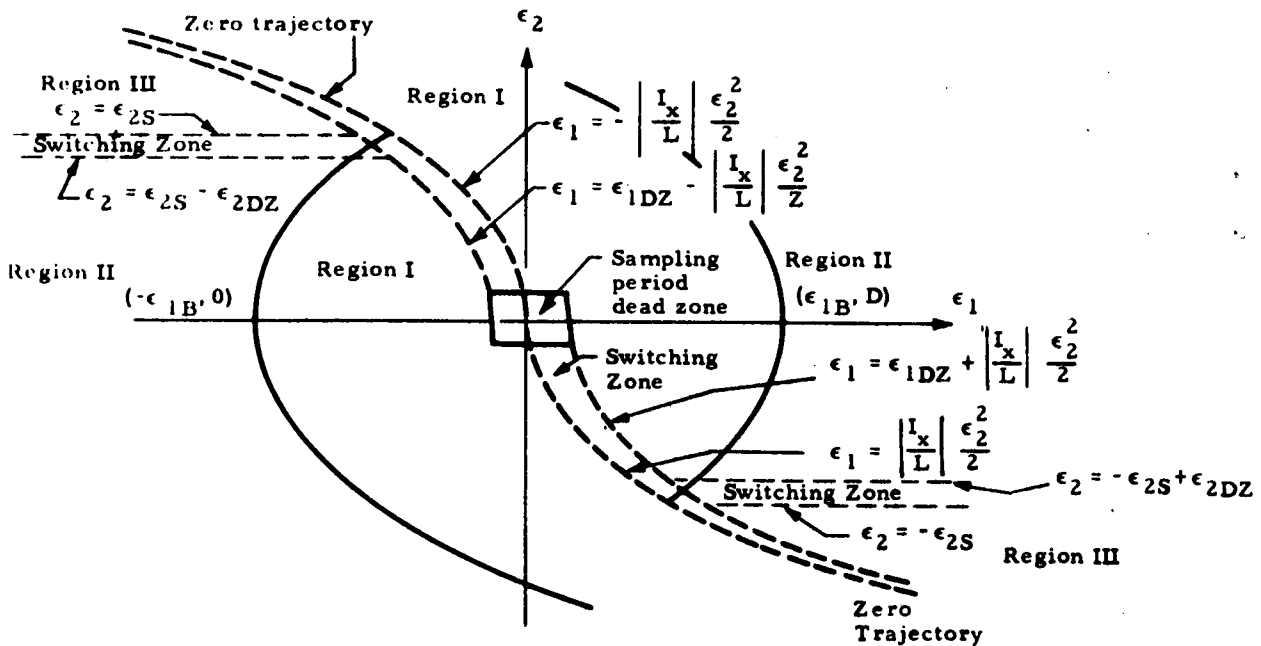


Fig. E-5 - Switching Zone for Raw Control Law

and the zone confined by

$$\left\{ \begin{array}{l} \epsilon_2 = -\epsilon_{2S} + \epsilon_{2DZ} \\ \epsilon_1 \geq \left|\frac{I_x}{L}\right| \frac{\epsilon_{2S}^2}{2} \end{array} \right\} \text{ and } \left\{ \begin{array}{l} \epsilon_2 = -\epsilon_{2S} \\ \epsilon_1 \geq \left|\frac{I_x}{L}\right| \frac{\epsilon_{2S}^2}{2} \end{array} \right\} \quad (E-16)$$

Based on the characteristics of switching, each section (divided by the zero trajectories) of the phase plane can be subdivided into three regions as shown in Fig. E-5. Region I is bounded by zero trajectories and parabolas passing through

$$\left(\left| \frac{I_x}{L} \right| \frac{\epsilon_{2S}^2}{2}, -\epsilon_{2S} \right) \text{ or } \left(- \left| \frac{I_x}{L} \right| \frac{\epsilon_{2S}^2}{2}, \epsilon_{2S} \right)$$

i.e.,

$$\epsilon_1 \leq - \left| \frac{I_x}{L} \right| \frac{\epsilon_2^2}{2} + \epsilon_{1B} \quad \text{and zero trajectories} \quad (\text{E-17a})$$

$$\epsilon_1 \geq - \left| \frac{I_x}{L} \right| \frac{\epsilon_2^2}{2} - \epsilon_{1B} \quad \text{and zero trajectories} \quad (\text{E-17b})$$

where

$$\epsilon_{1B} = \left| \frac{I_x}{L} \right| \epsilon_{2S}^2.$$

Within this region, the system is first accelerated to the switching zone bounded by the parabolas then decelerated to the sampling period dead zone. Region II is outside the parabola passing through

$$\left| \frac{I_x}{L} \right| \frac{\epsilon_{2S}^2}{2}, -\epsilon_{2S} \quad \text{or} \quad - \left| \frac{I_x}{L} \right| \frac{\epsilon_{2S}^2}{2}, \epsilon_{2S} \quad \text{and bounded by } |\epsilon_2| = \epsilon_{2S}$$

i.e., $\epsilon_1 \geq - \left| \frac{I_x}{L} \right| \frac{\epsilon_2^2}{2} + \epsilon_{1B} \quad \text{and} \quad \epsilon_2 \geq -\epsilon_{2S}$ (E-18a)

or

$$\epsilon_1 \leq - \left| \frac{I_x}{L} \right| \frac{\epsilon_2^2}{2} - \epsilon_{1B} \quad \text{and} \quad \epsilon_2 \leq \epsilon_{2S} \quad (\text{E-18b})$$

The system is first accelerated toward the switching zone bounded by straight lines, once in this zone, the system is co-acting toward the switching zone bounded by parabolas. Finally, the system is decelerated toward the sampling period dead zone. Region III is bounded by

$$\epsilon_1 \geq - \left| \frac{I_x}{L} \right| \frac{\epsilon_2^2}{2} \quad \text{and} \quad \epsilon_2 \leq \epsilon_{2S} \quad (\text{E-19a})$$

or

$$\epsilon_1 \leq - \left| \frac{I_x}{L} \right| \frac{\epsilon_2^2}{2} \quad \text{and} \quad \epsilon_2 \geq \epsilon_{2S} \quad (\text{E-19b})$$

The pure analog implementation of the raw control law can be easily obtained because all the switching lines are expressed by algebraic equations in terms of vehicle rotational state variables. A digital program has been written for the raw control law.

E.10 FINE CONTROL LAW

Once the error and error rate of the system is within the sampling period dead zone, fine control law is used to guide the state of the system into the minimum impulse bit dead zone. No definite rules govern the combination of jet firing sequence and time. However, as a rule of thumb, if at the sampling time the state of the system is just outside of the minimum impulse bit dead zone or near the ϵ_1 -axis, minimum impulse bit is used for control, and if at the sampling time the state of the system is near the boundaries of the sampling period dead zone the jet firing for a complete sampling period is used for control.

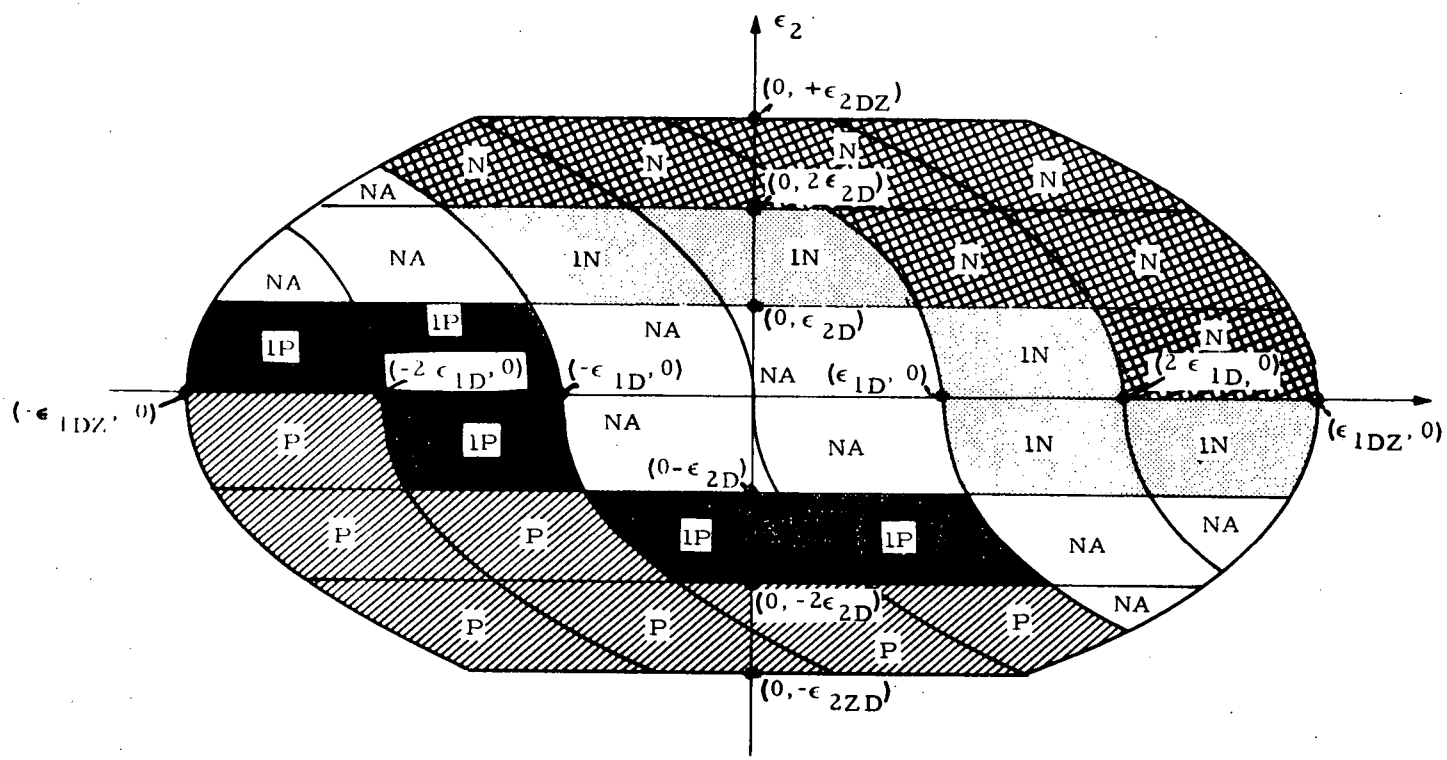
Obviously, the optimal firing logic depends on the sizes of the minimum impulse bit dead zone and the sampling period dead zone. The latter dead zone can then be subdivided into five regions with each region requiring a different control effort. For $T_s = 3 T_m$, the regions and their control effort are given in Fig. E-6. The boundaries of these regions are parabolas and horizontal lines. A digital computer has been written which implements this fine control law.

E.11 IMPLEMENTATION OF THE ACTUAL OPTIMUM SWITCHING LINE IN THE PRESENCE OF A TIME DELAY

For $\tau = 0$, Eqs. (E-9) and (E-10) can be reduced to equations for optimum switching line without time delay

$$(\epsilon_1'')_{sw} = \frac{I_x}{2L} \left[(\epsilon_2'')_{sw} \right]^2 \quad \text{for the lower switching line}$$

$$(\epsilon_1'')_{sw} = -\frac{I_x}{2L} \left[(\epsilon_2'')_{sw} \right]^2 \quad \text{for the upper switching line}$$



1P = 1 positive pulse

1N = 1 negative pulse

P = positive thrust for all T_s

N = negative thrust for 1 T_s

NA = zero thrust for T_s

Fig. E-6 - Optimal Firing Logic for Fine Control Law
(assumed sample period = 3' Tm)

or

$$(\epsilon_1'')_{sw} = -\frac{I_x}{2L} (\epsilon_2'')_{sw} \left[(\epsilon_2'')_{sw} \right] \quad (E-20)$$

Since the implementation of Eqs. (E-9) and (E-10) are considerably different from that of Eq. (E-20), it requires a major reprogramming effort. However, for most cases, the time delay and L/I_x are fairly small. Eqs. (E-7) and (E-8) can be approximated by:

$$(\epsilon_2)_{sw} \approx (\epsilon_2'')_{sw}$$

$$(\epsilon_1)_{sw} \approx (\epsilon_1'')_{sw} + (\epsilon_2'')_{sw} \tau$$

The approximated switching lines can be written as

$$(\epsilon_1'')_{sw} + (\epsilon_2'')_{sw} \tau \approx -\frac{I_x}{2L} (\epsilon_2'')_{sw} \left| (\epsilon_2'')_{sw} \right|$$

which has the same form as Eq. (E-20). The only change in the program for raw control law is to replace (ϵ_1) by $\epsilon_1 + \epsilon_2 \tau$. For fine control law, a complete new design is required but the general guideline remains unchanged.

Appendix F

**TIME-VARYING COEFFICIENTS GENERATED
BY DATA PREPROCESSOR PROGRAMS**

Appendix F

The time-varying coefficients for the 6-D EOM (Eqs. (4.1-16) through (4.1-20)) of Section 4.1 were computed with an IBM 7094 digital computer program. This program reduces the raw aerodynamic, configuration trajectory data into time-varying coefficients suitable for use on the analog as well as input data for the Control Gain Synthesis digital computer program. A simplified block diagram of the program is shown in Fig. F-1. Plots of some of the input trajectory and aerodynamic data and all the time-varying coefficients for the 6-D EOM are included. Approximations are straight-line segments between specified computation points.

The input data used in this computation were derived mainly from the GDC-B9U Booster and complimented by the GDC-B9T Booster.

Some of the fast data transfer analog strip chart plots of the time-varying coefficients are shown on page F-25.

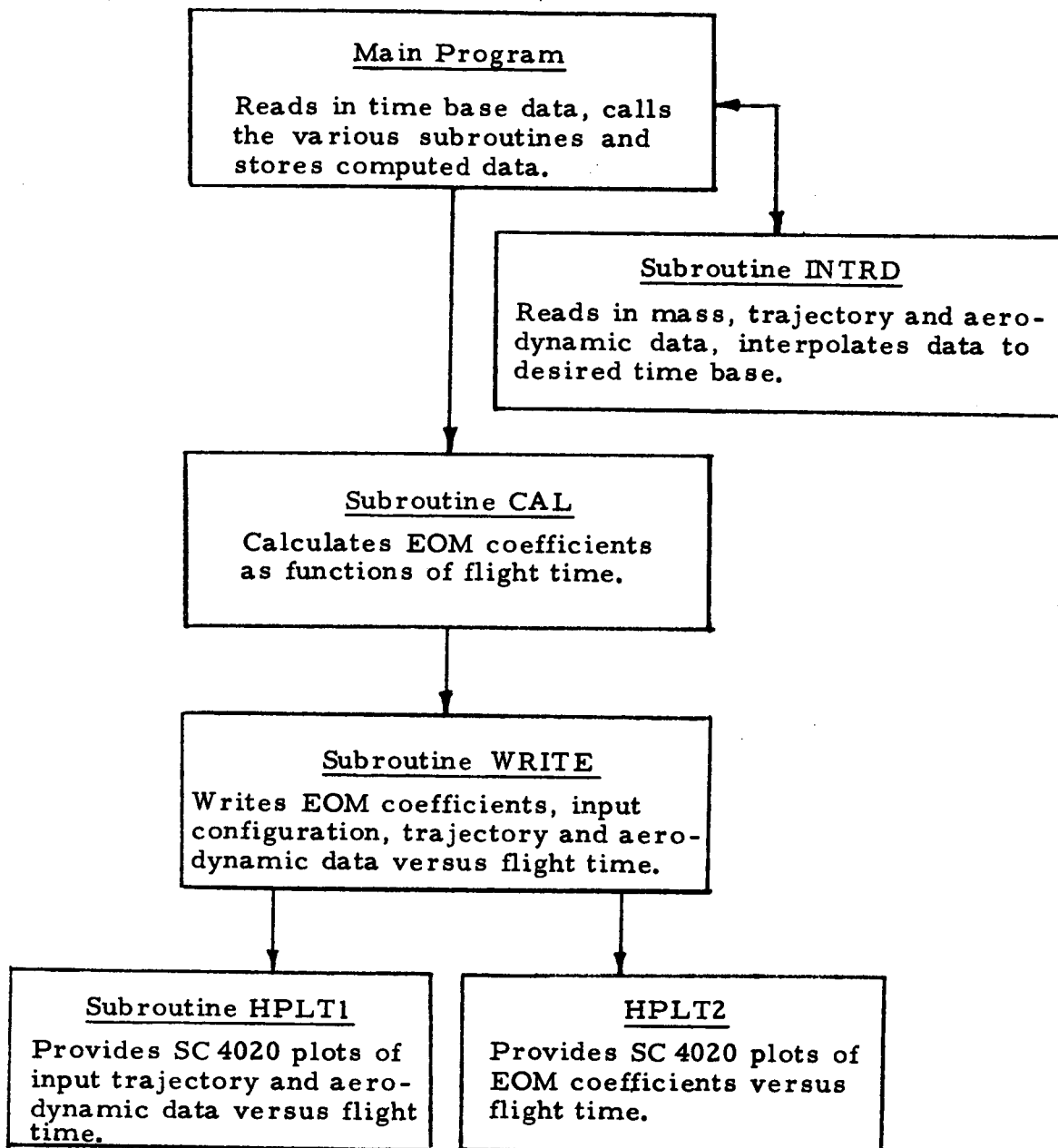
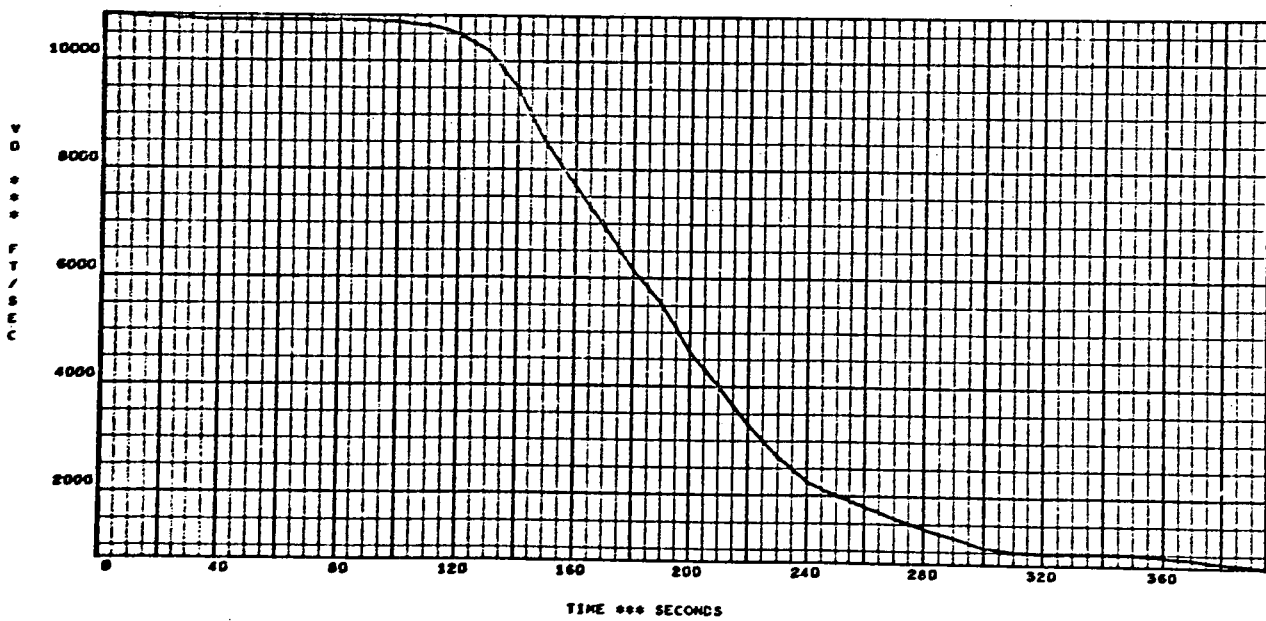
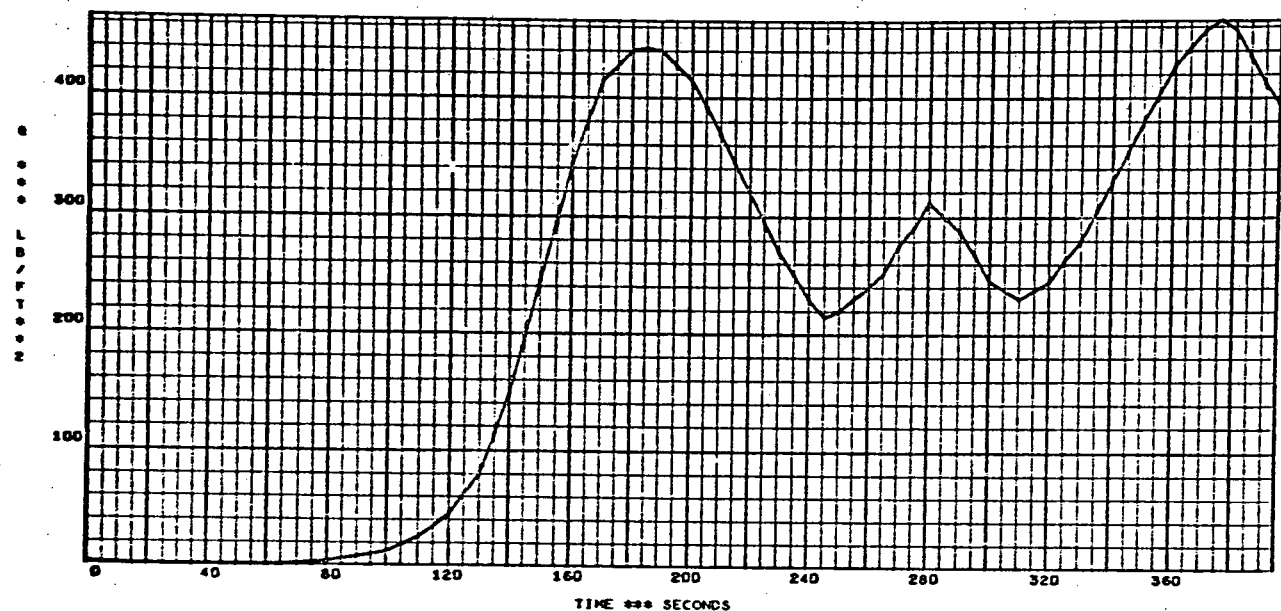


Fig. F-1 - Flow Chart of IBM 7094 Digital Data Program to Calculate and Plot Shuttle EOM Coefficients

SHUTTLE REENTRY

JOB NO 422500

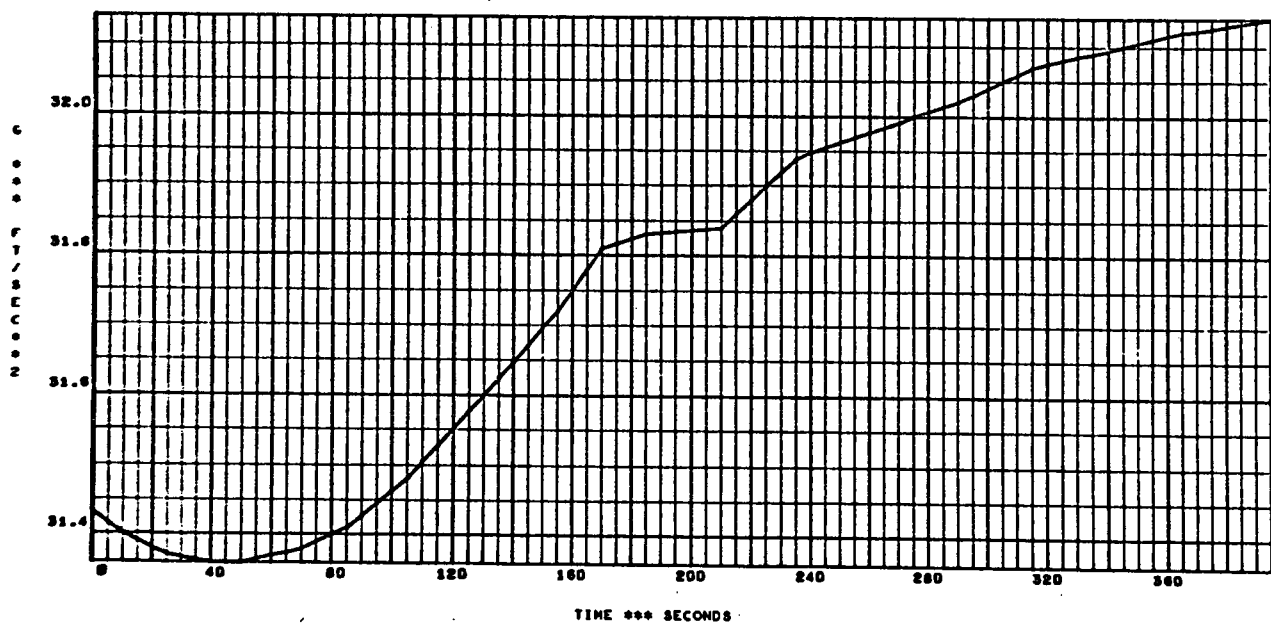
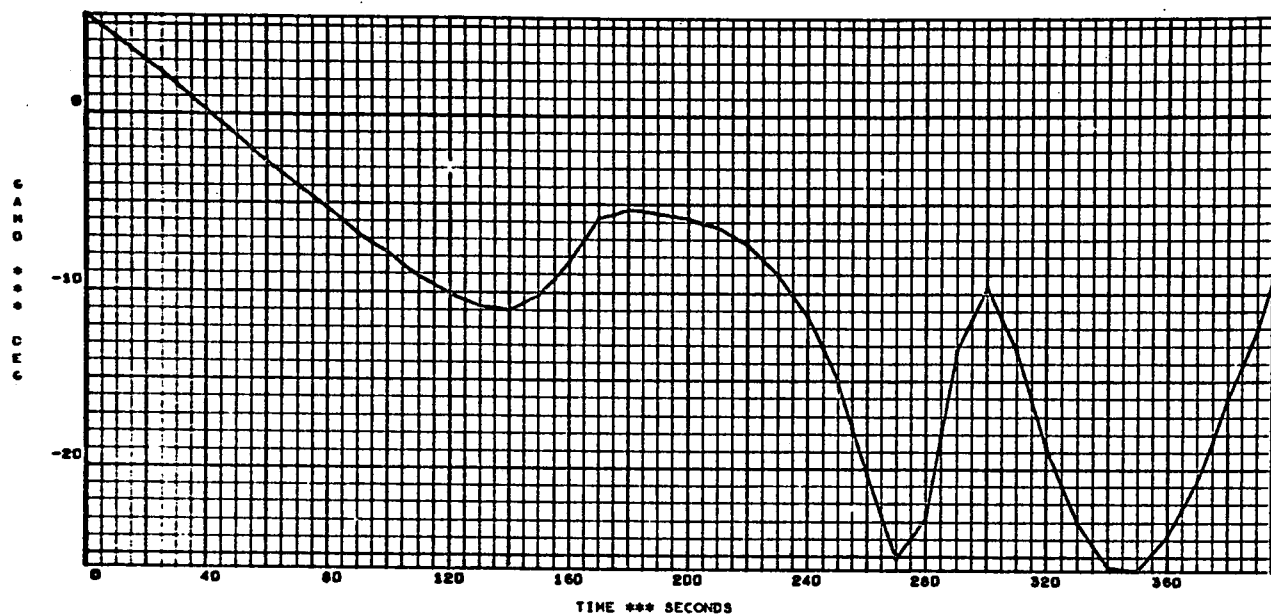
PAGE 1





SHUTTLE REENTRY

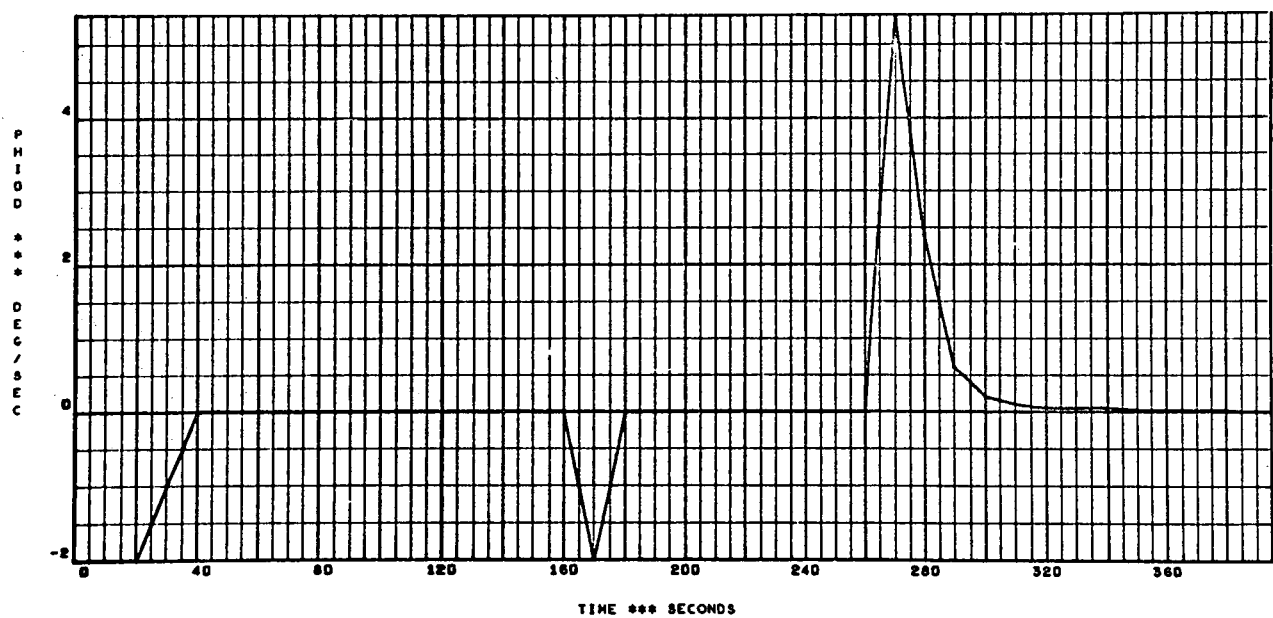
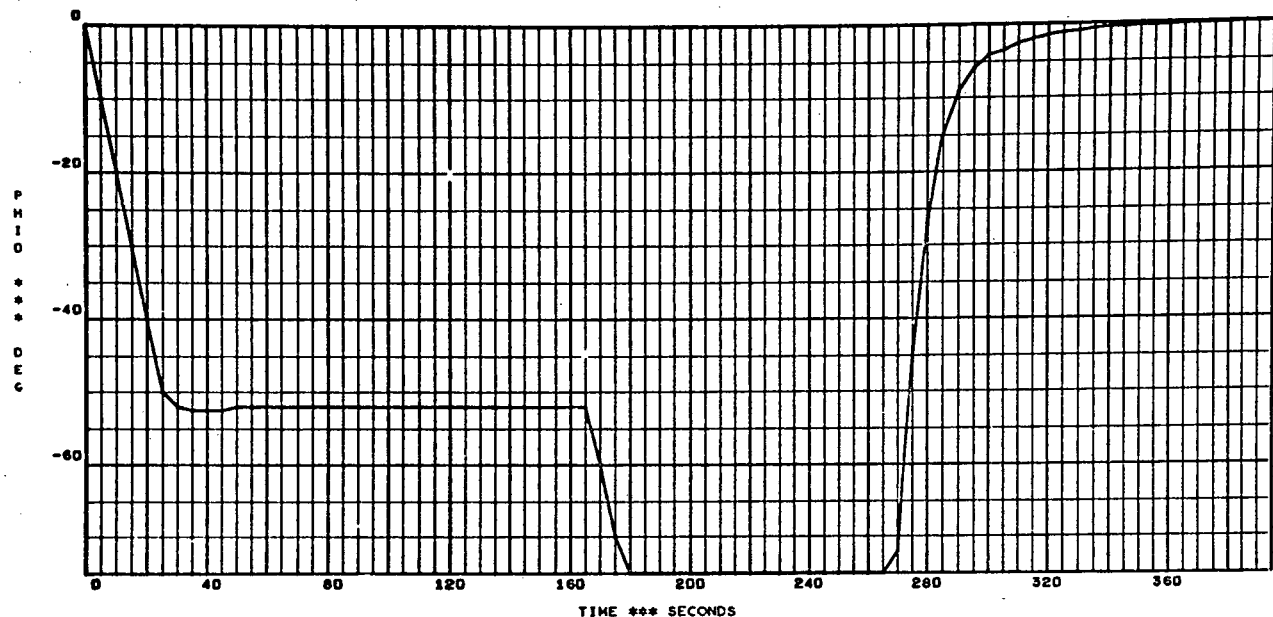
JOB NO 422500 PAGE 2





JOB NO 422500 PAGE 4

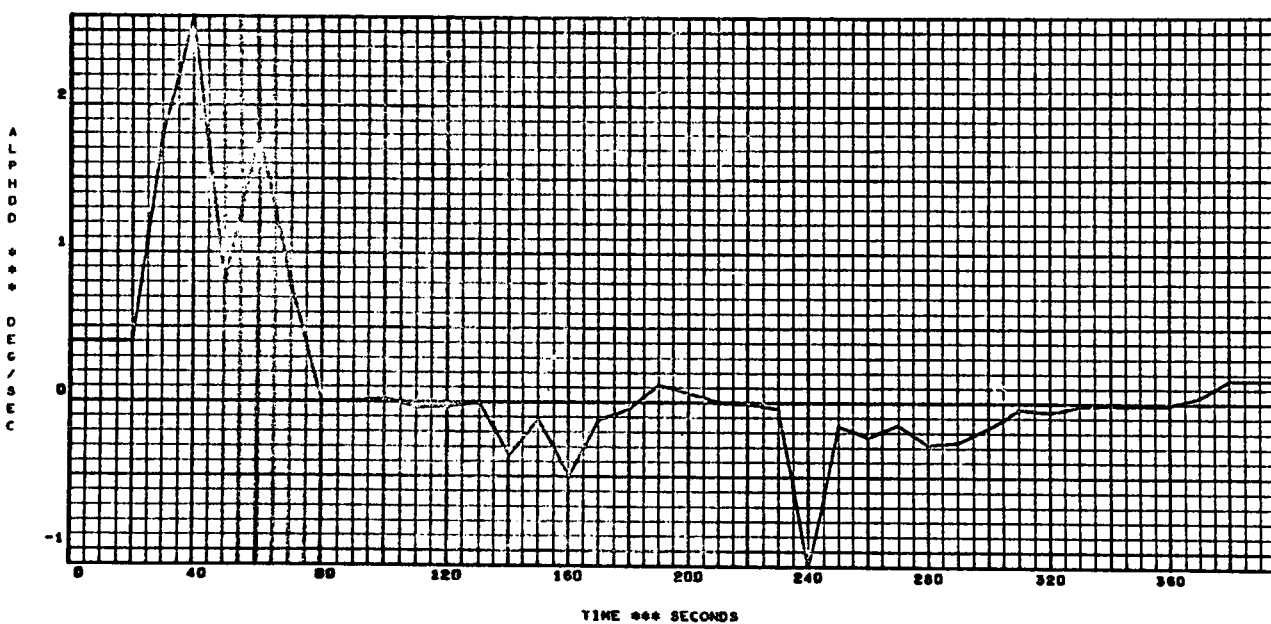
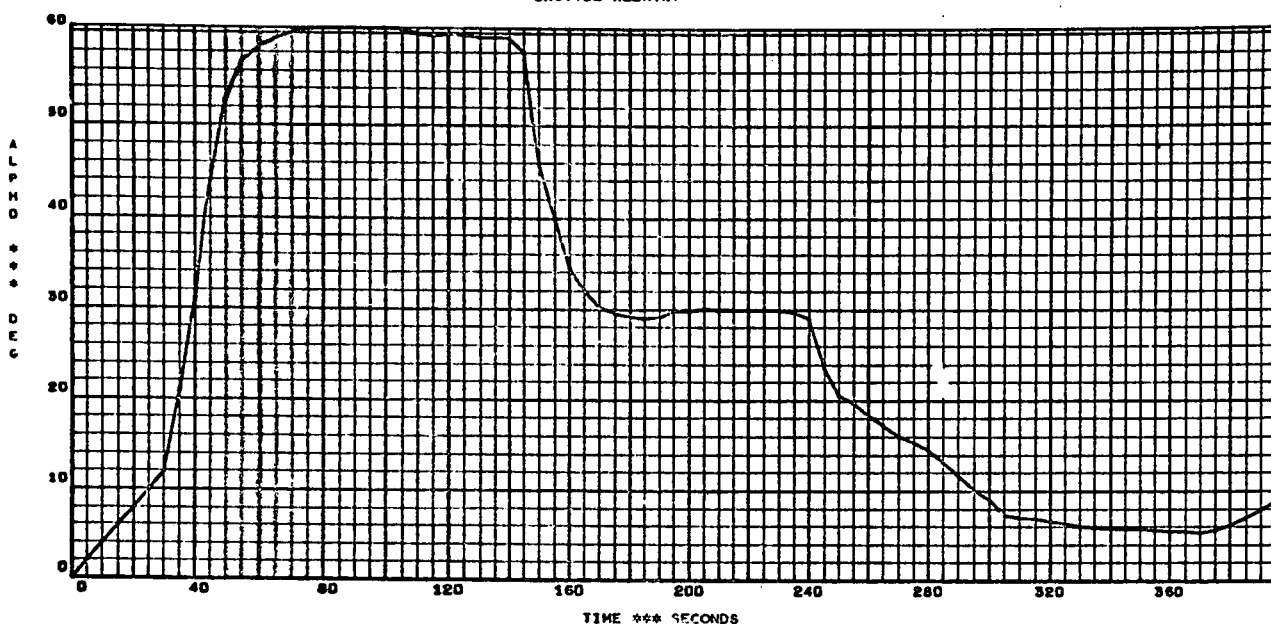
SHUTTLE REENTRY





SHUTTLE REENTRY

JOB NO 422500 PAGE 3

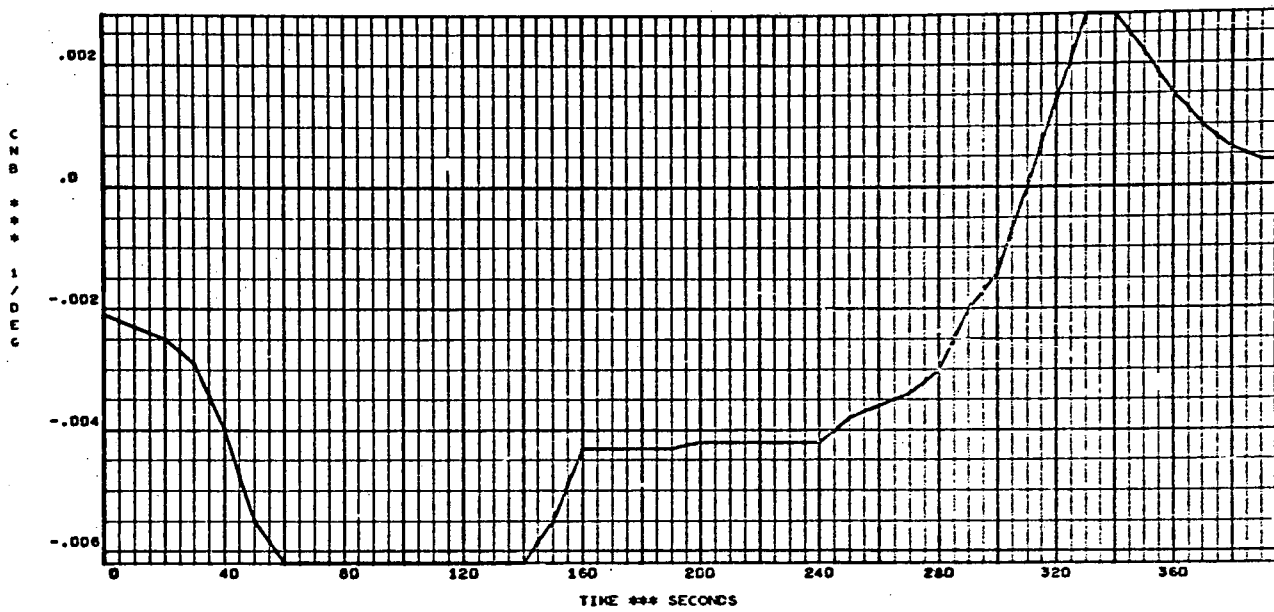
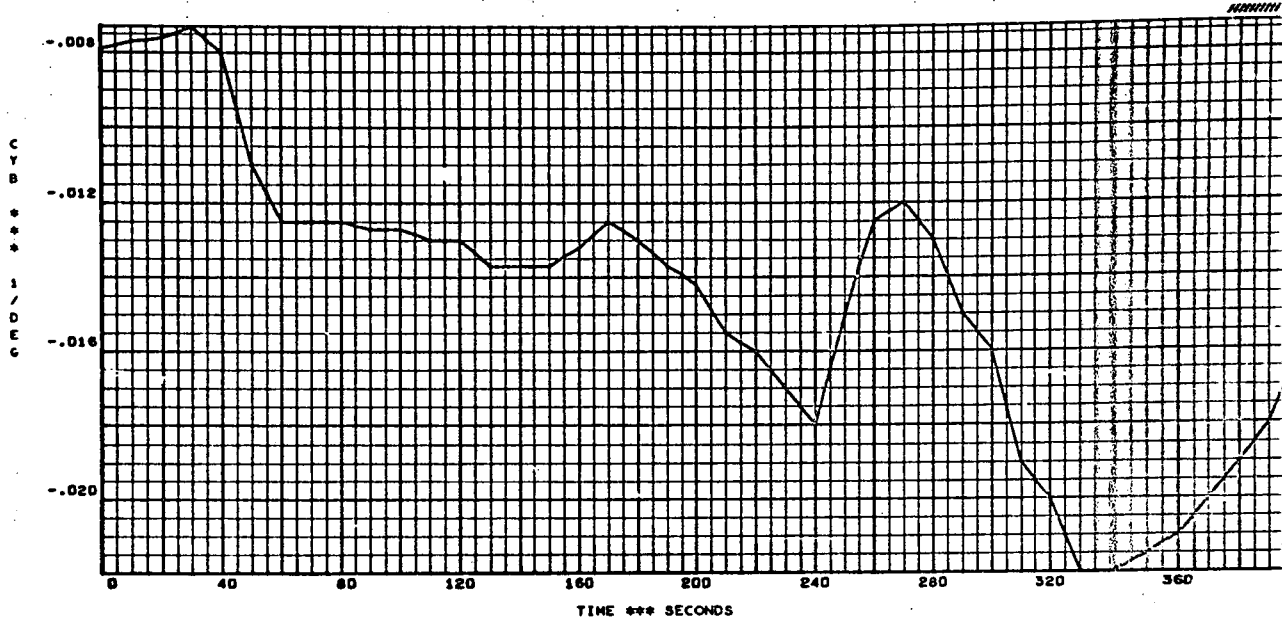




JOB NO 4225889

PAGE 9

SHUTTLE REENTRY

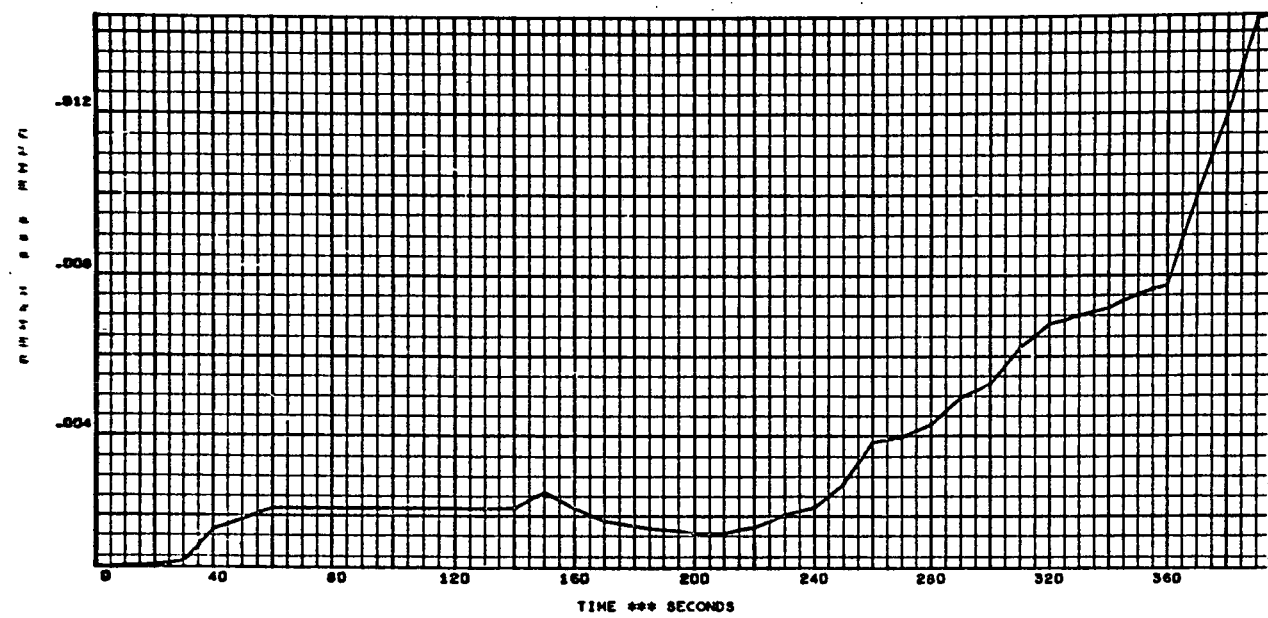
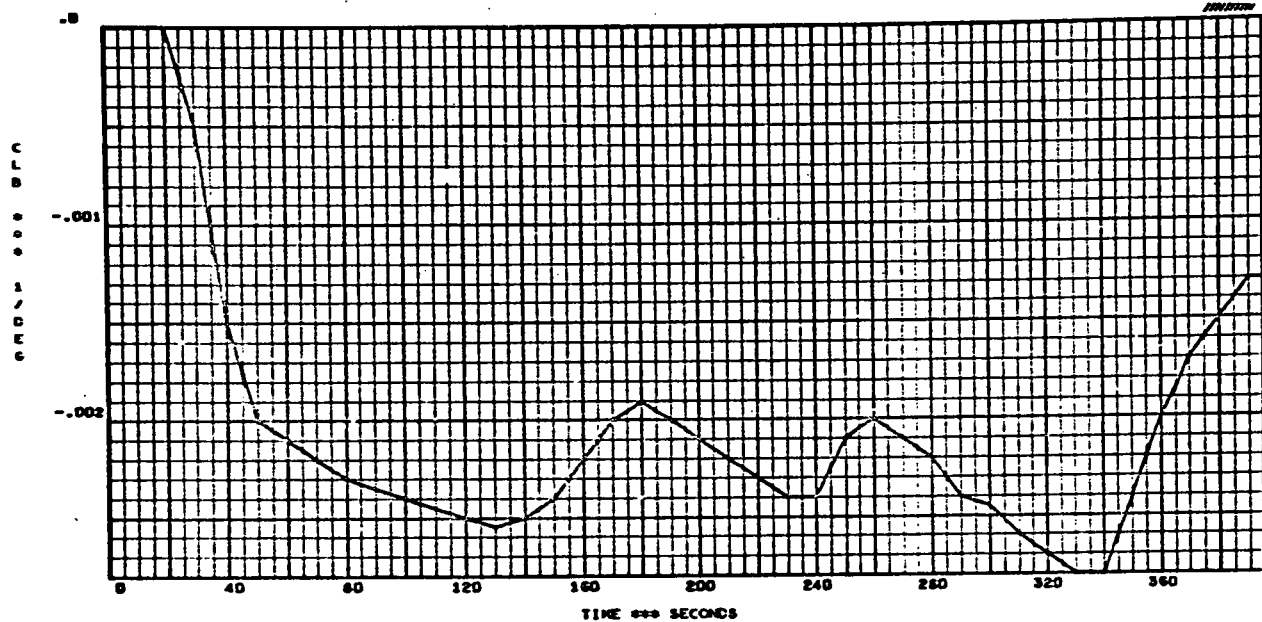




JOB NO 422500

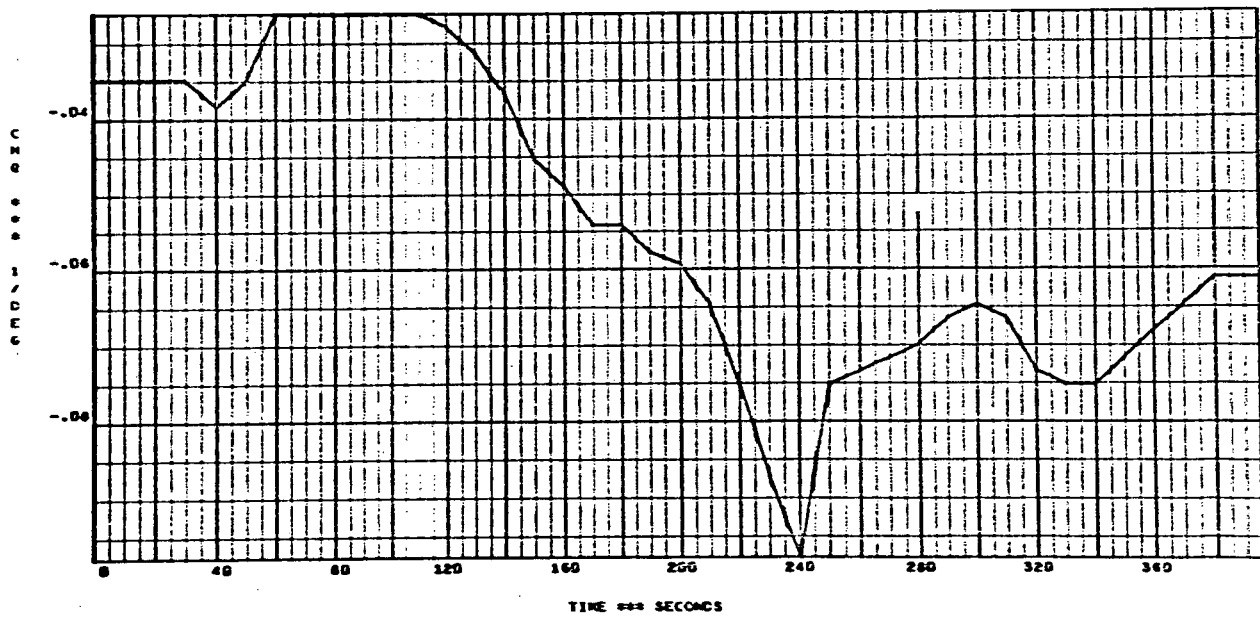
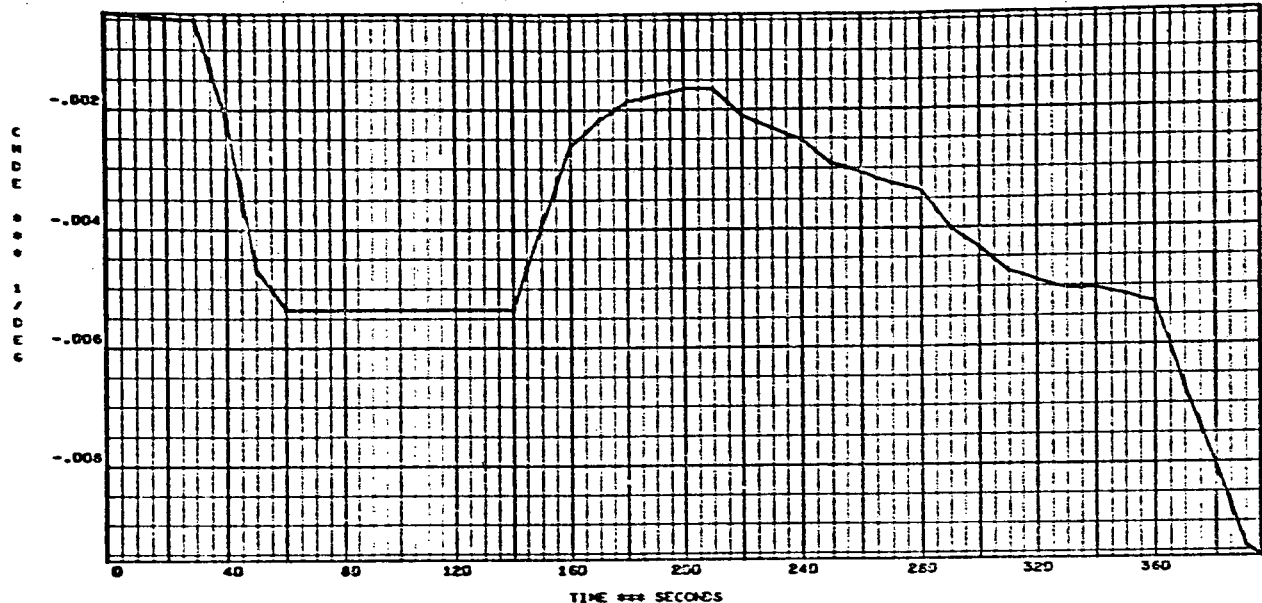
PAGE 6

SHUTTLE REENTRY



JOB NO 422500 PAGE 10

SHUTTLE REENTRY

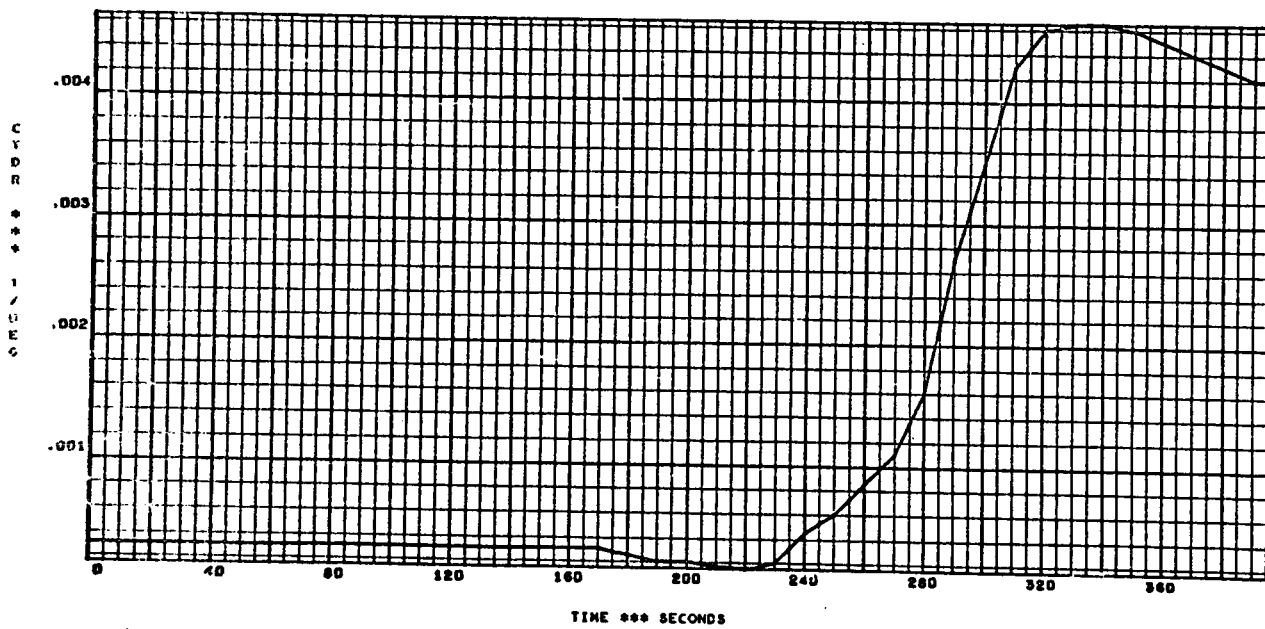
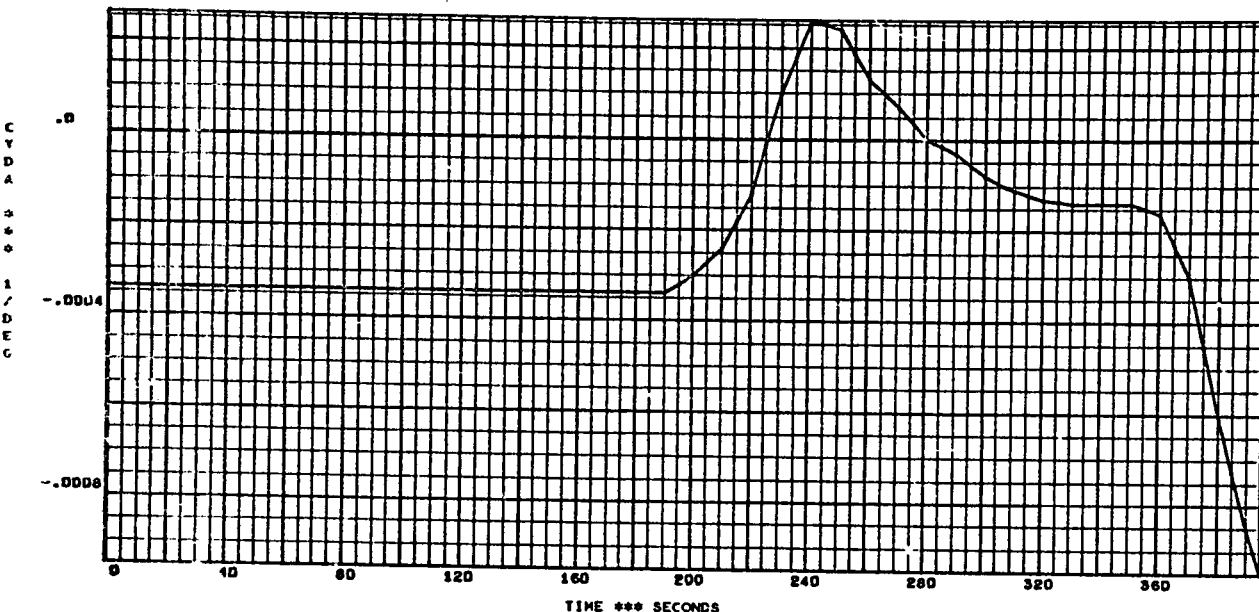




SHUTTLE REENTRY

JOB NO 422500

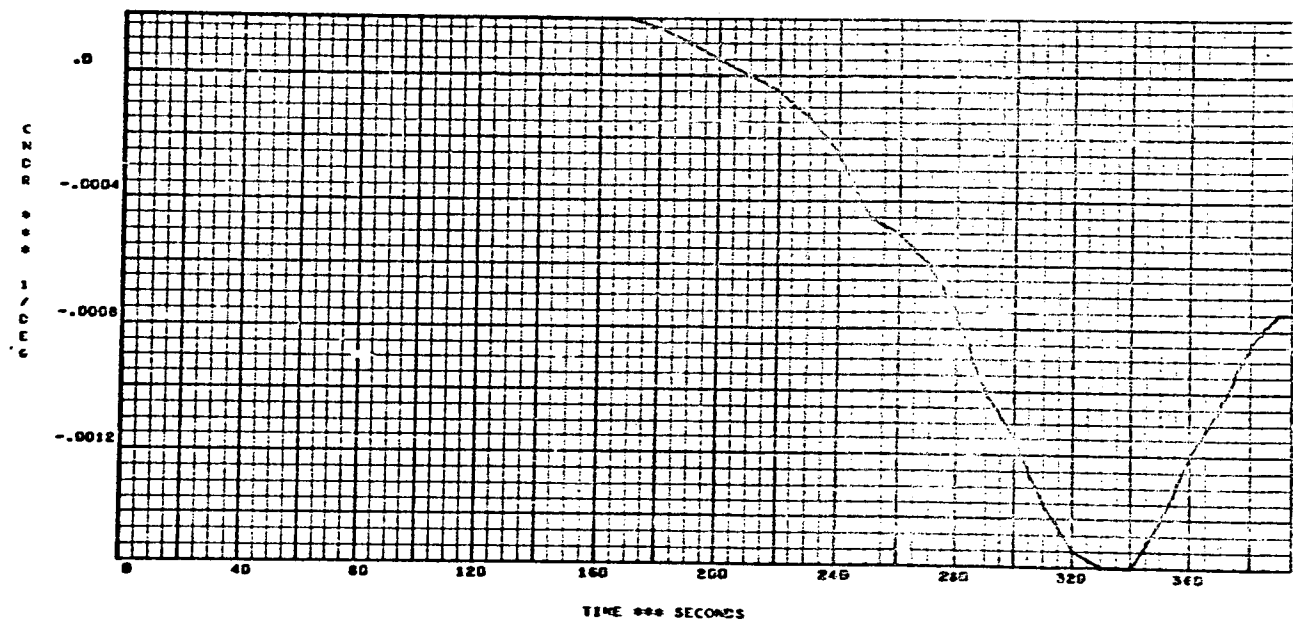
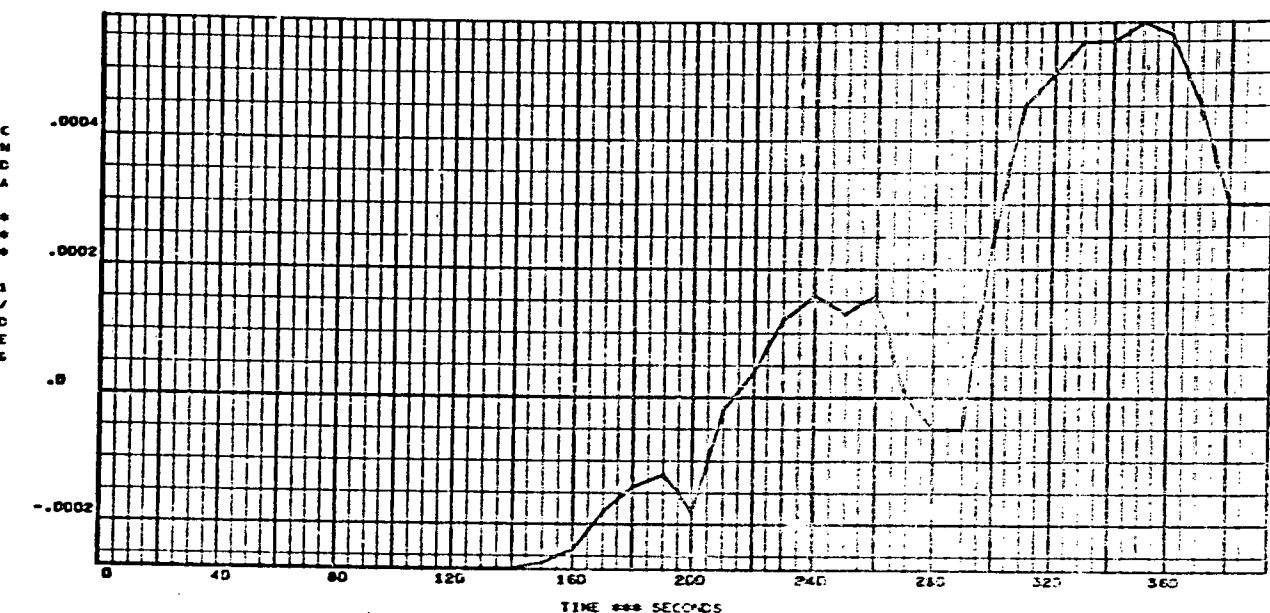
PAGE 10





SHUTTLE REENTRY

JOB NO 422506 PAGE 16

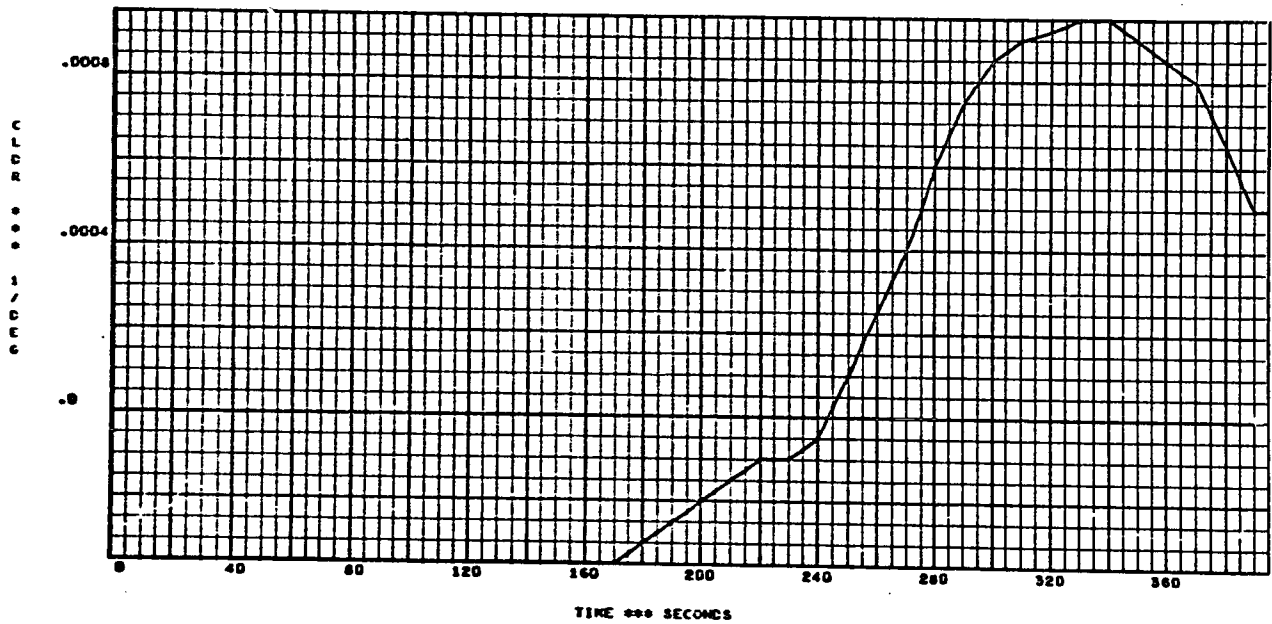
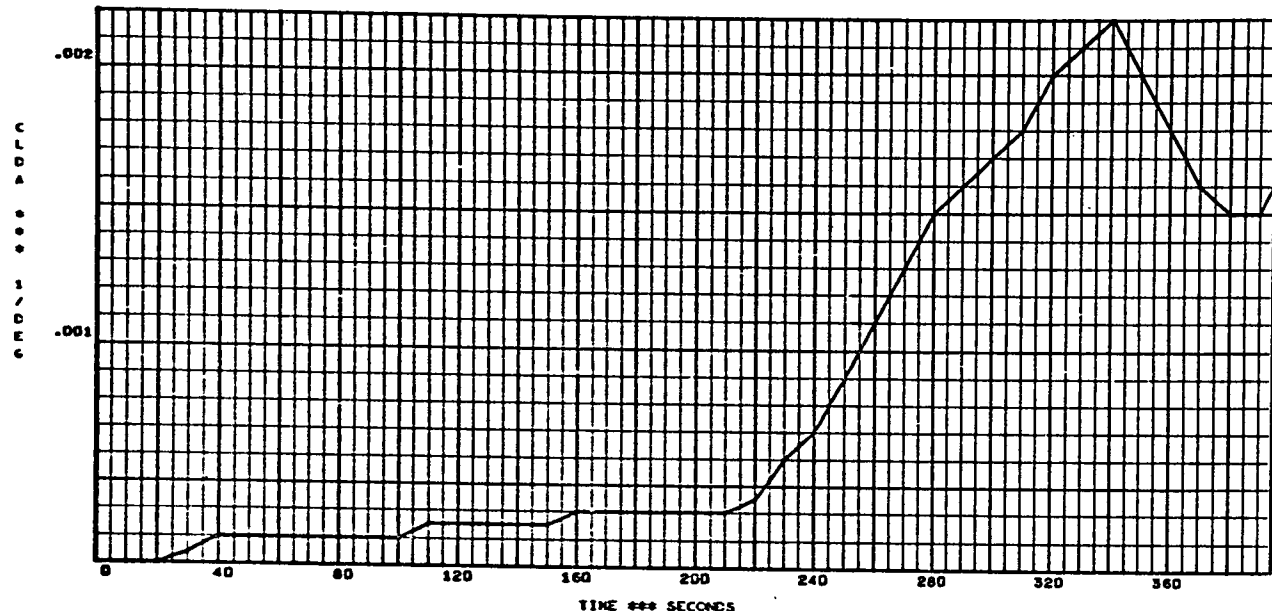


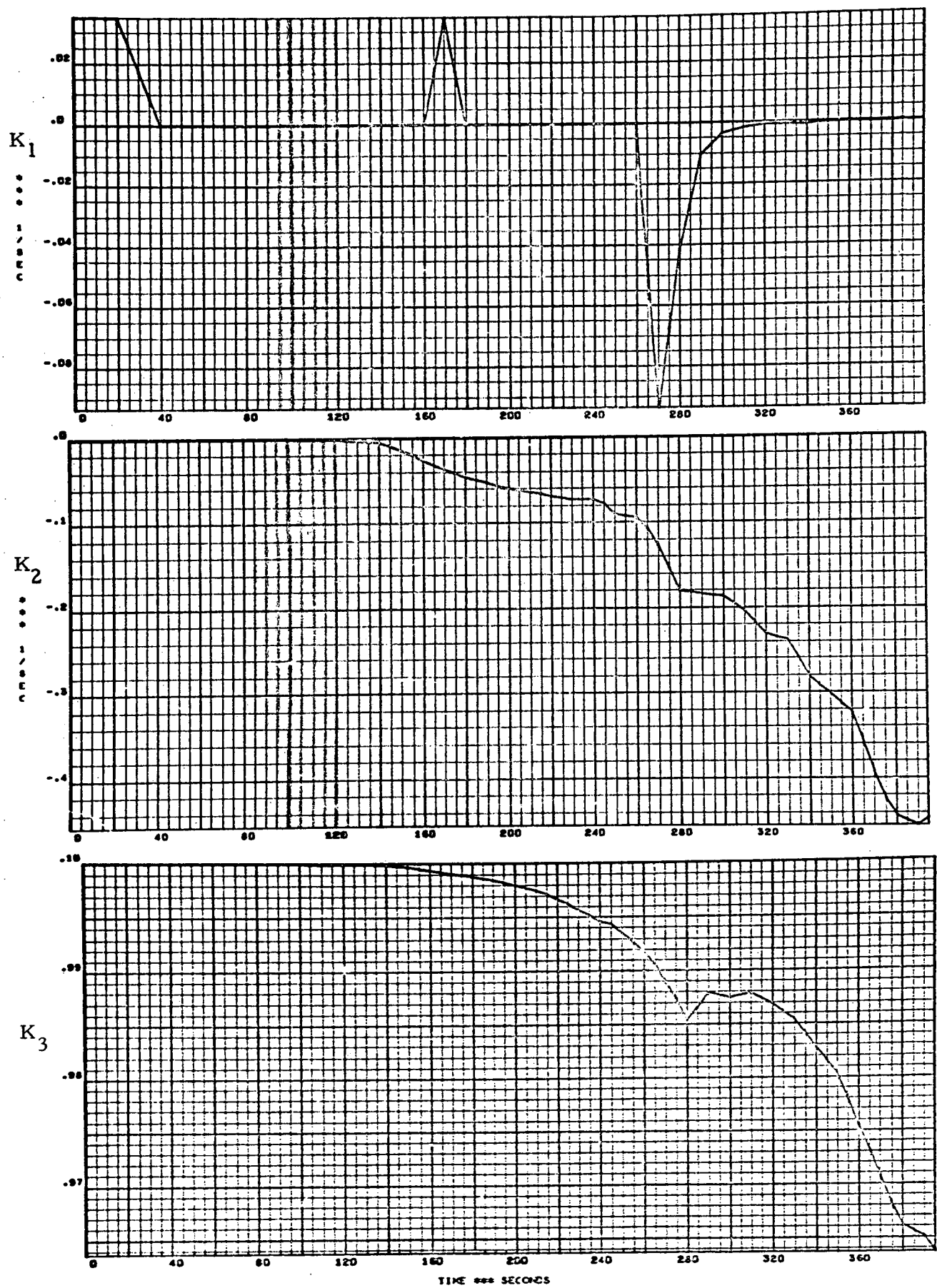


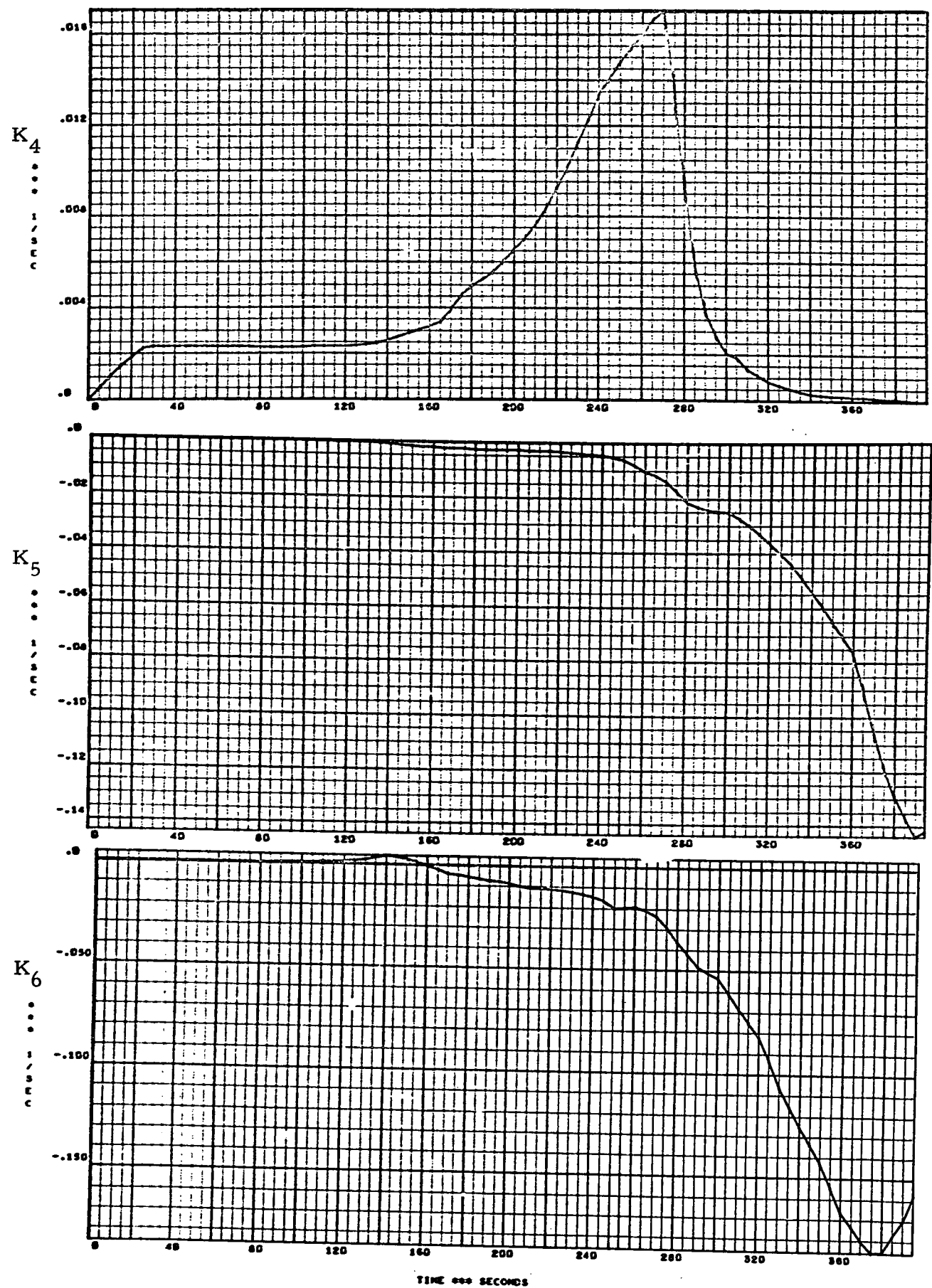
SHUTTLE REENTRY

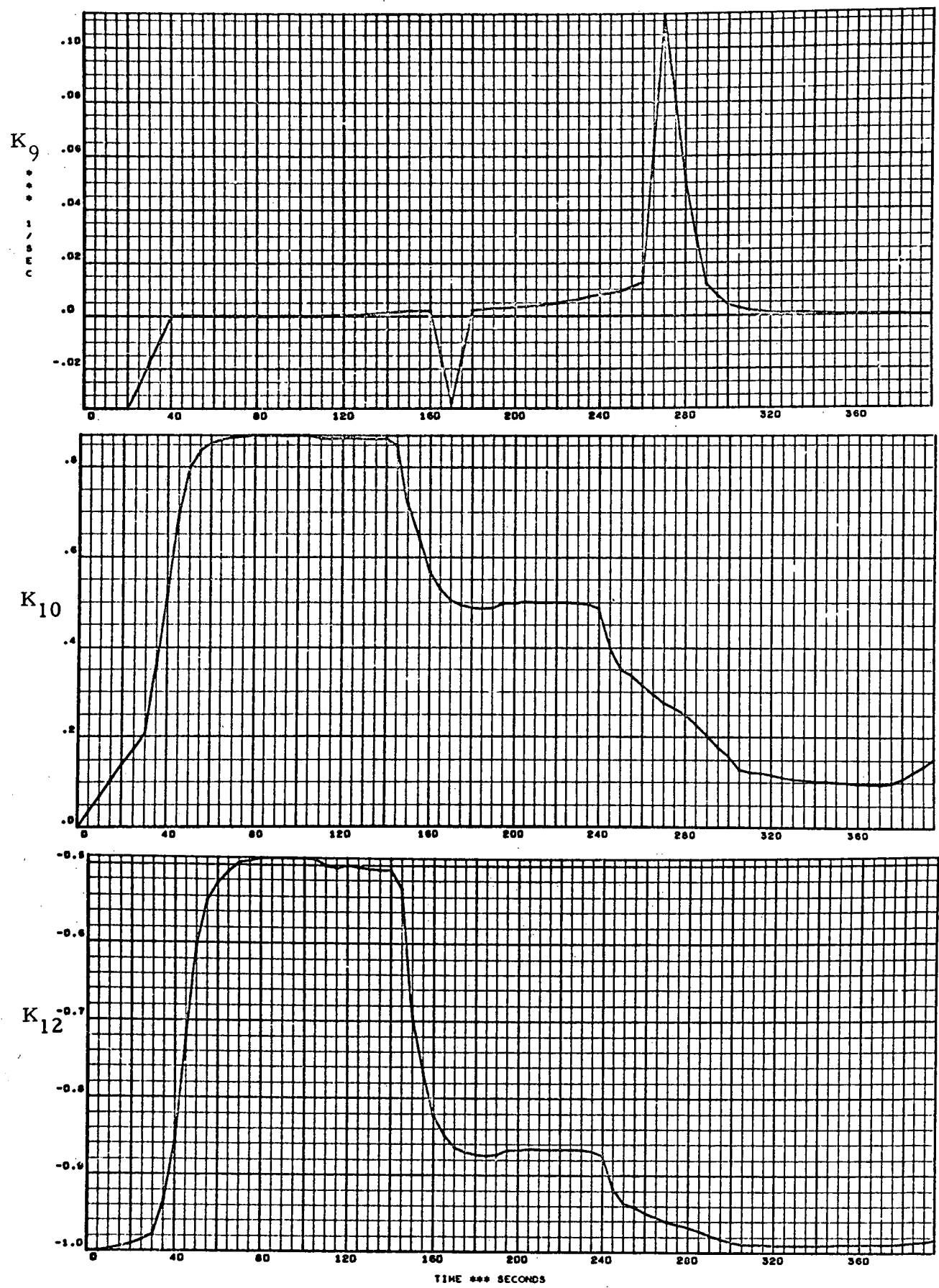
JOB NO 422500

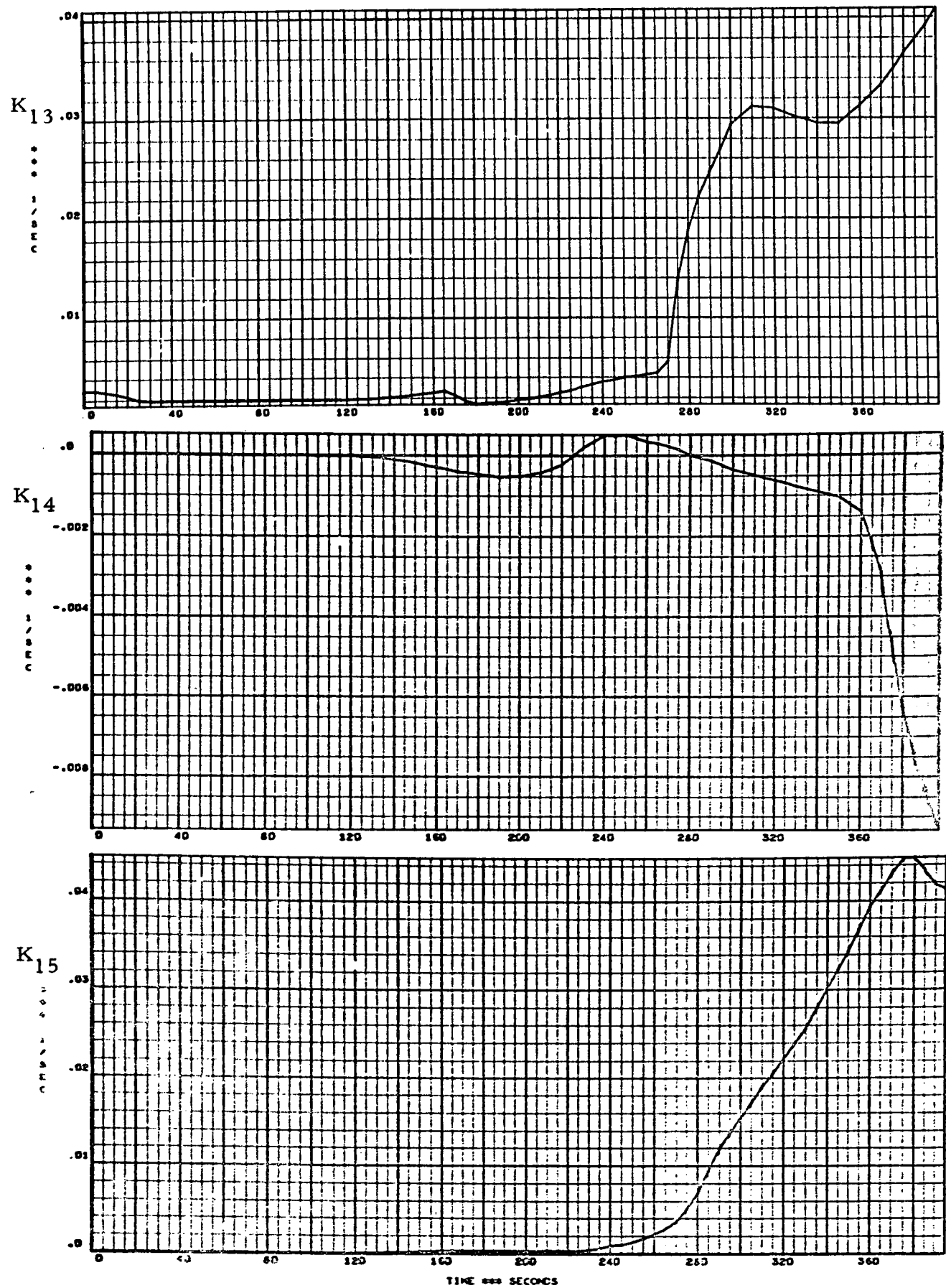
PAGE 13

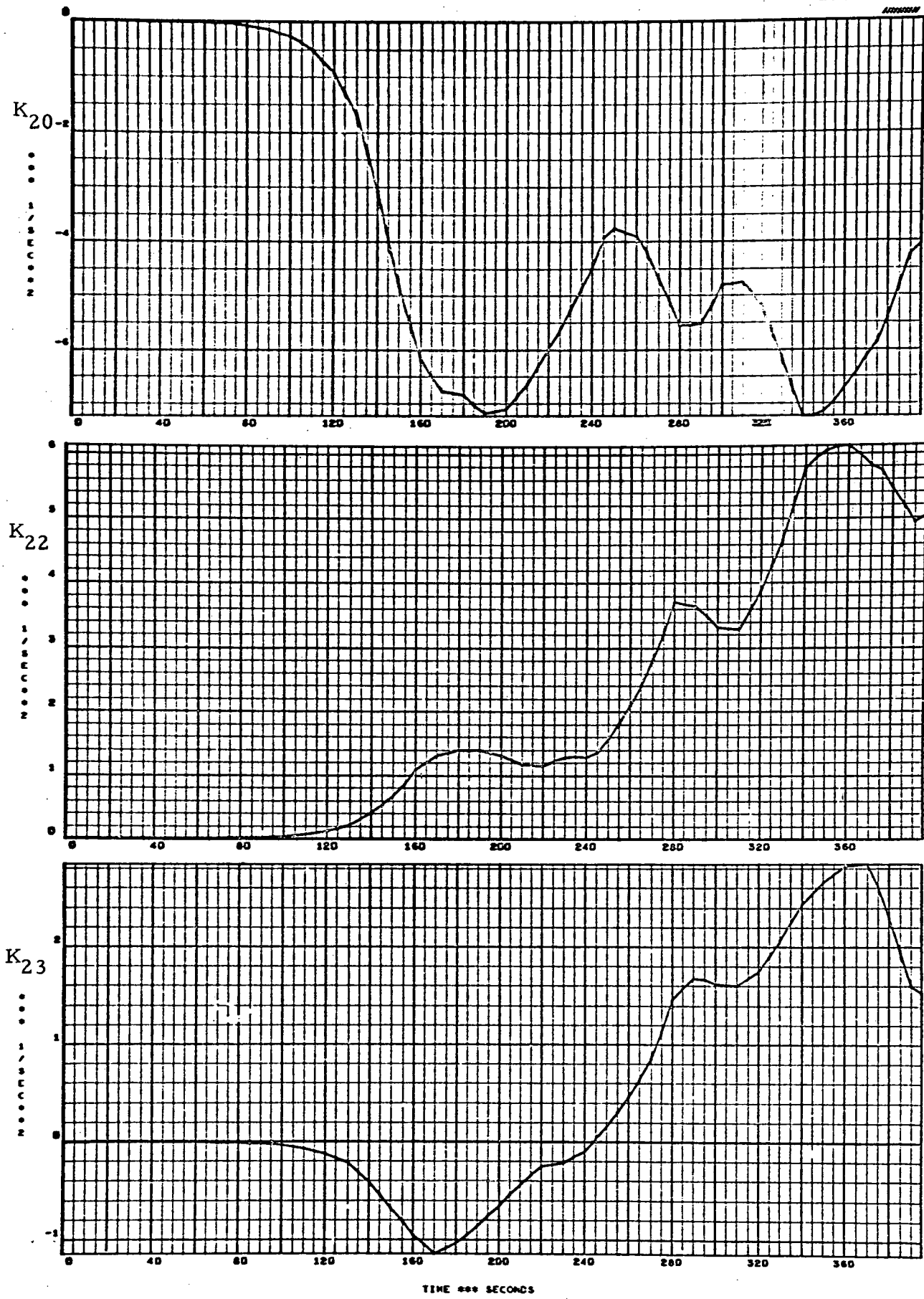


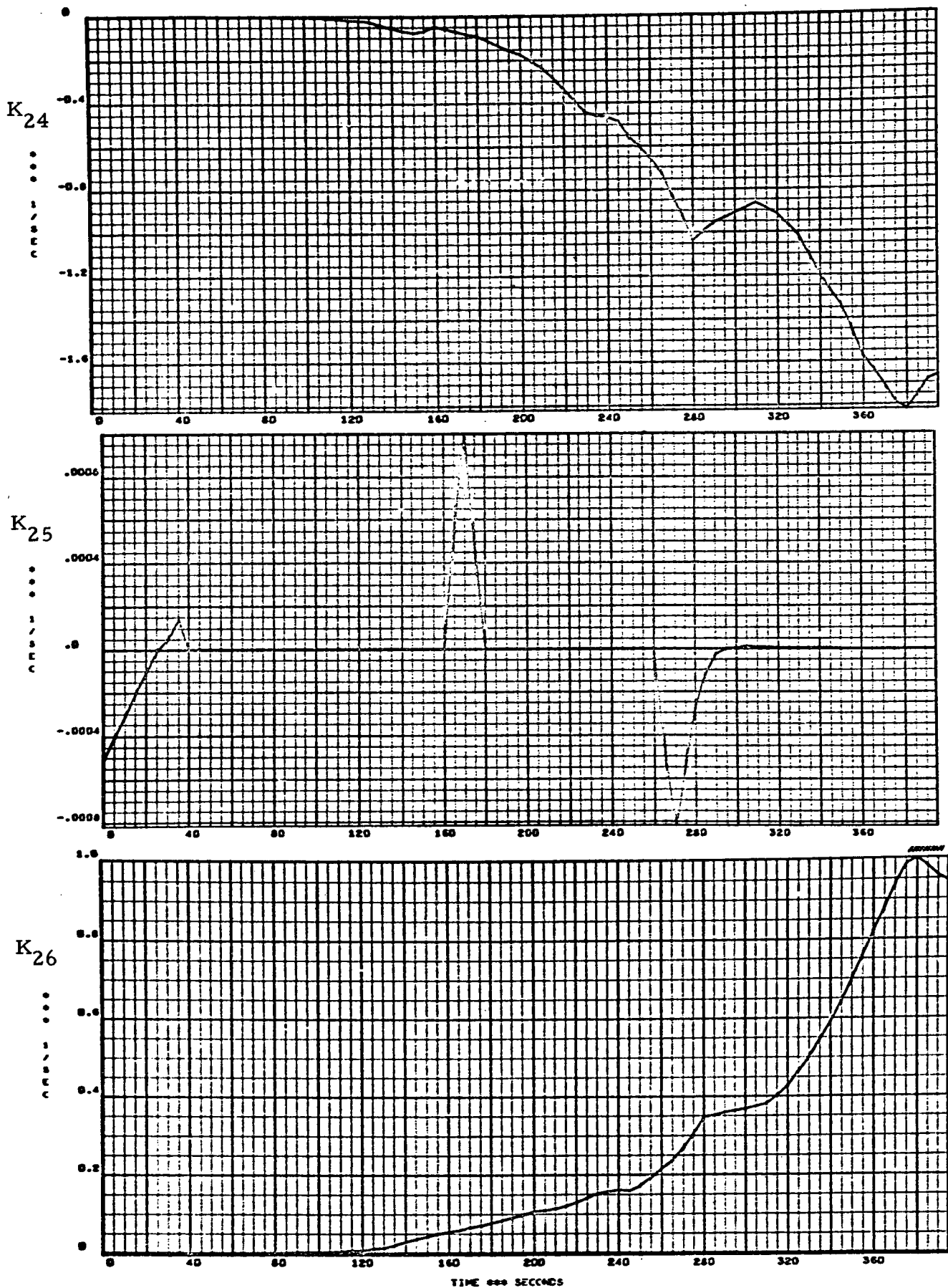




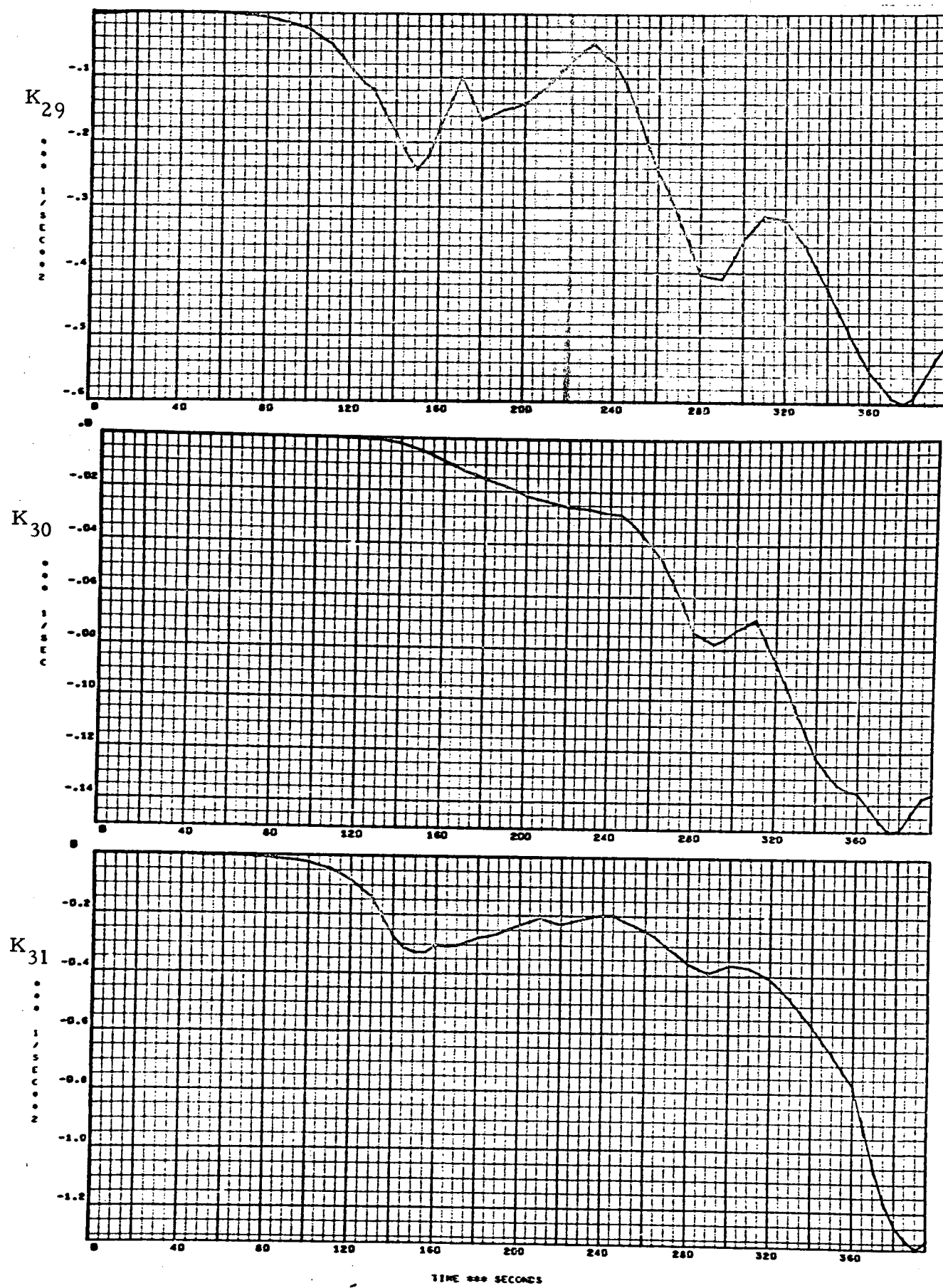


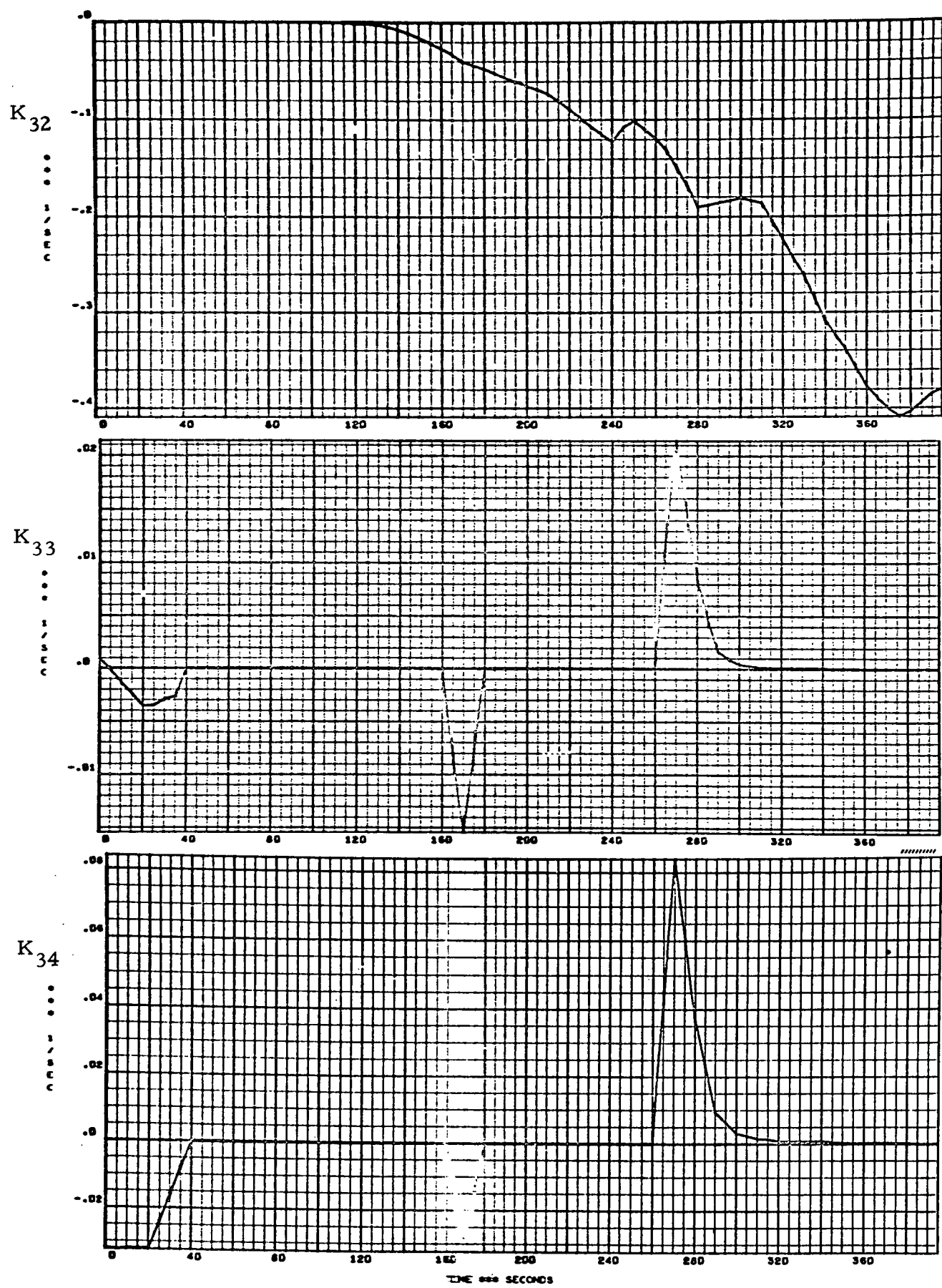




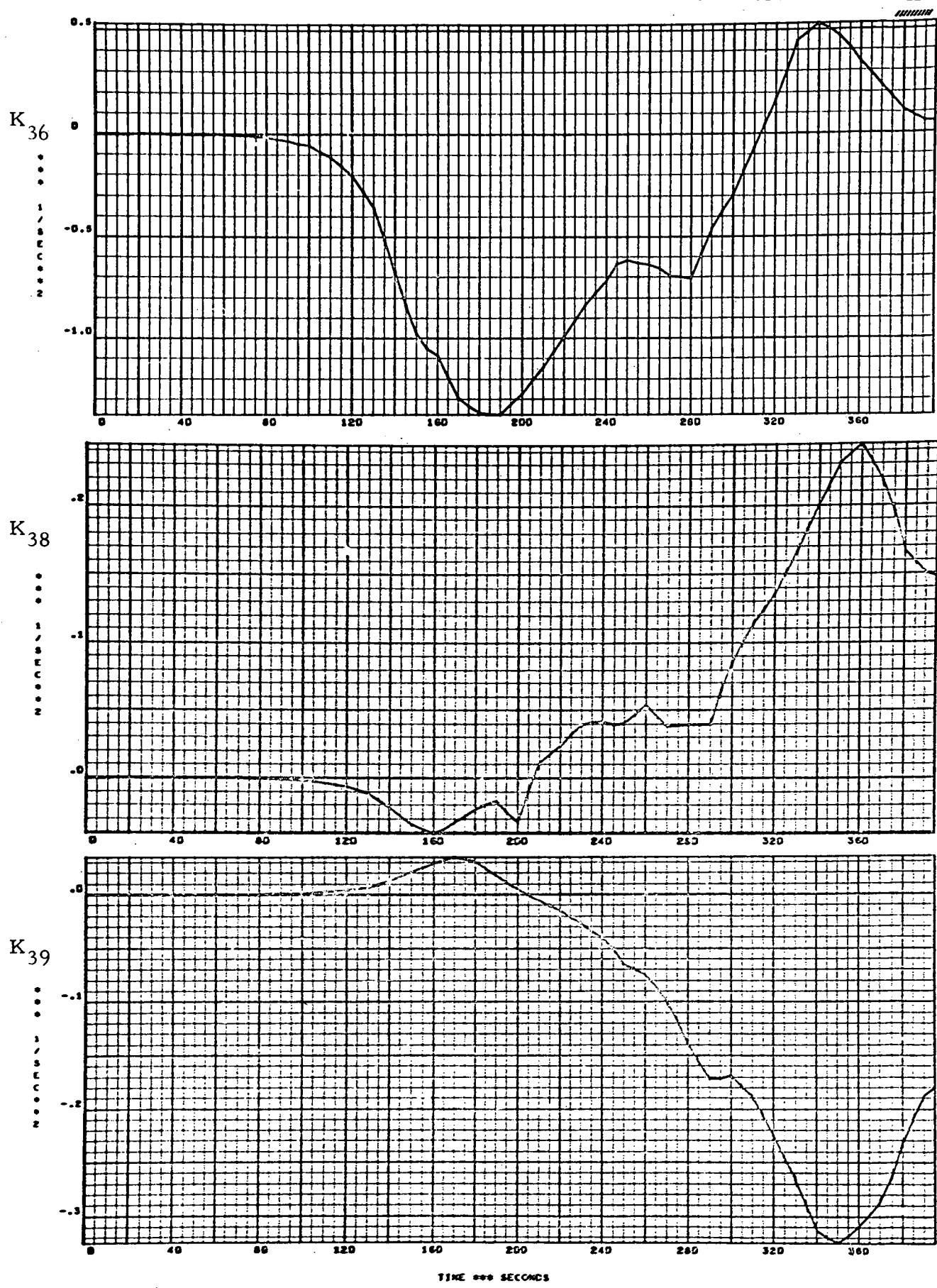


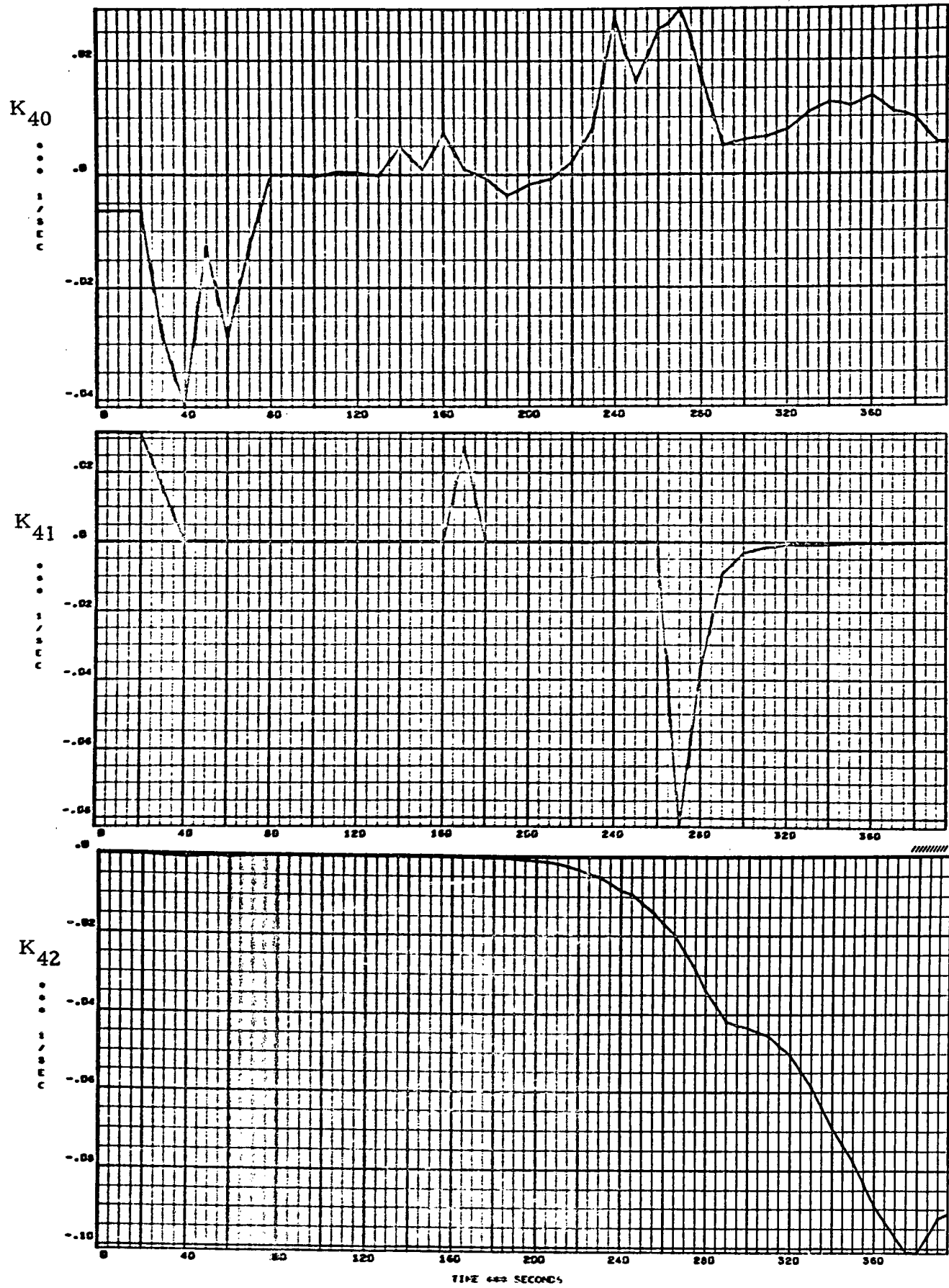
K_{27} and K_{28} are constants.



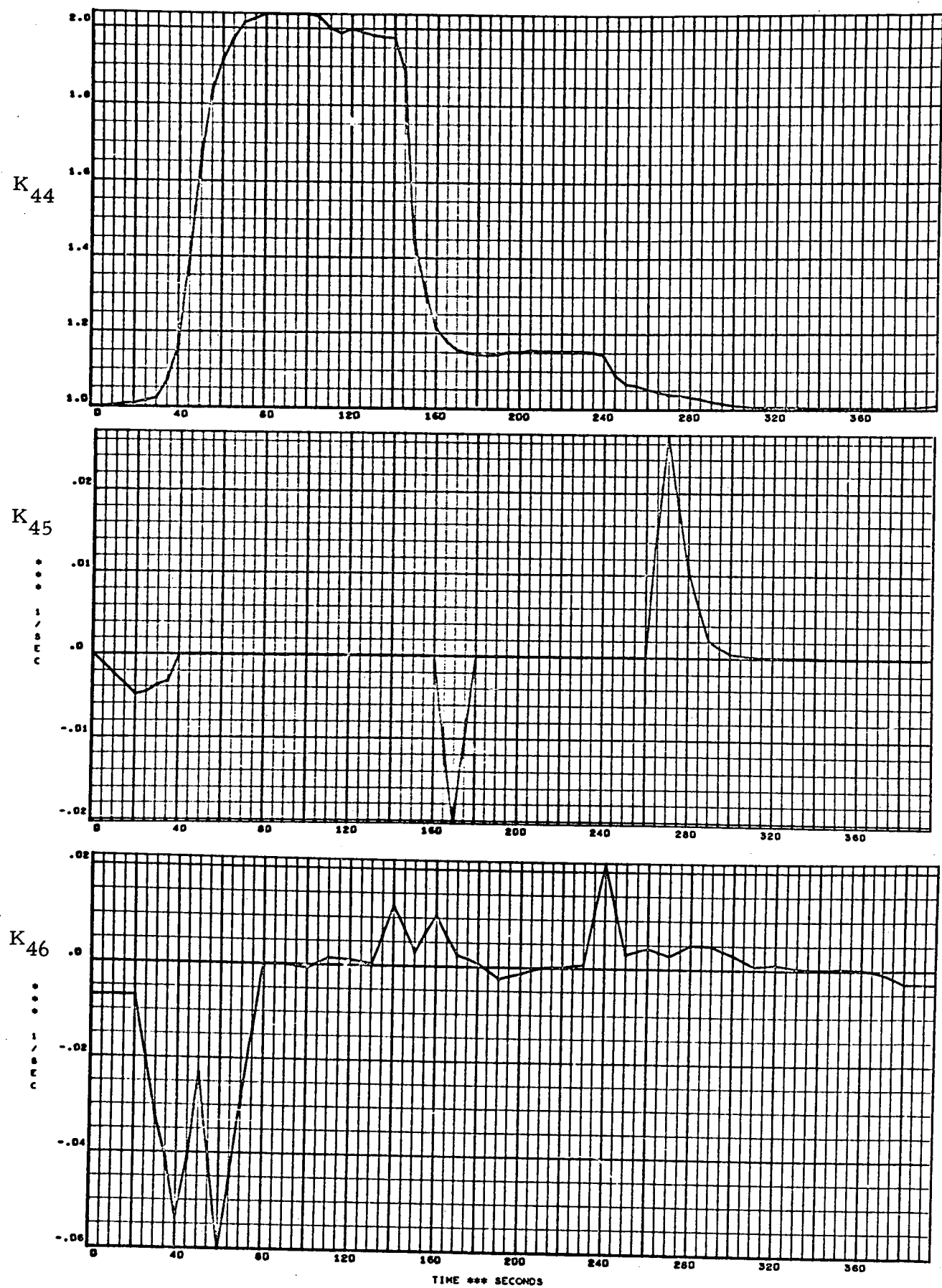


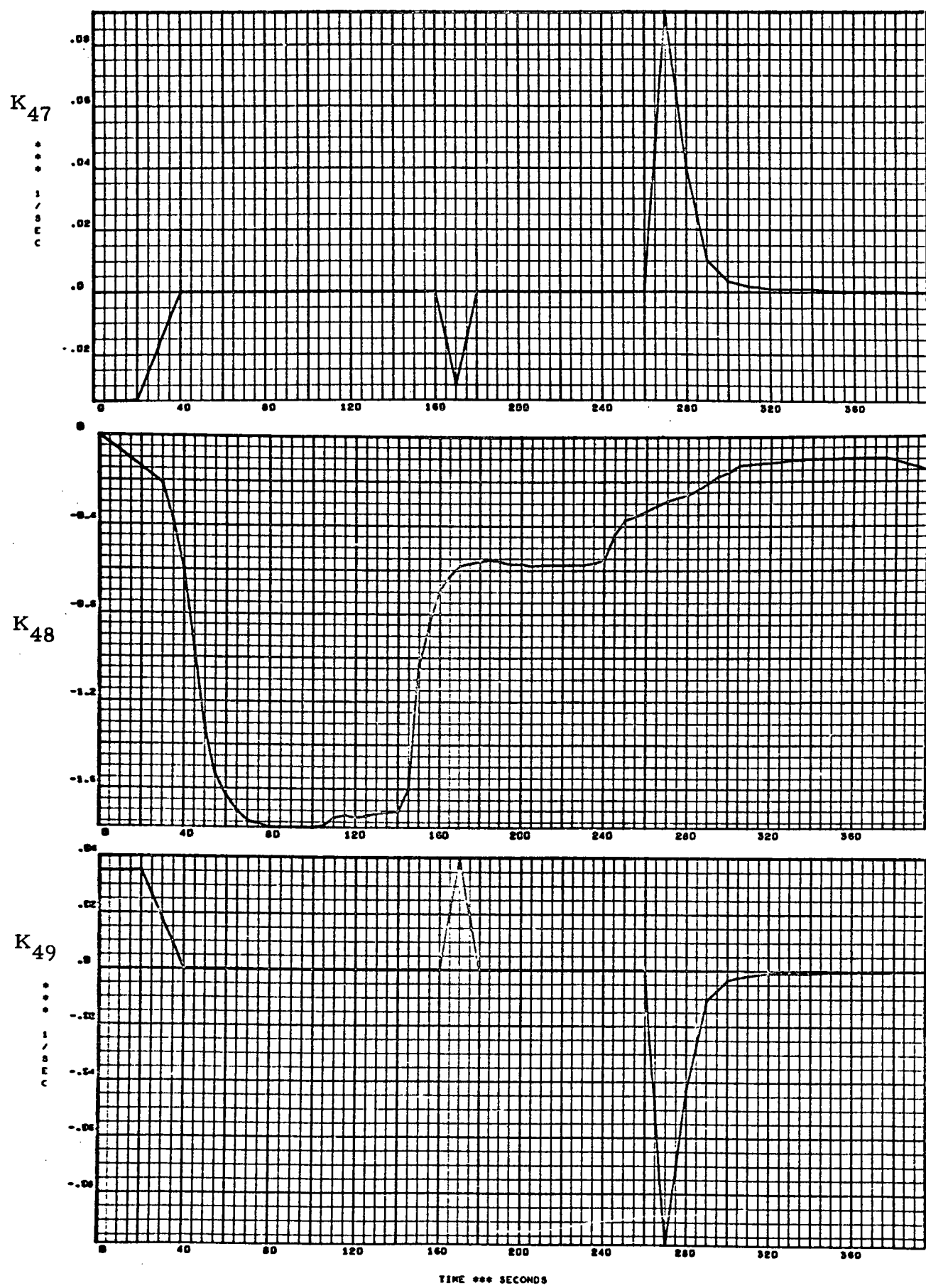
K_{35} is a constant.

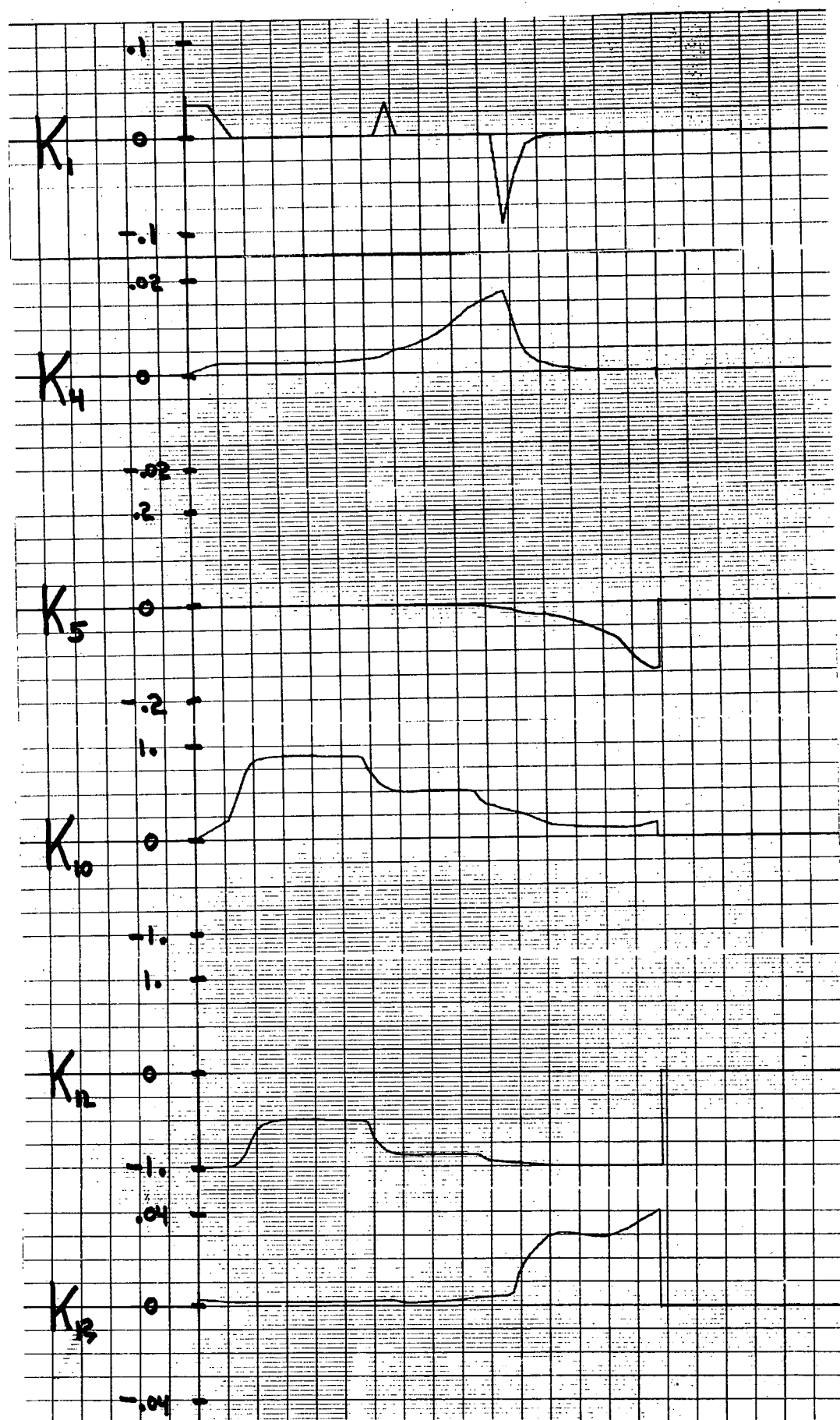




K_{43} is a constant.







Appendix G

SHUTTLE REENTRY CONTROL GAINS SYNTHESIS PROGRAM
AND SOME REPRESENTATIVE RESULTS

Appendix G

The block diagram shown in Fig. G-1 gives the general outline of the Control Gains Synthesis program. A simple description of each subroutine is also given.

Aerodynamic control gain schedules and root locus plots are given on pages G-3 through G-7. Representative plots of APS control gain schedules and root locus plot are given on pages G-8 and G-9, respectively. GDC/B-9U data are used in the synthesis. The control law used is the one described in Section 4.3. The design goal is:

Longitudinal Control

$$\omega_{sp} = 2 \text{ rad/sec} \quad \xi_{sp} = 0.8$$

Lateral Control

$$\omega_{dr} = 1 \text{ rad/sec} \quad \xi_{dr} = 0.8$$

$$T_s = 10 \quad T_r = 0.1$$

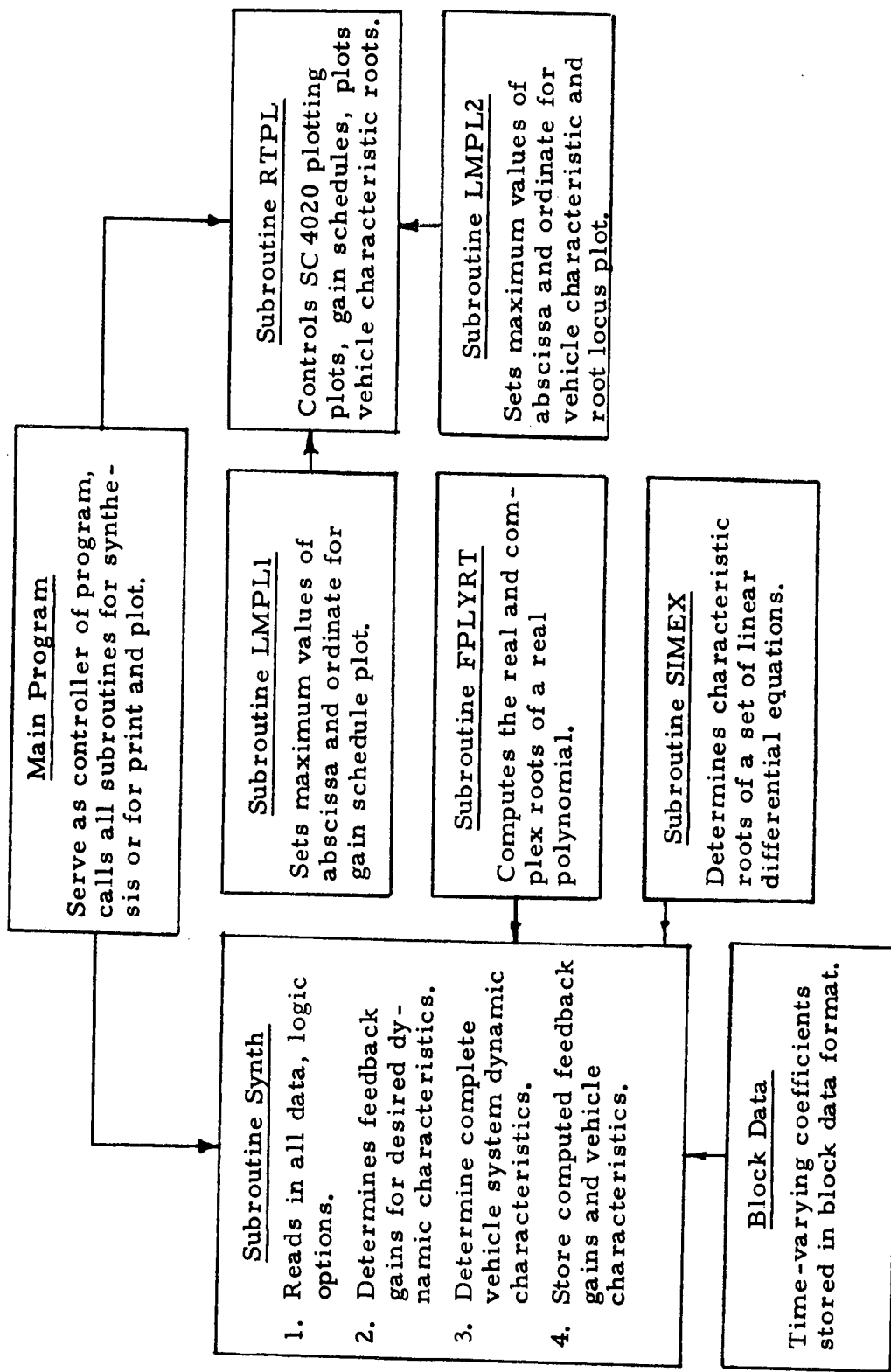
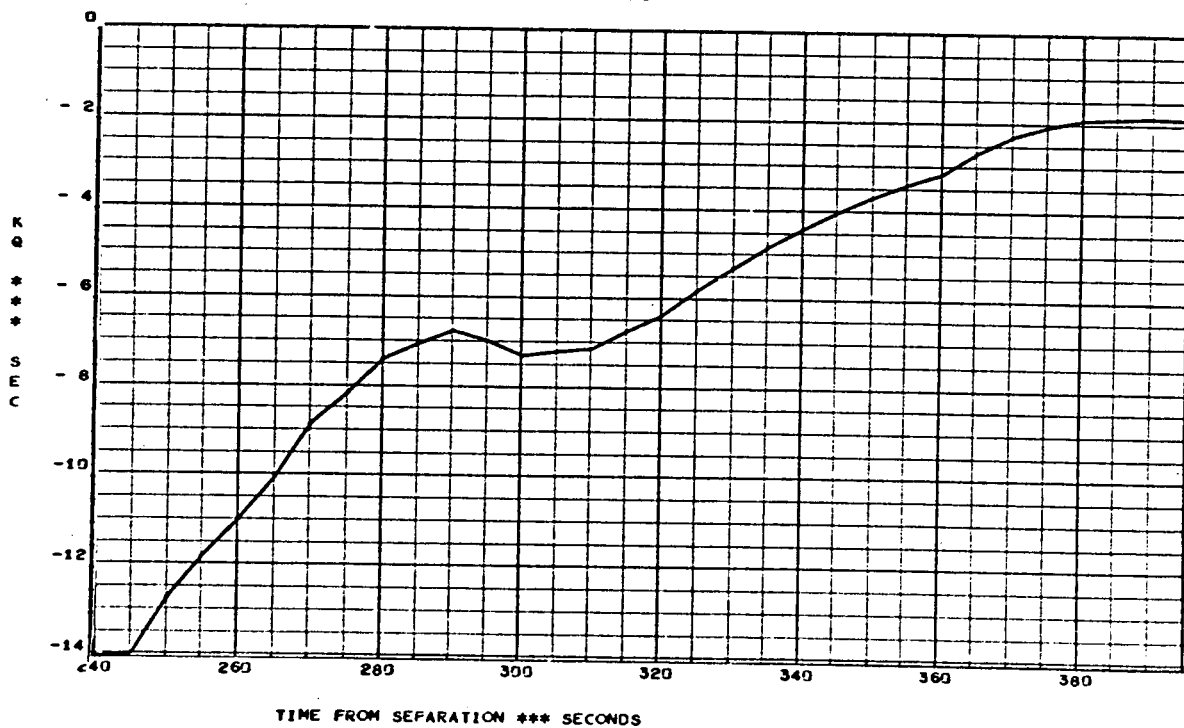
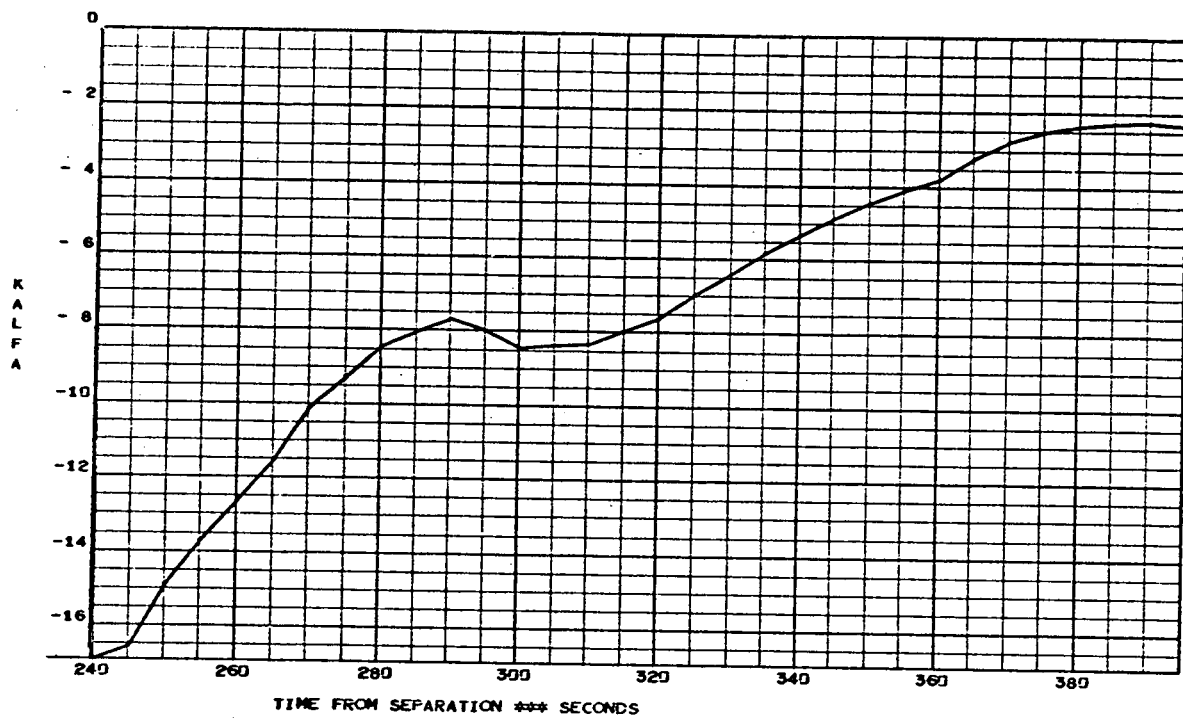


Fig. G-1 - Diagram of IBM 1108 Digital Program Used to Synthesize Control Gains for Shuttle Reentry

GDC BOOSTER B9U, LATERAL TS=10, TR=1, Z=.7, WN=1., LONG Z=.6, WN=2.

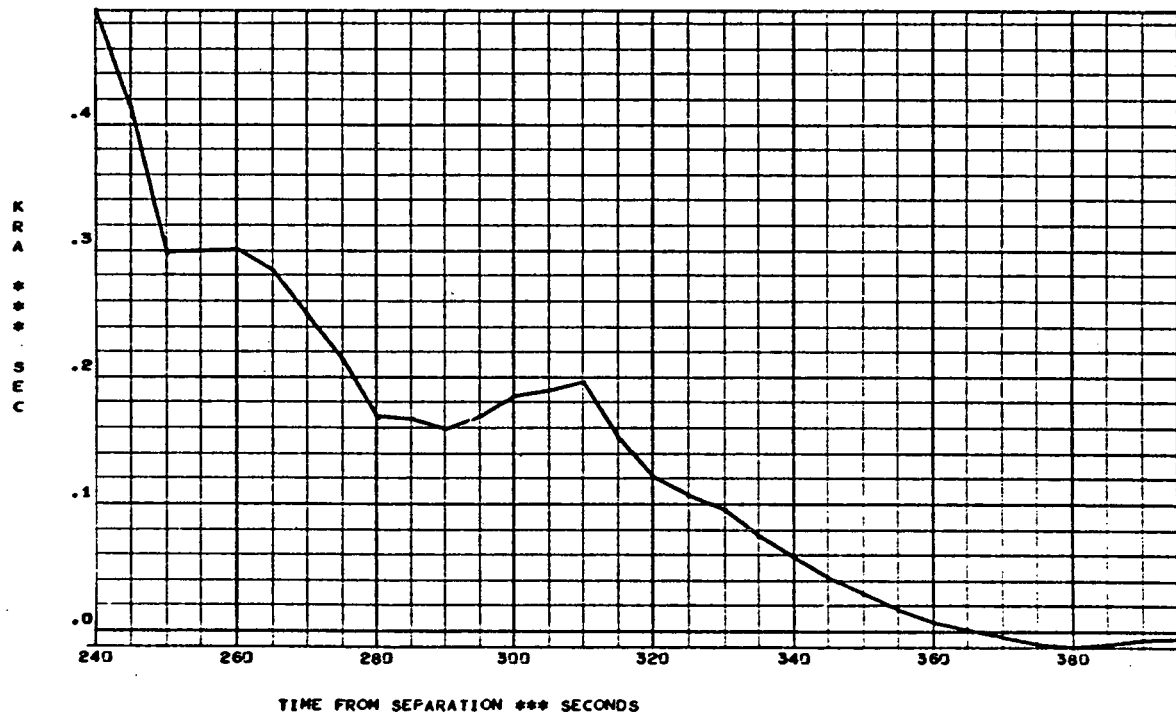
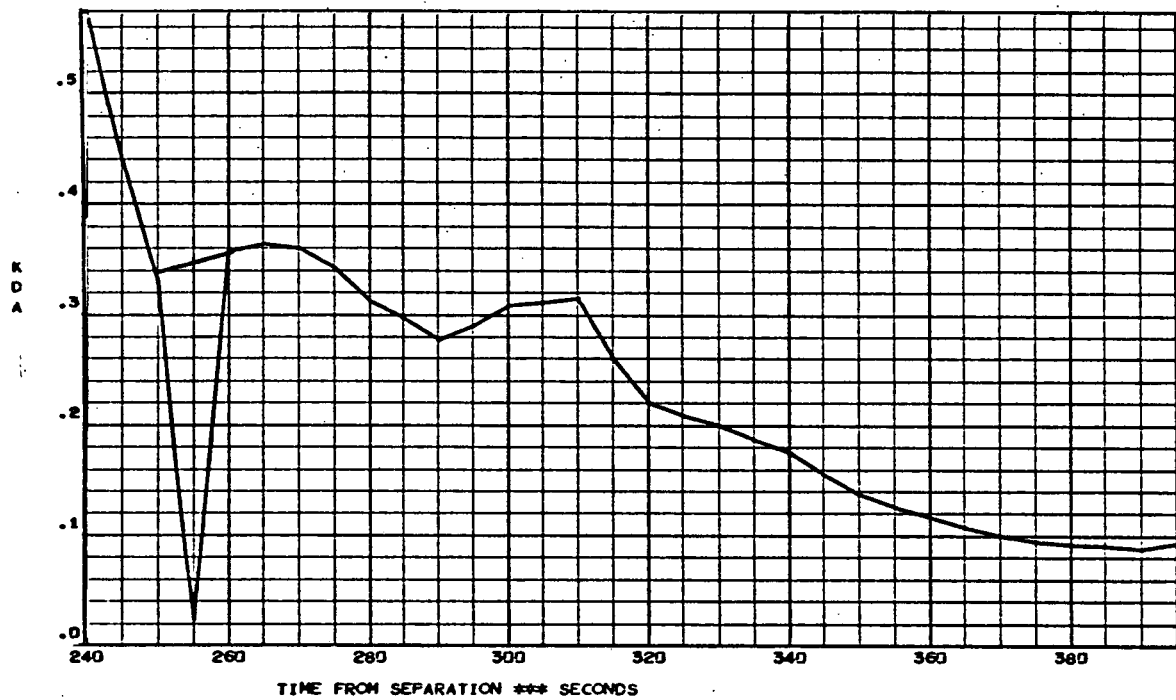
JOB NO 422500

PAGE 8



GOC BOOSTER B9U, LATERAL TS=10, TR=1, Z=.7, WN=1., LONG Z=.8, WN=2.

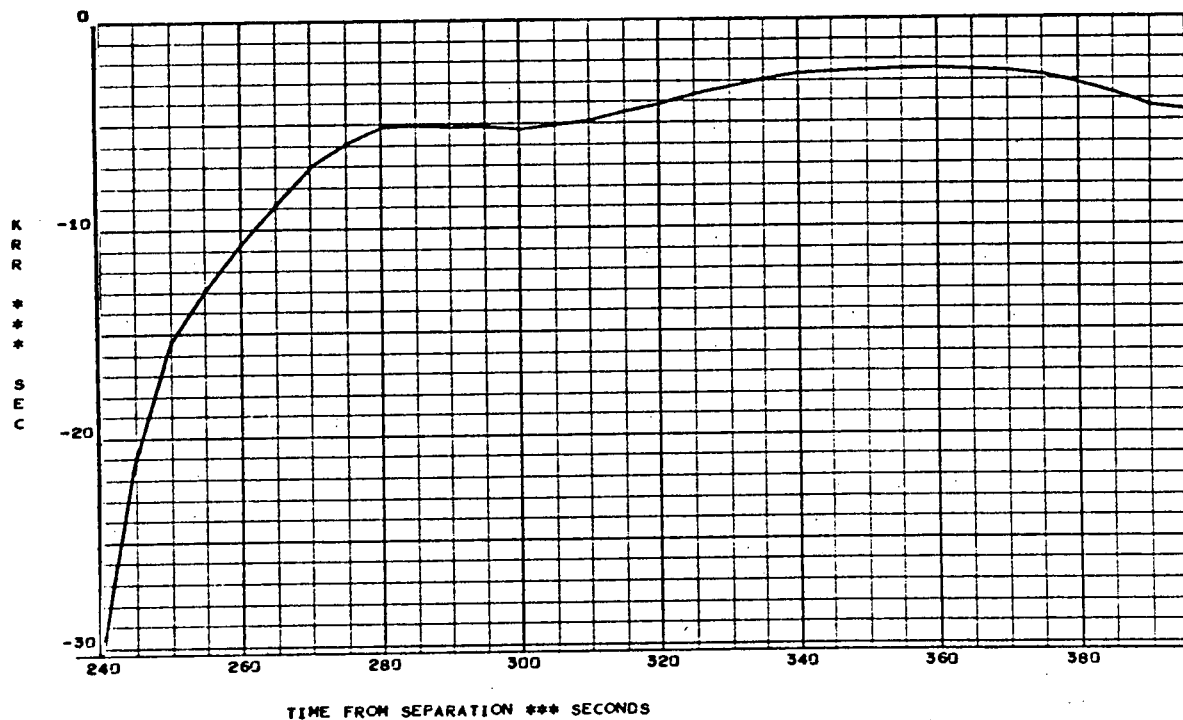
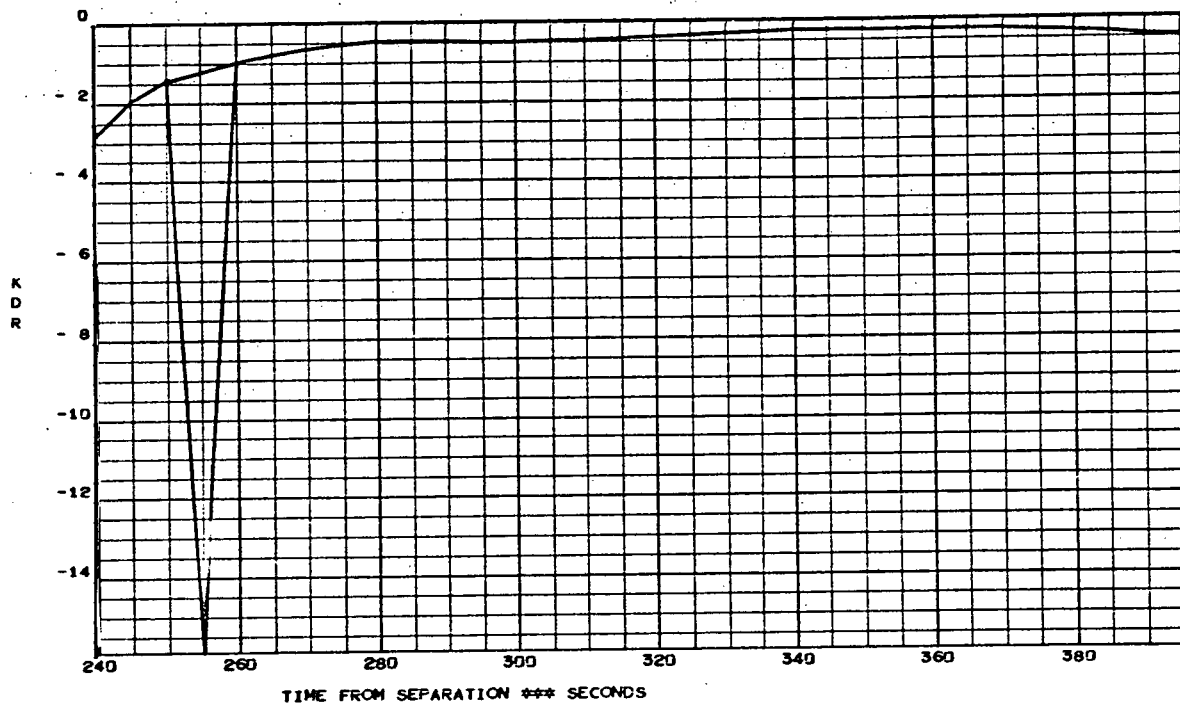
JOB NO 422500 PAGE 5



GDC BOOSTER B9U, LATERAL TS=10, TR=1, Z=.7, WN=1., LONG Z=.8, WN=2.

JOB NO 422500

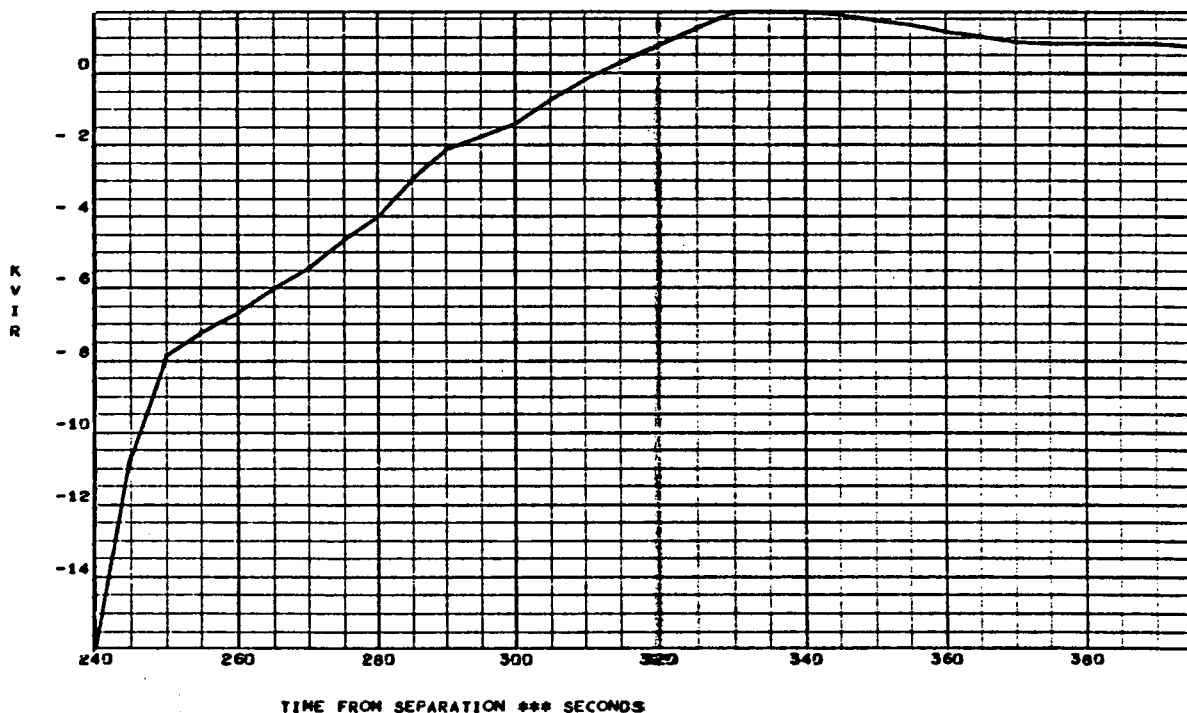
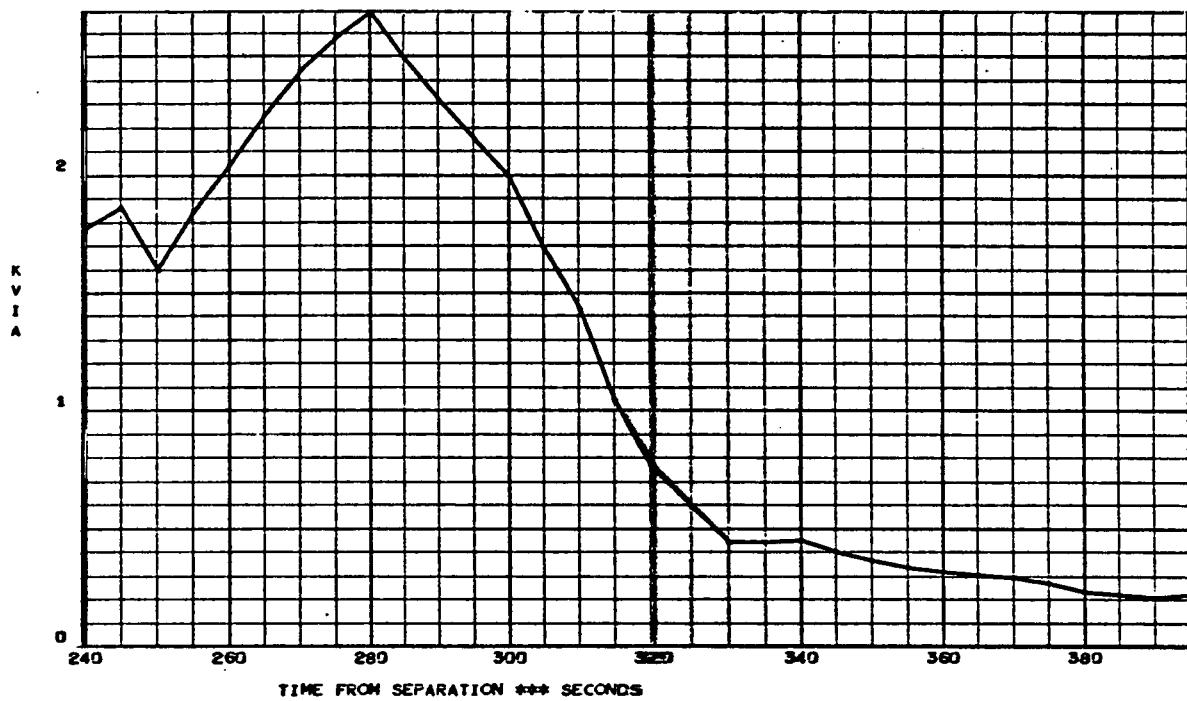
PAGE 6



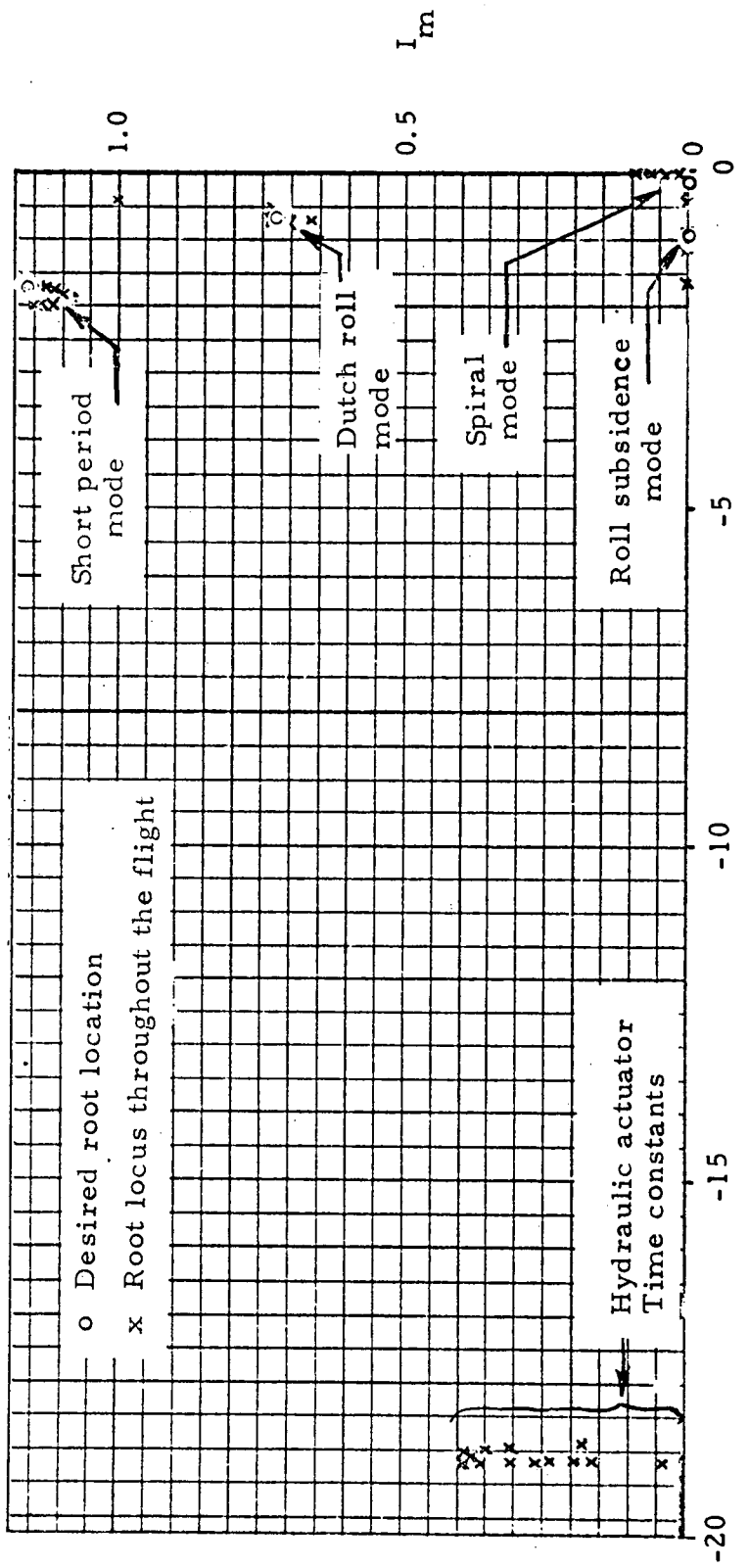
GDC BOOSTER B9U, LATERAL TS=10, TR=1, Z=.7, W=1., LONG Z=.8, W=2.

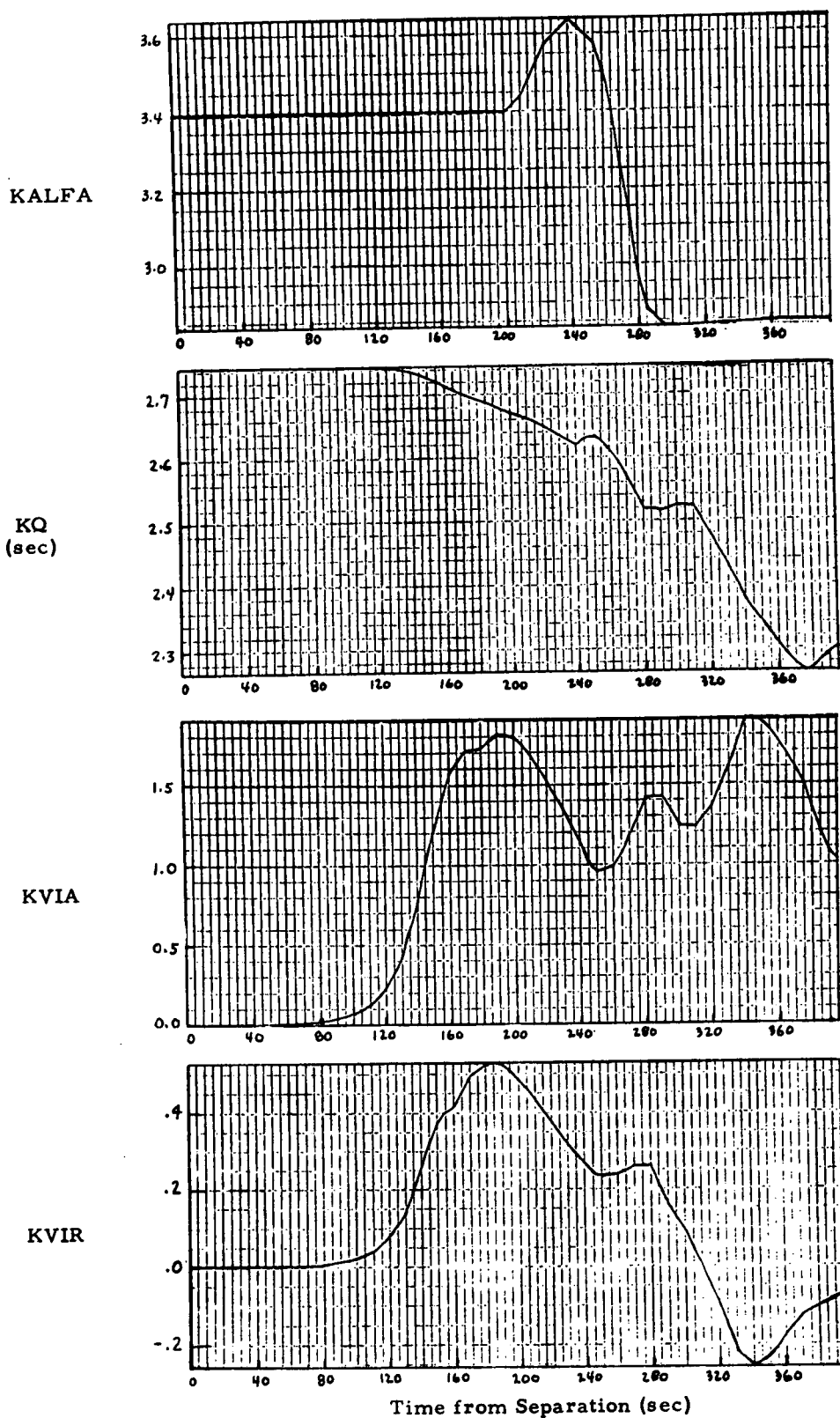
JOB NO 422500

PAGE 7

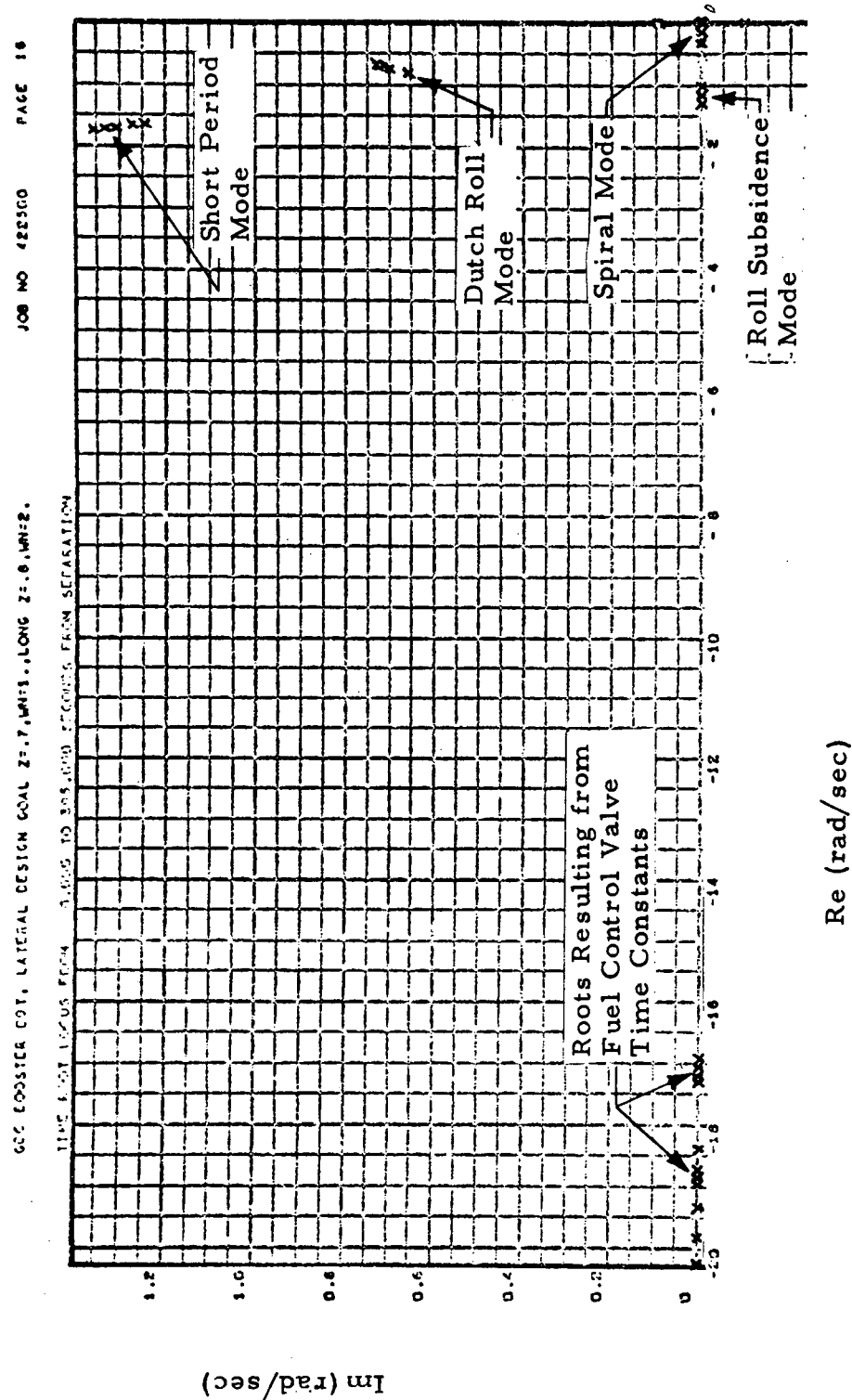


TIME ROOT LOCUS - GDC B9U SHUTTLE





- Representative Plots of the GDC/B-9U APS Control Gain Schedules



Root Locus Plot for the Entire Reentry Phase of the
GDC/B9-U with APS Control System

Appendix H

**SHUTTLE REENTRY SIMULATION PROGRAM
AND SOME REPRESENTATIVE RESULTS**

Appendix H

The block diagram shown in Fig. H-1 gives a general outline of the Shuttle Reentry Simulation program. Simple descriptions of each subroutine are also given.

Table H-1 shows the definition of the variables used in the plots.

Pages H-4 through H-19 give the SC-4020 plots of the Shuttle Reentry Simulation program using optimized APS gains. Pages H-4 through H-11 are the simulation of the GDC/B-9U Reentry with an alternate pulse type of disturbance. The APS control is turned off at 240 sec after separation. Pages H-12 through H-19 are the simulation with step input. The roll, pitch and yaw APS thrusters are turned off at 180, 160 and 240 sec after separation, respectively.

Table H-1
DEFINITIONS

<u>Quantity</u>	
ALFAC	commanded perturbational angle of attack
PHIC	commanded perturbational bank
ALFAC	angle of attack
P, Q, R	X, Y, Z body attitude rates
PHIX, PHIY, PHIZ	X, Y, Z body attitude error
PHI, THETA, PSI	Euler angles
ALFAD	rate of change of angle of attack
BETAD	rate of change of sideslip angle
BETA	sideslip angle
MX, MY, MZ	APS control moments in X, Y, Z body axes
PD, QD, RD	X, Y, Z body attitude accelerations
DELA	aileron deflection
DELE	elevon deflection
DELR	rudder deflection

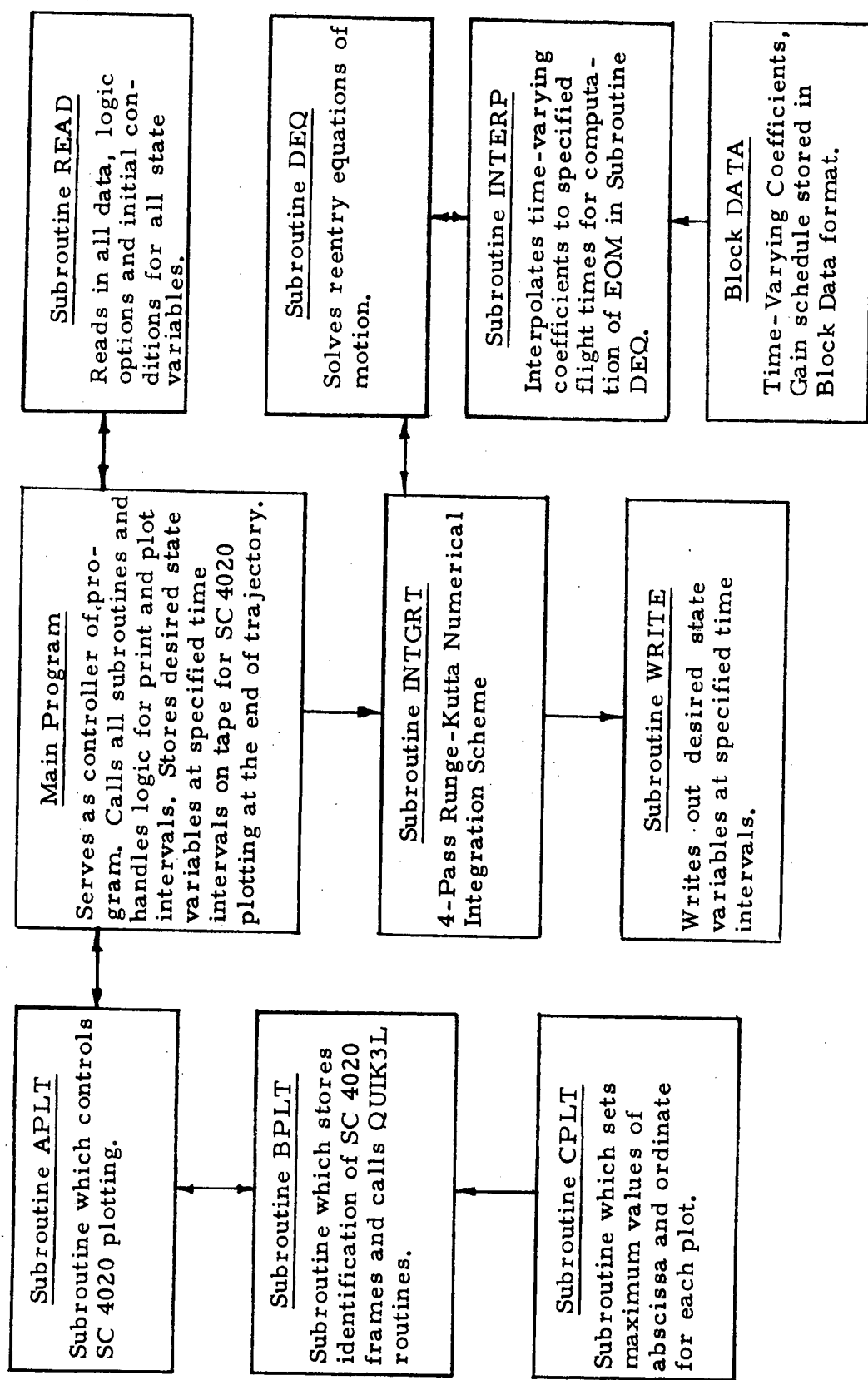
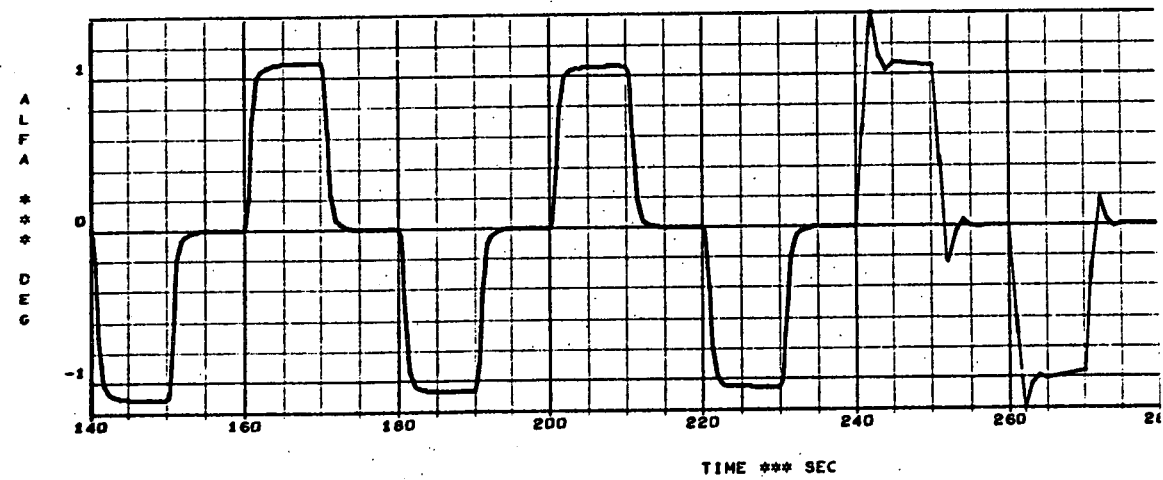
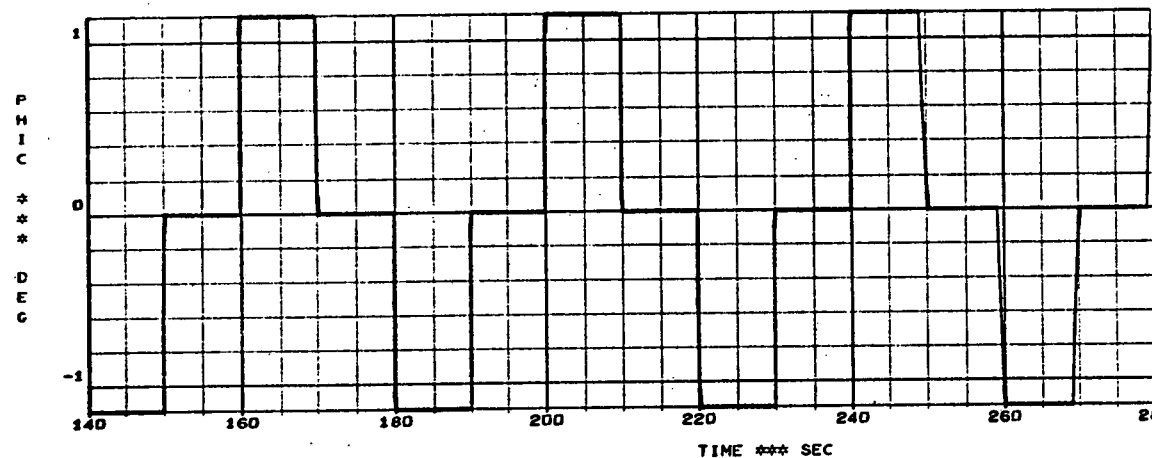
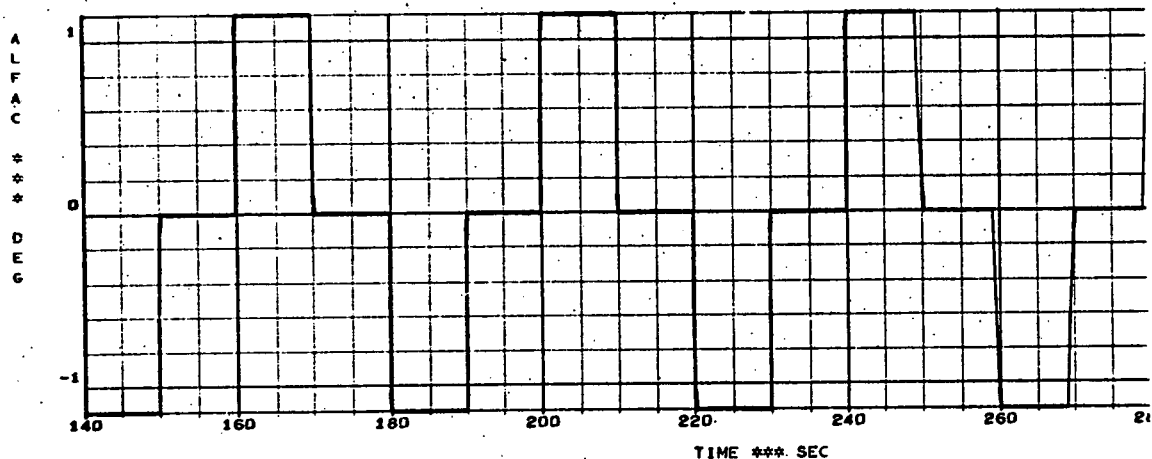


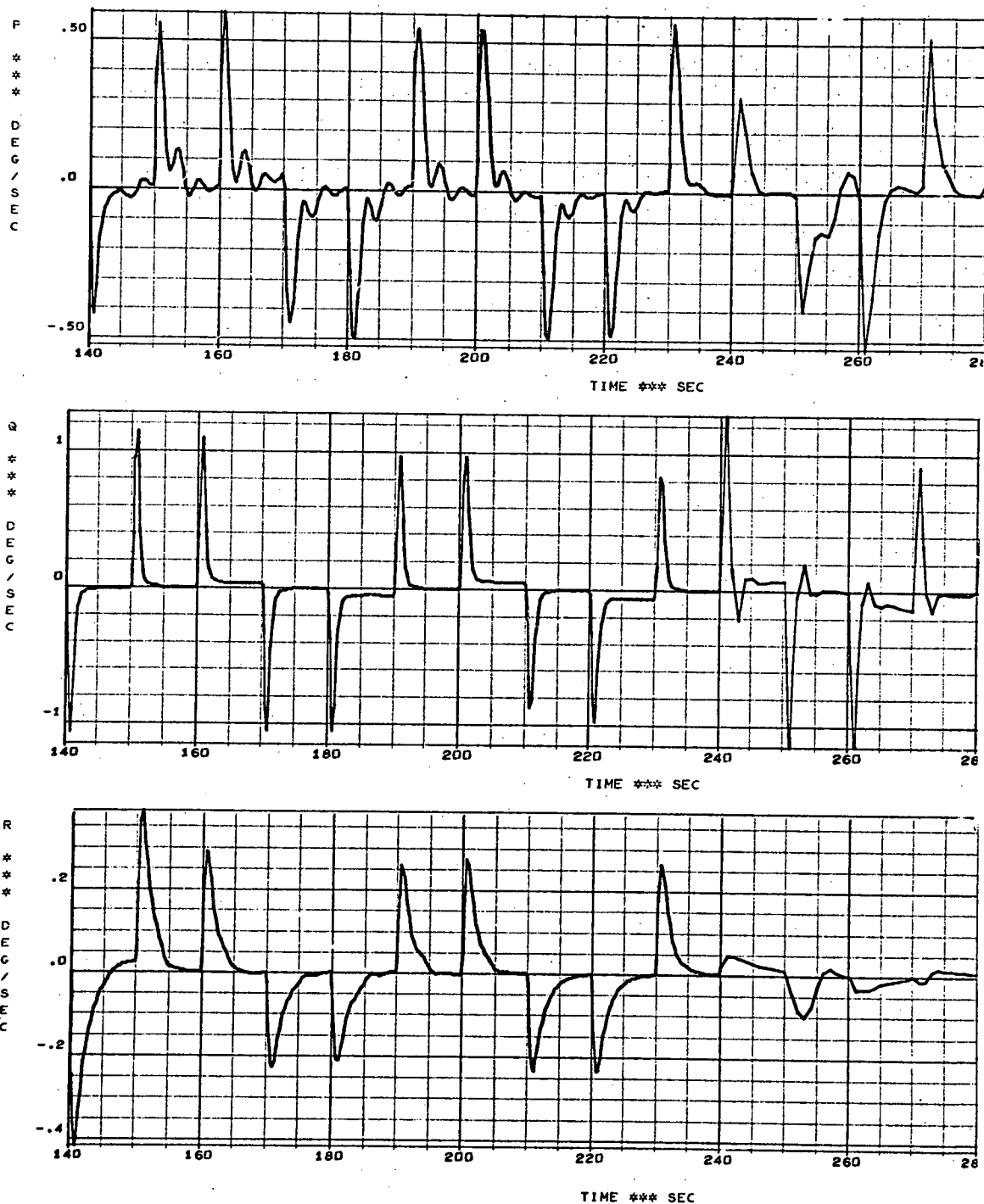
Fig. H-1 - Block Diagram of IBM 1108 Digital Program Used to Perform Shuttle Reentry Simulation

GRC BOOSTER 9U.



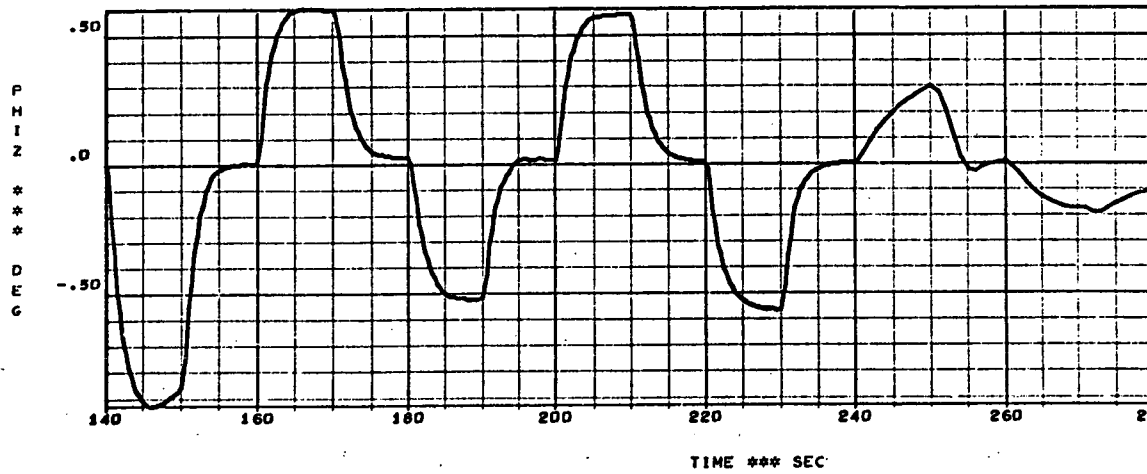
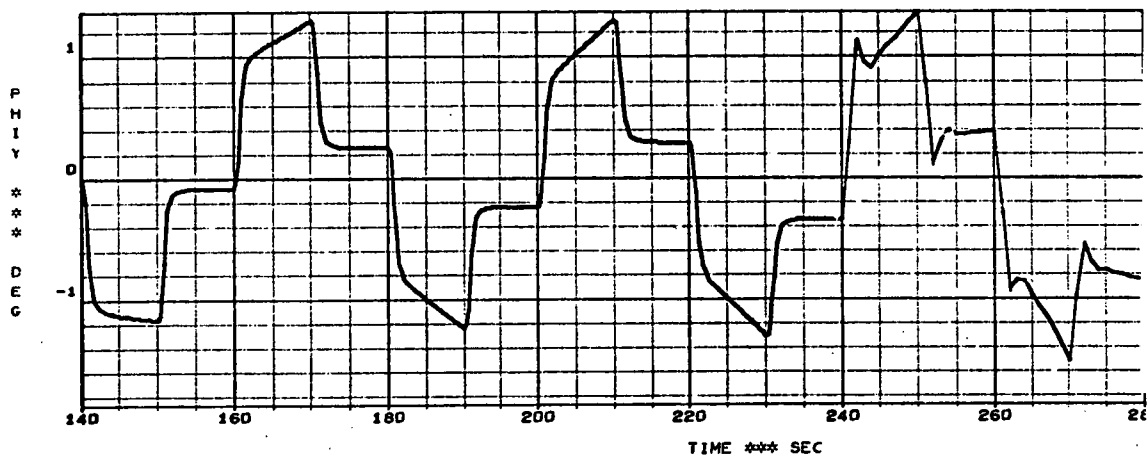
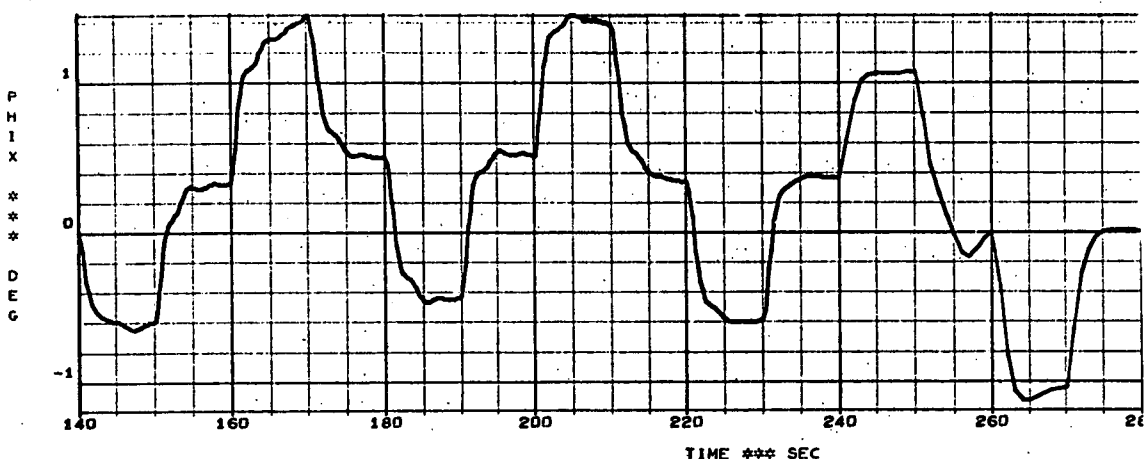
RECORDED BY
RECORDED BY
RECORDED BY
RECORDED BY

GDC BOOSTER 9U,



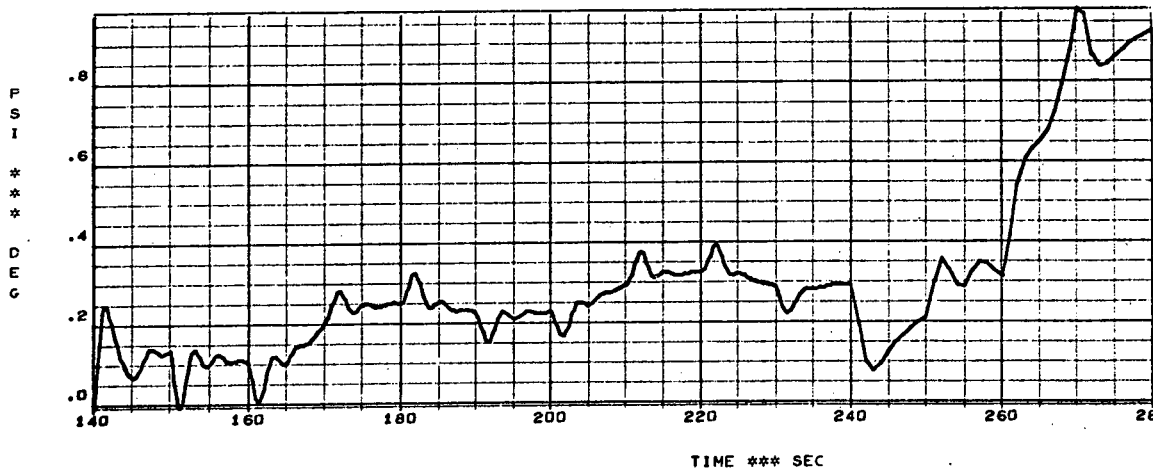
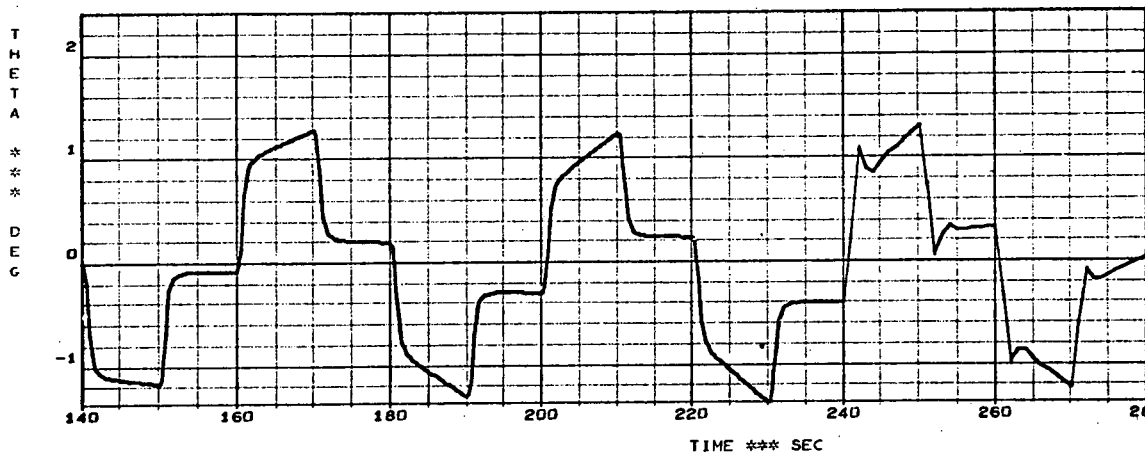
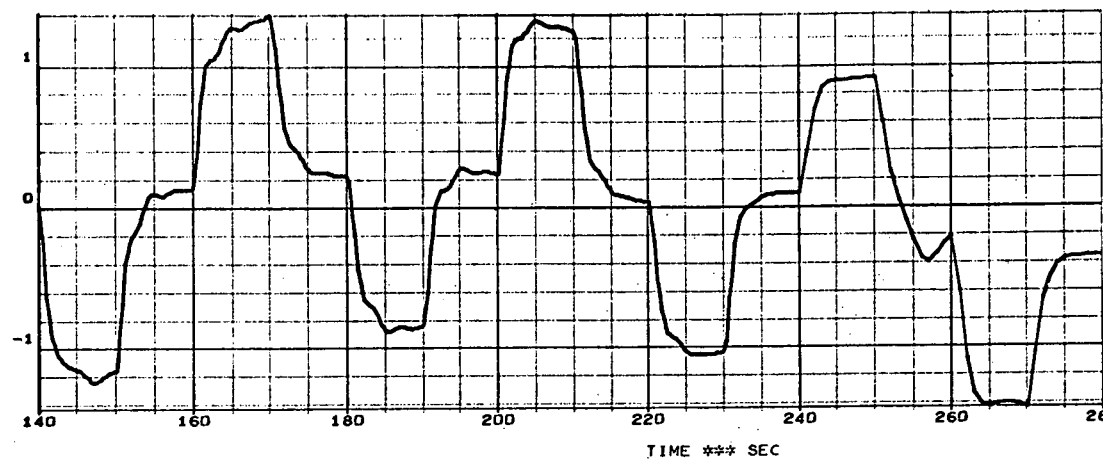


GDC BOOSTER 9U



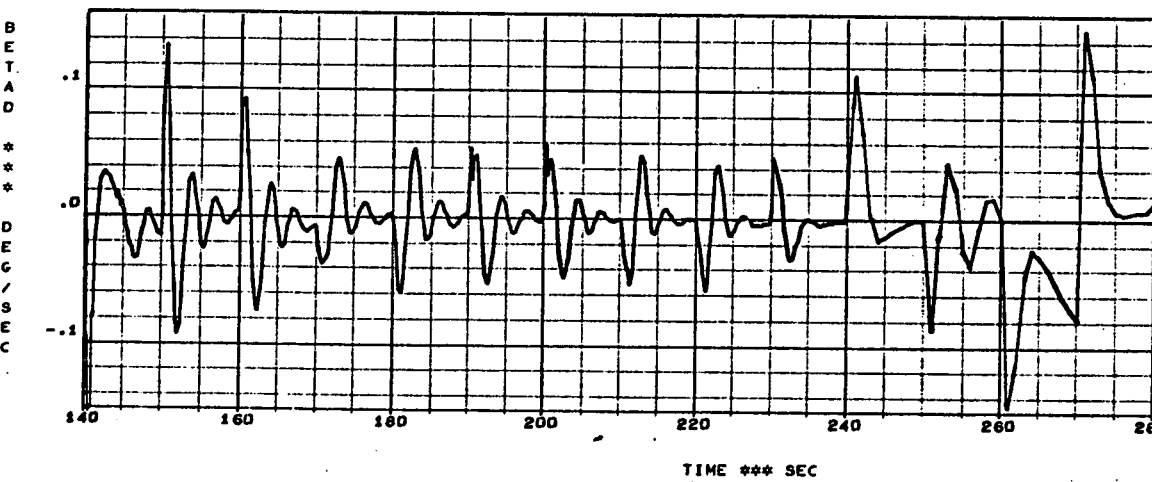
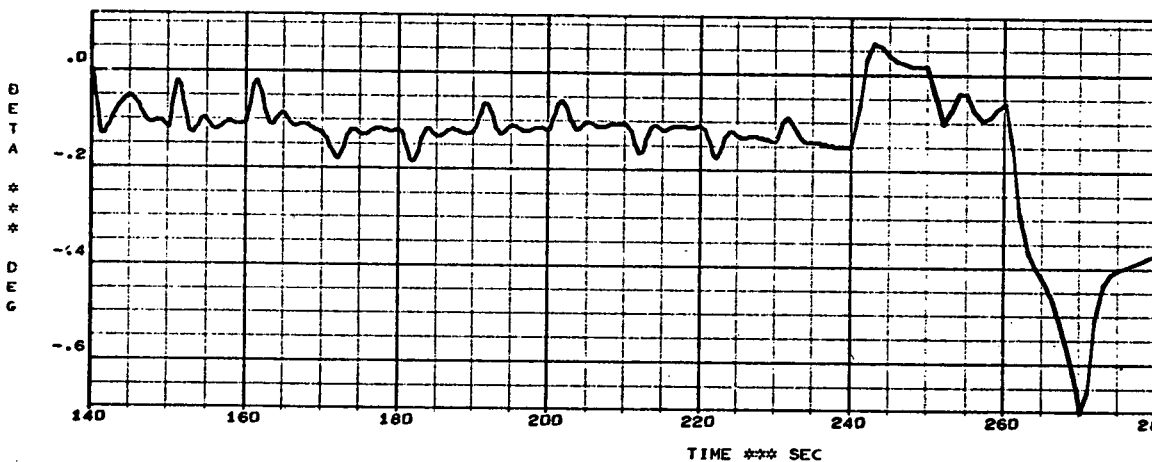
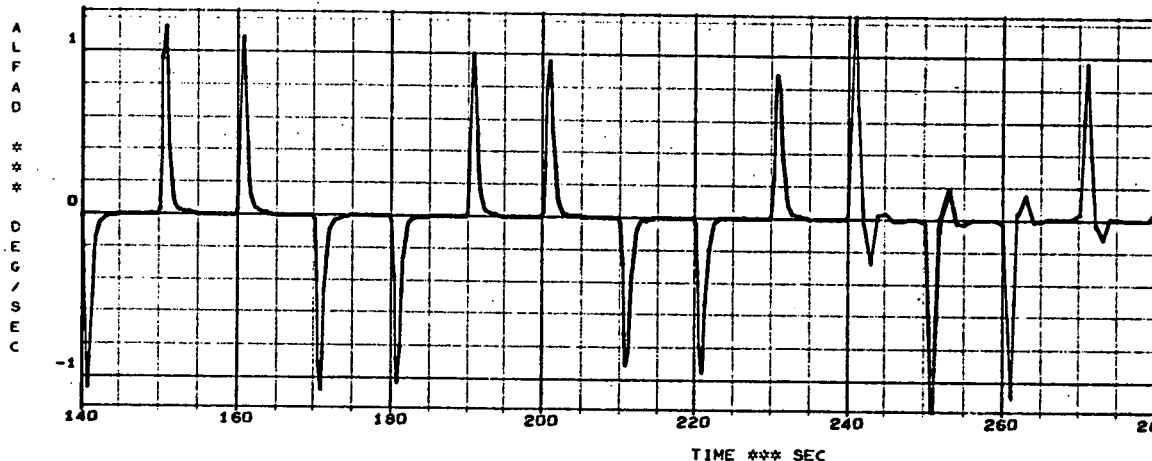
LMS
HREC
D225700-II
140-280 SEC
MPCV TEST DATA

GDC BOOSTER 9U



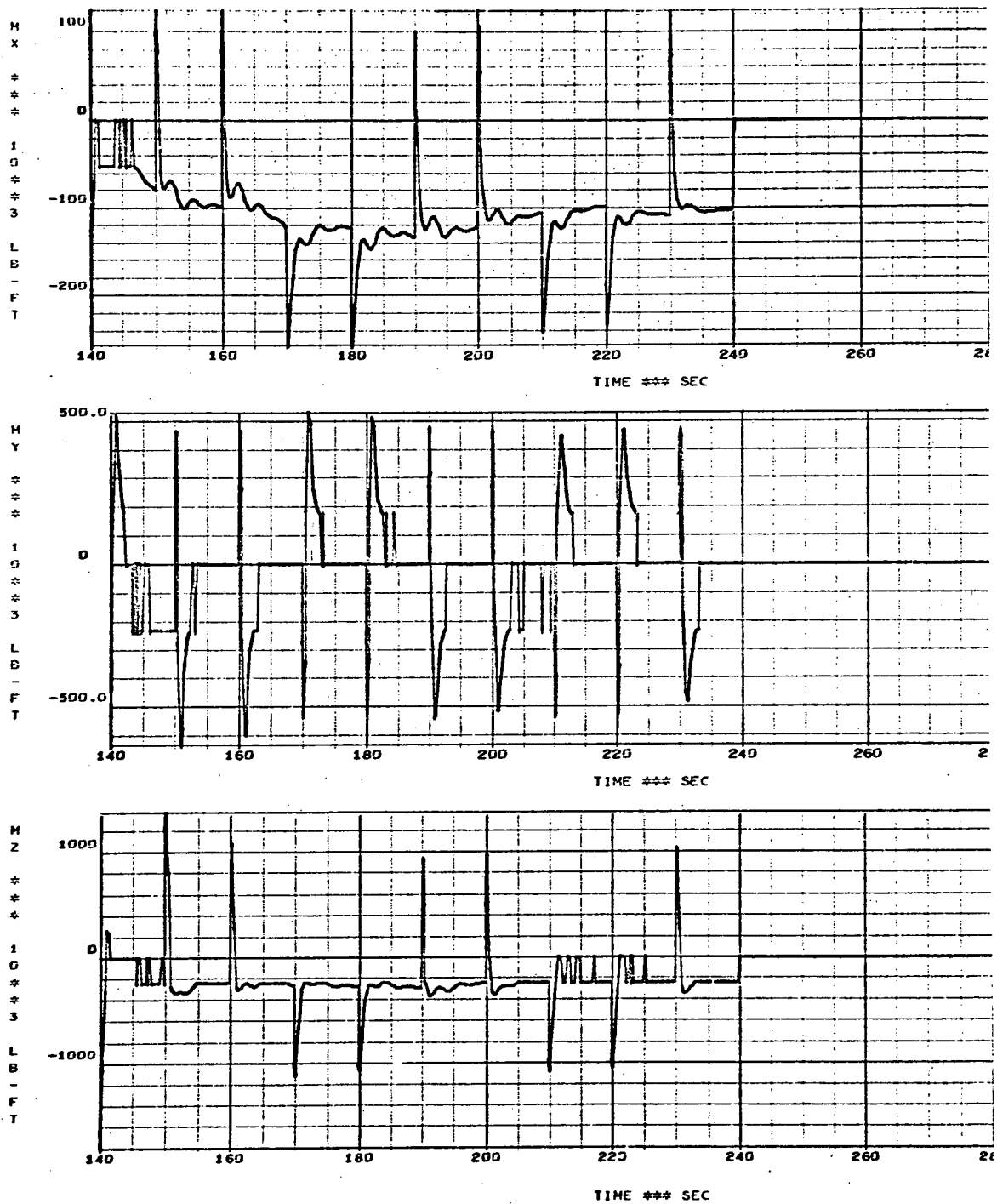


CDC DOOSTER 9U



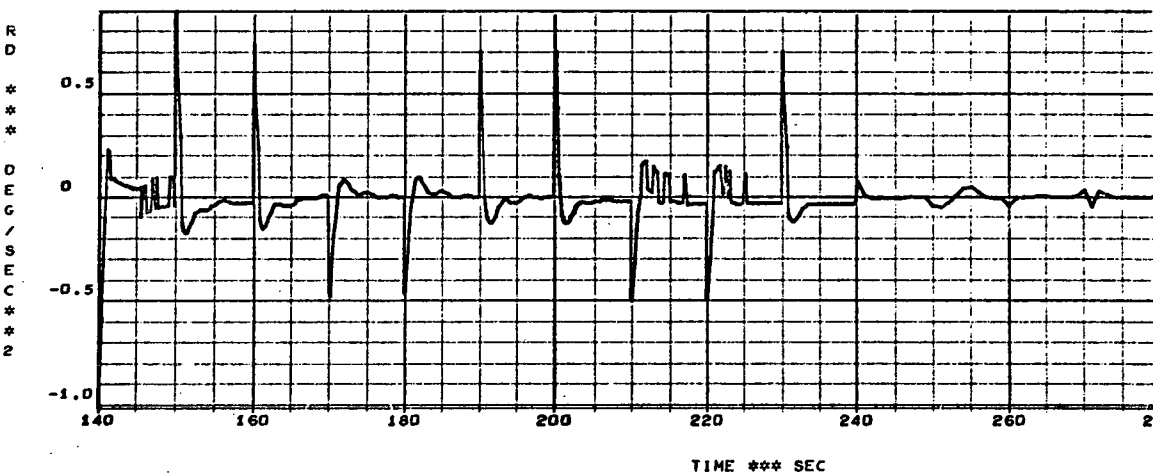
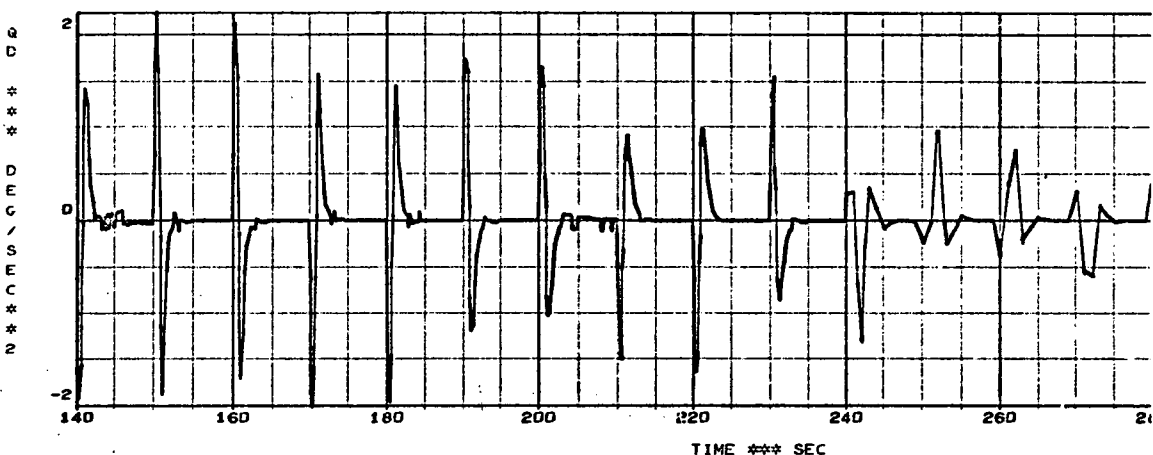
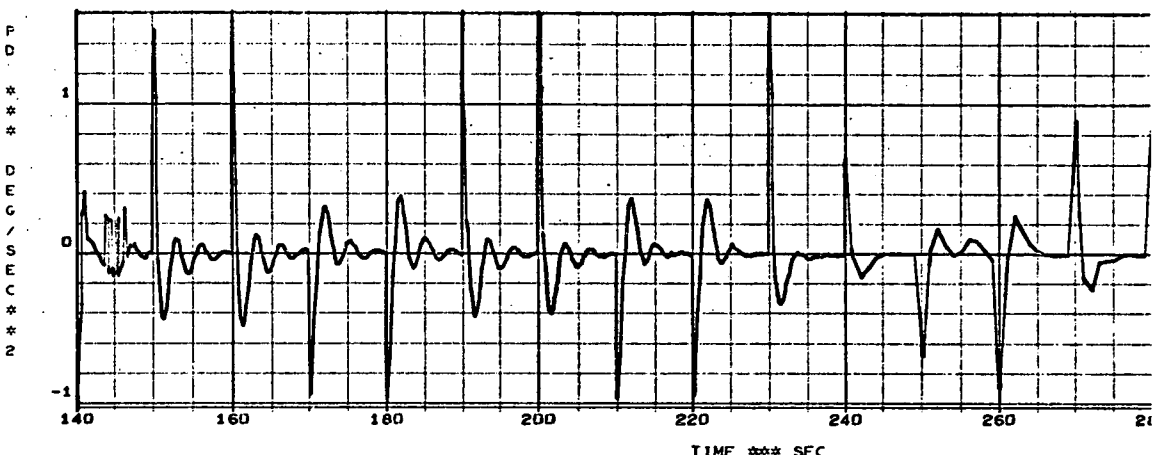
U.S. GOVERNMENT
PRINTED IN U.S.A.
BY GOVERNMENT CONTRACTOR
NOT PURCHASED BY GOVERNMENT

GDC BOOSTER 9U



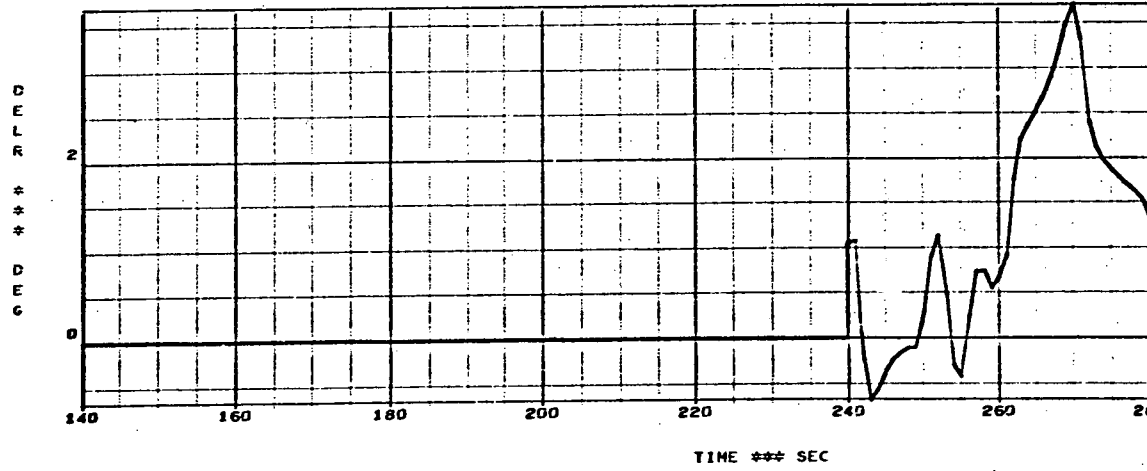
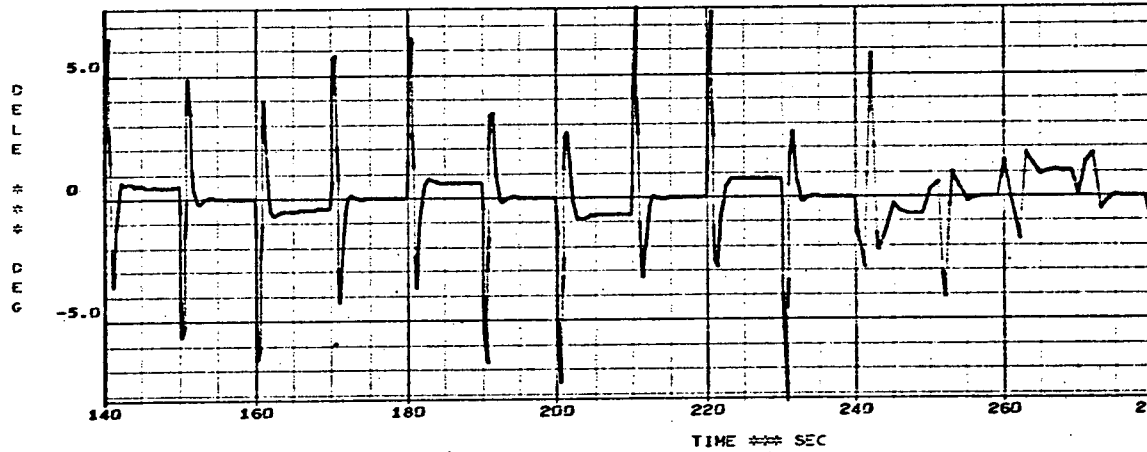
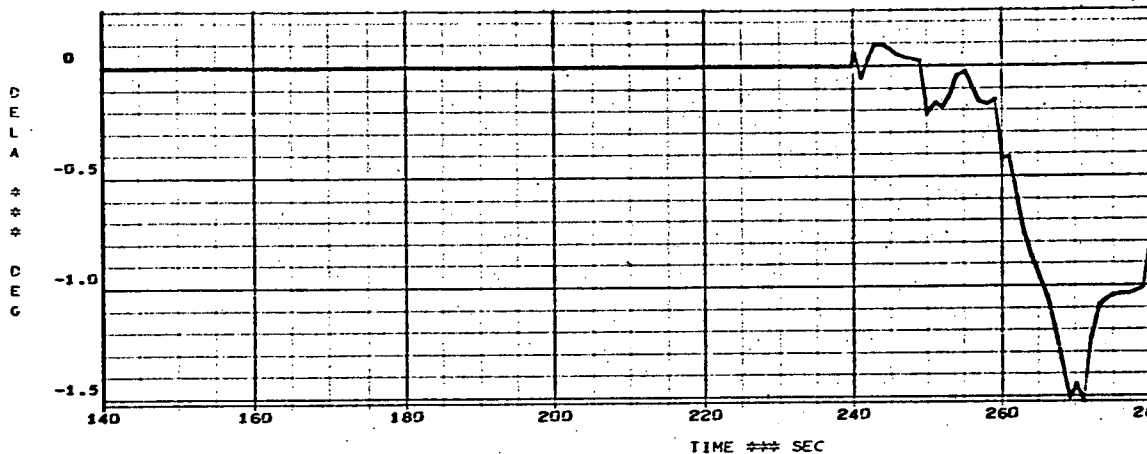
174
175
176
177
178
179
180

GDC BOOSTER 9U,



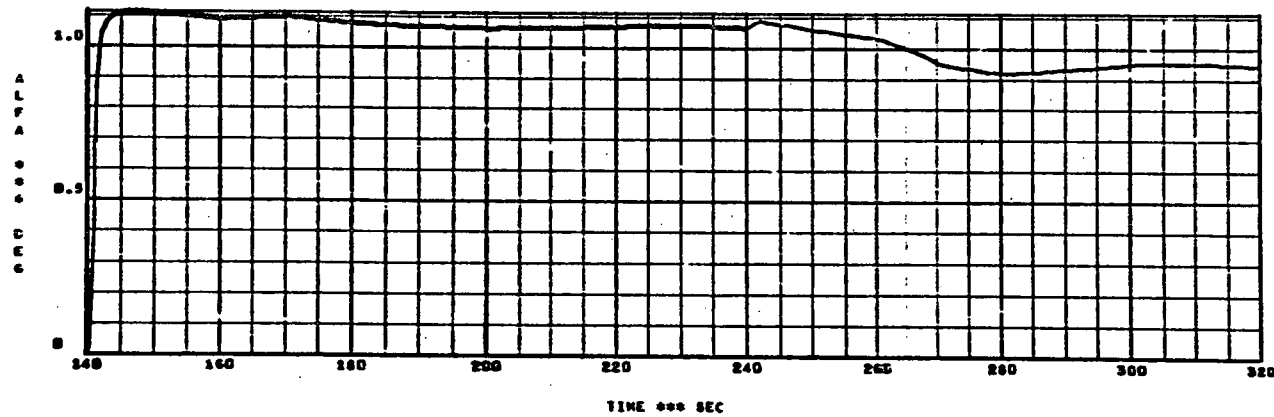
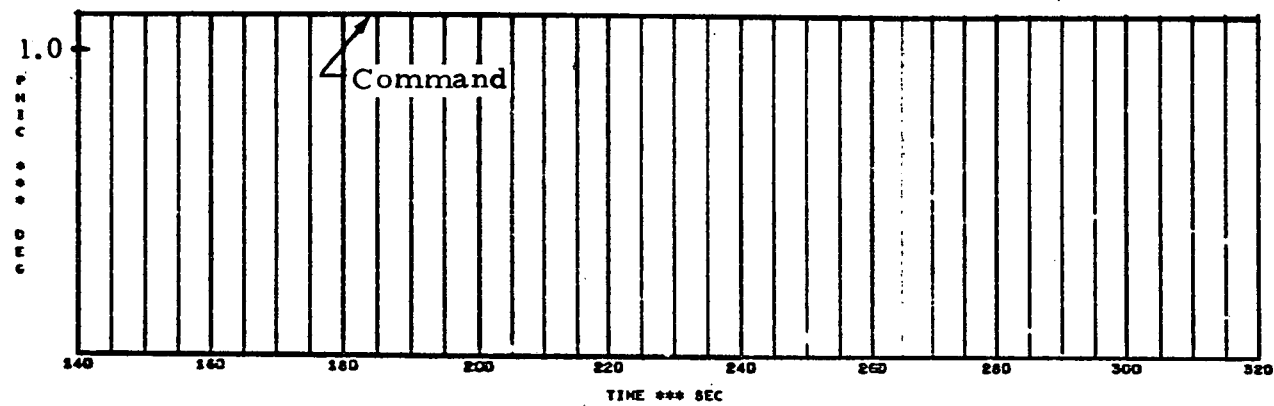
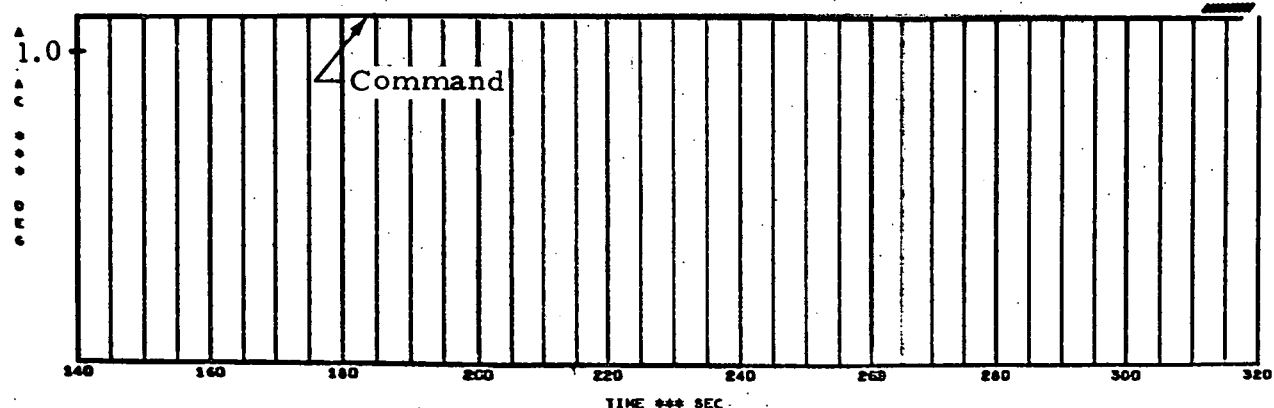
DATA
RECORD
FORMAT
SPECIFICATIONS
REV 1
1968

CCC BOOSTER 9U.



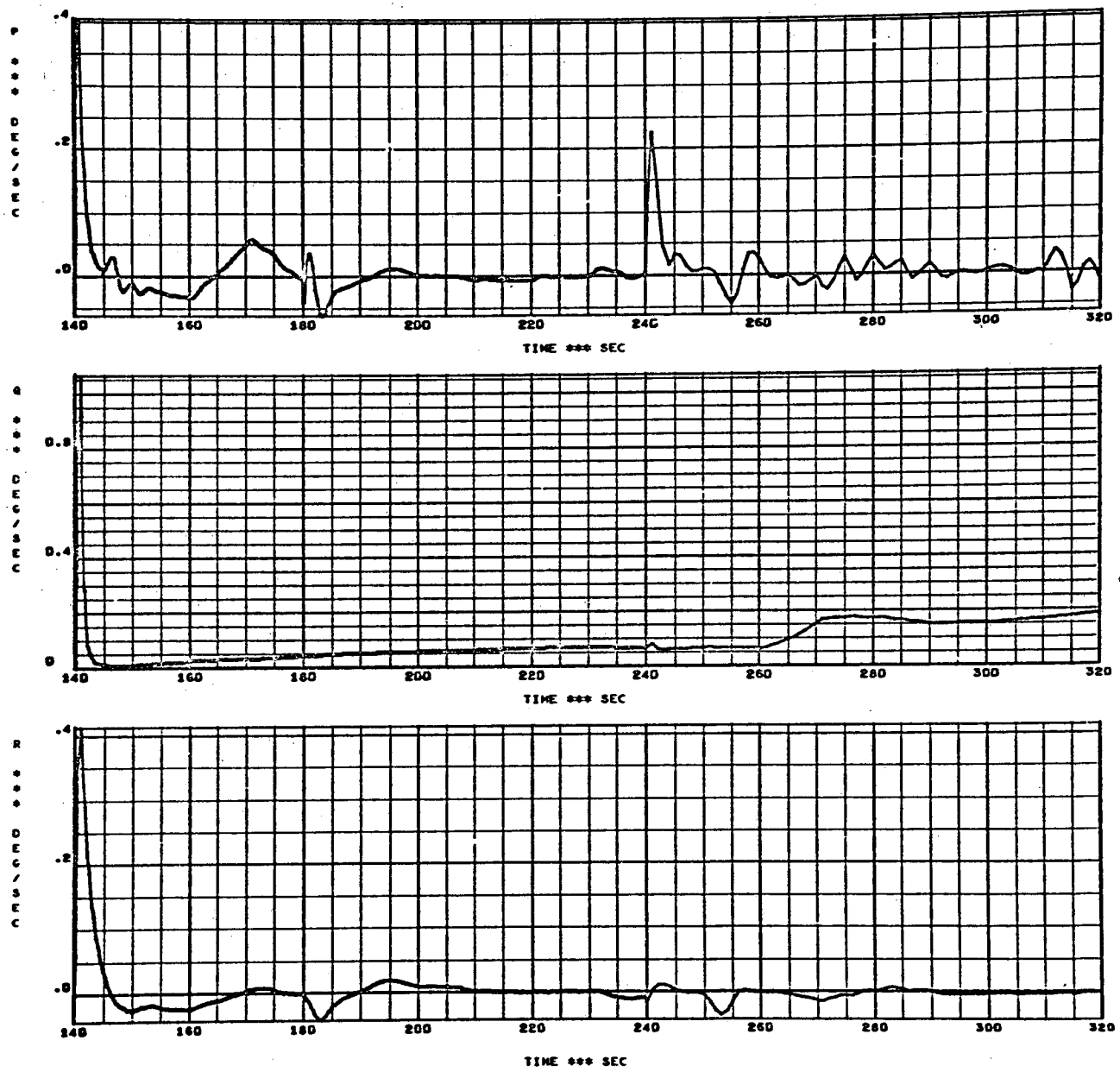


GDC BOOSTER SU.



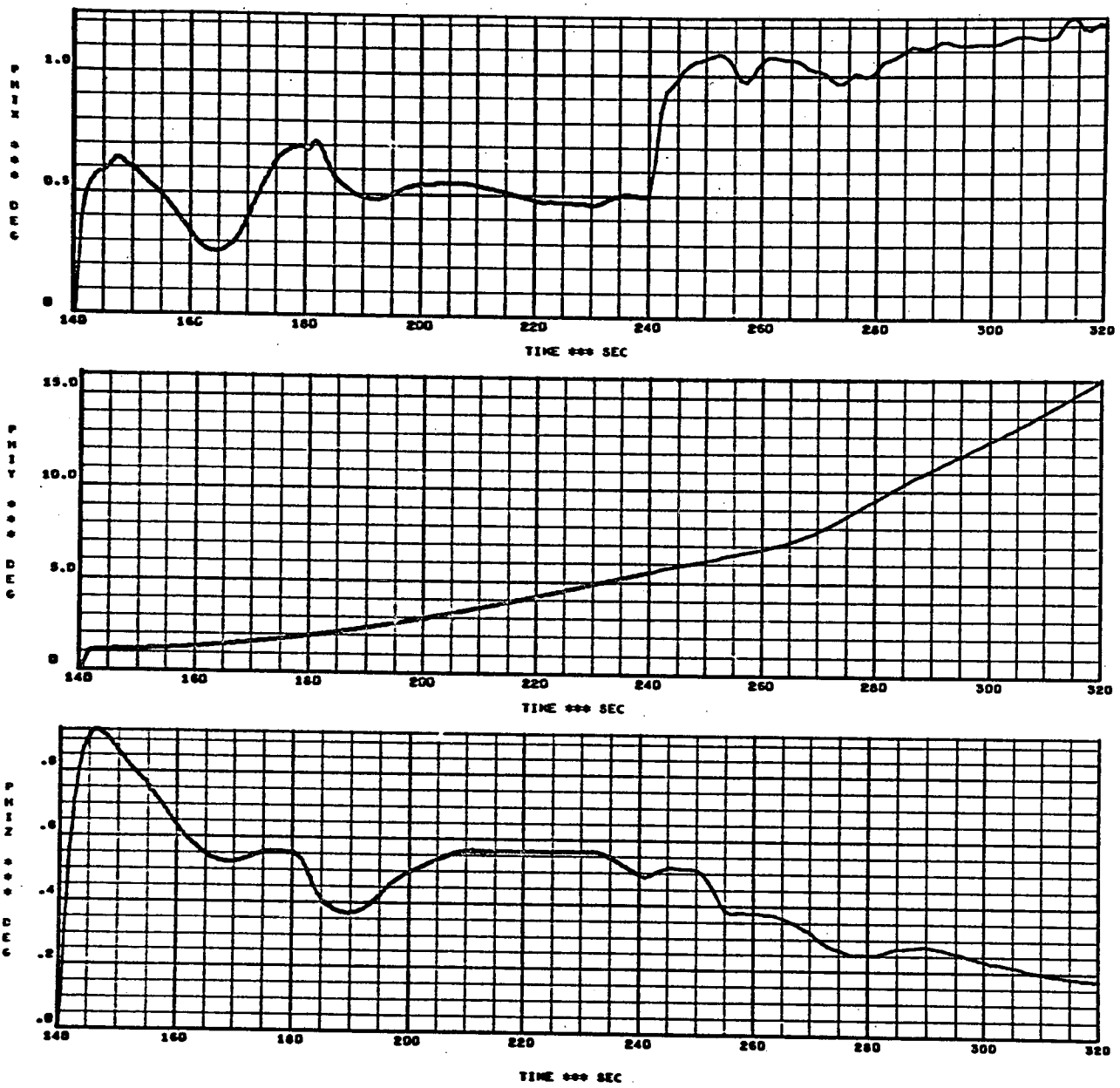


GDC BOOSTER 9U.S.



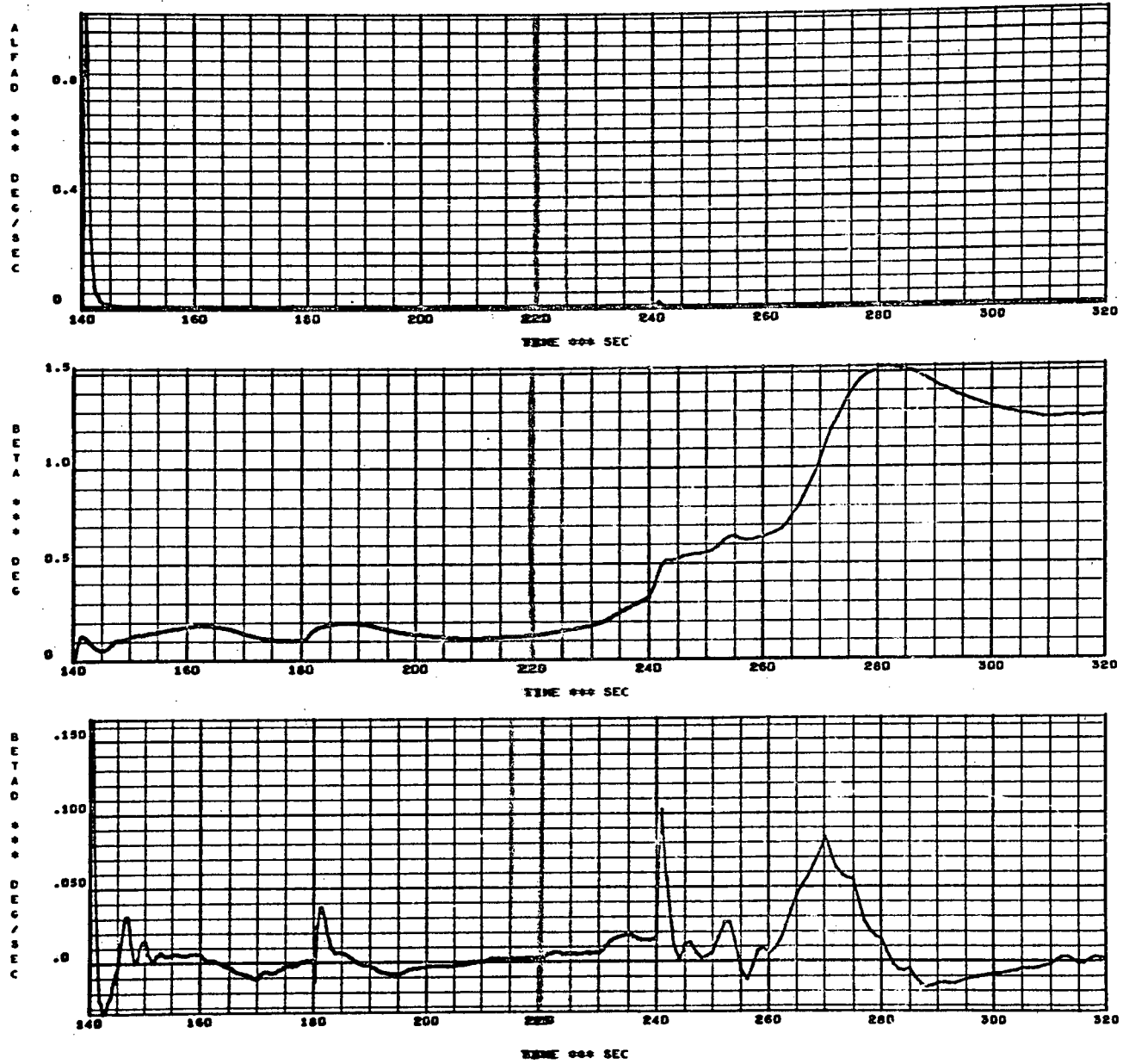


GDC BOOSTER SWL



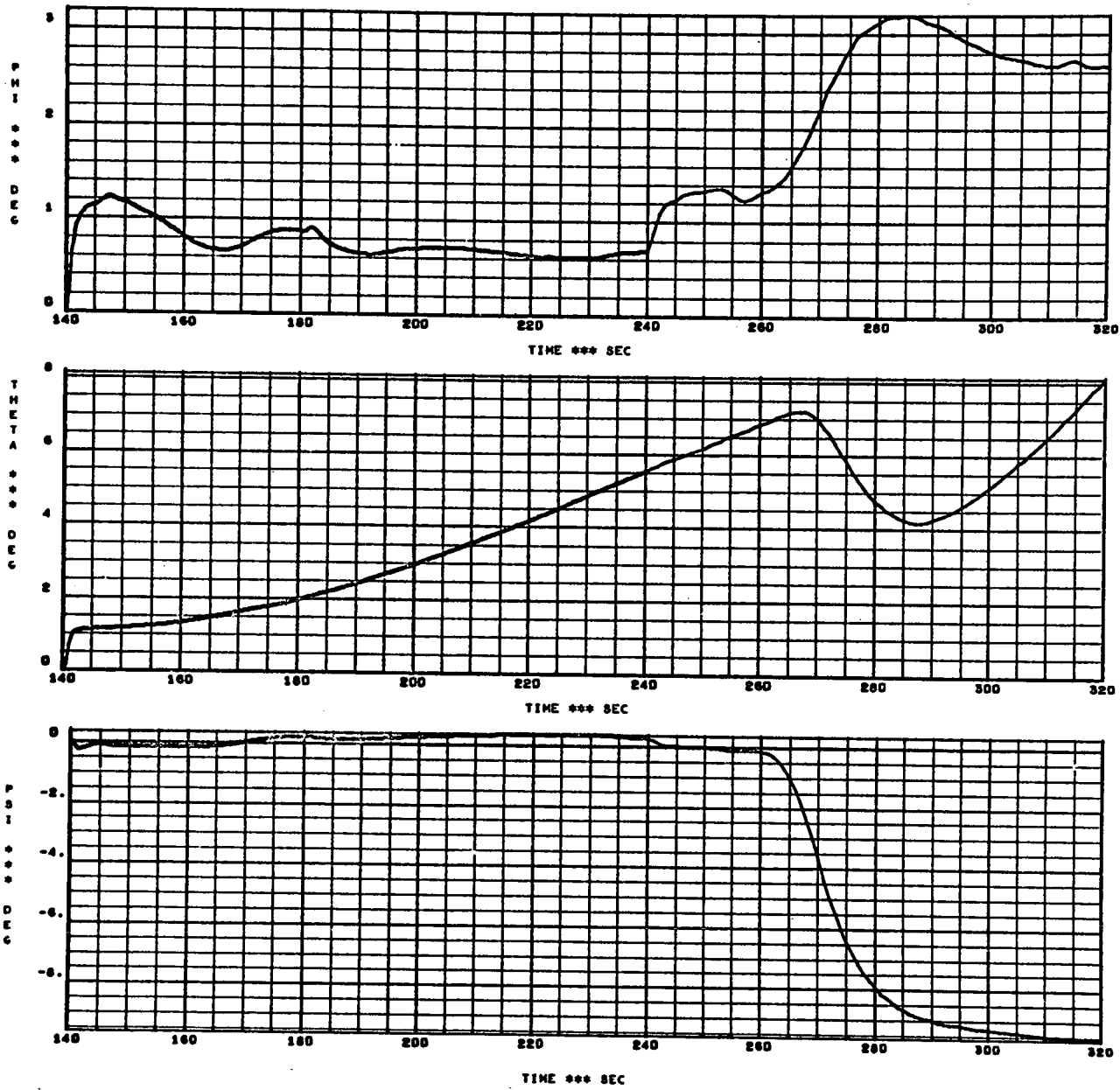


GDC BOOSTER 9U.



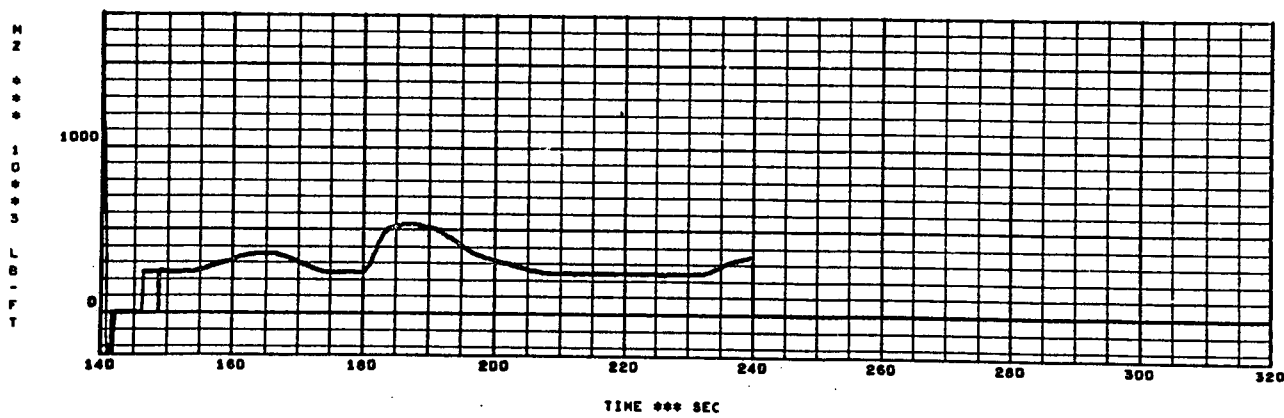
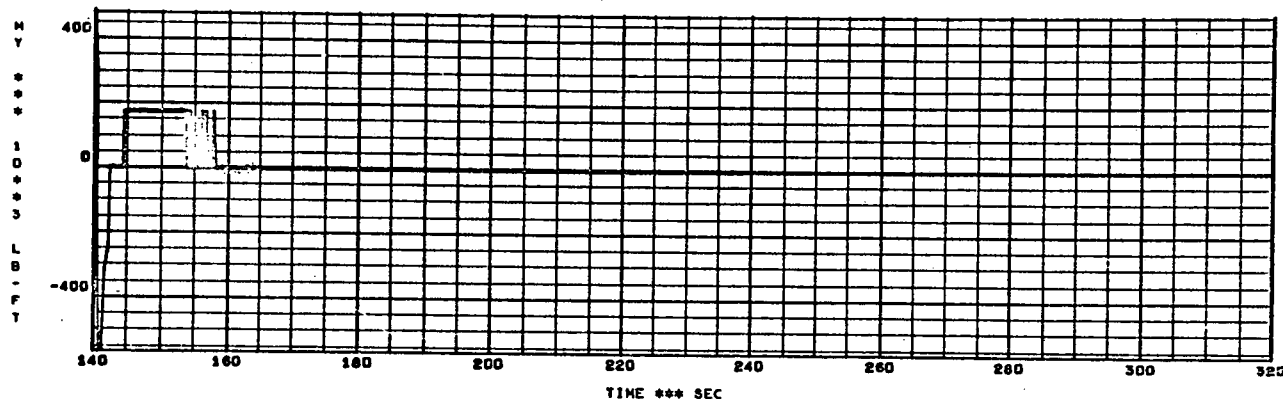
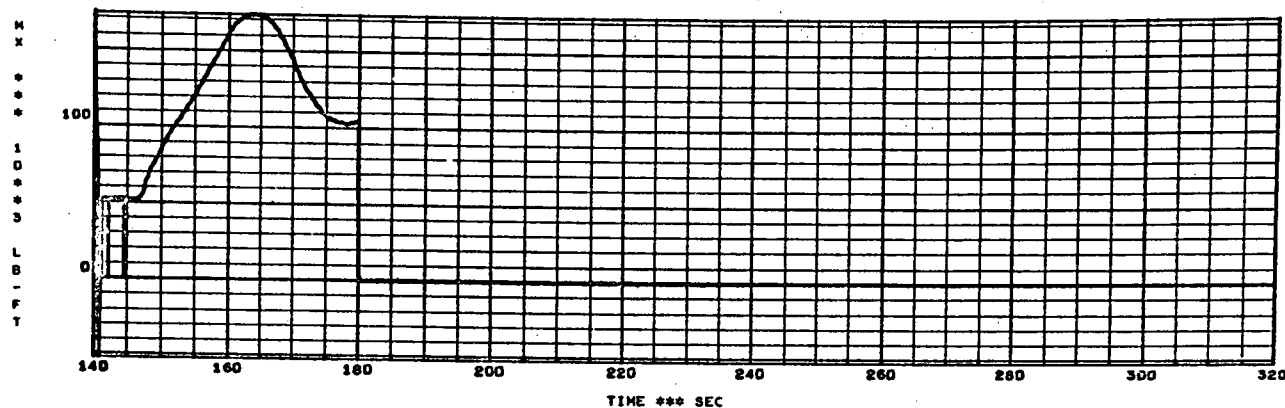


GDC BOOSTER 9U.



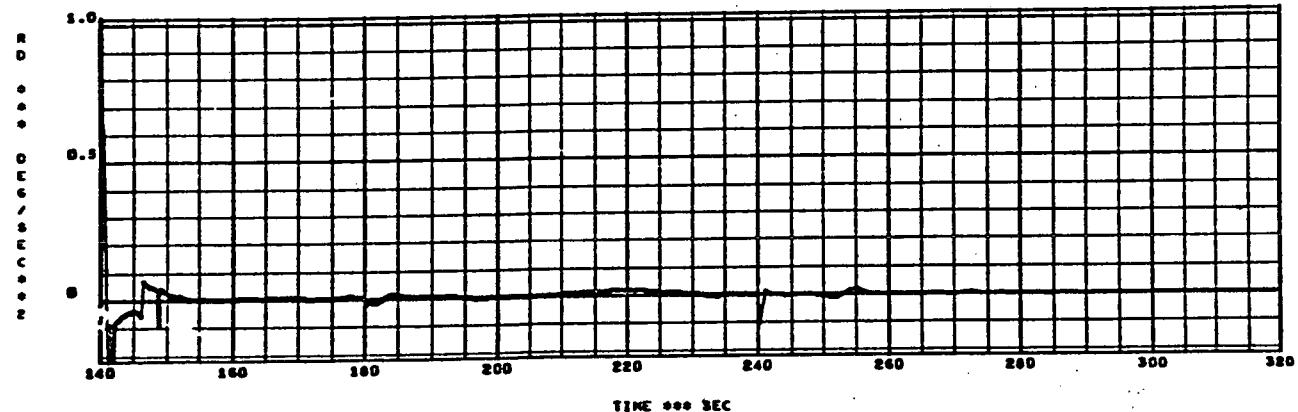
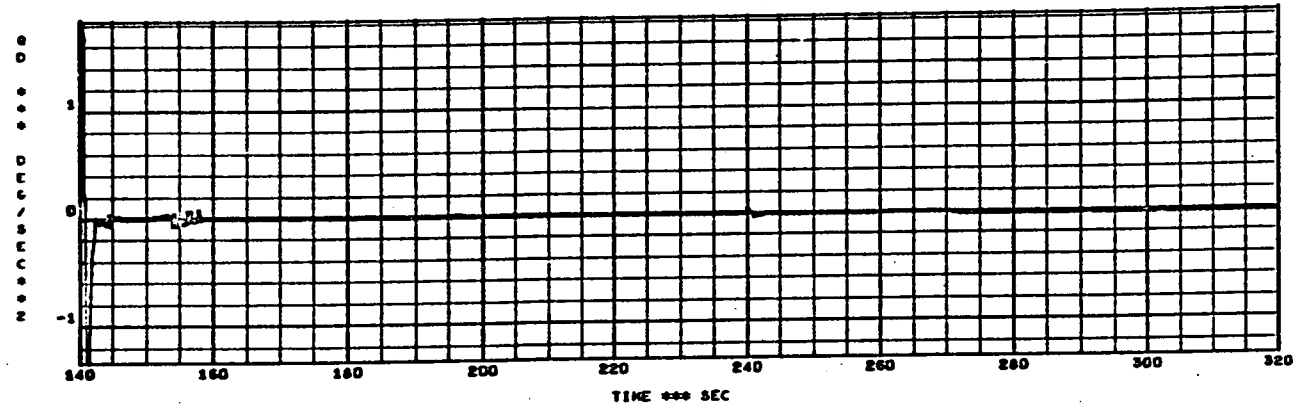
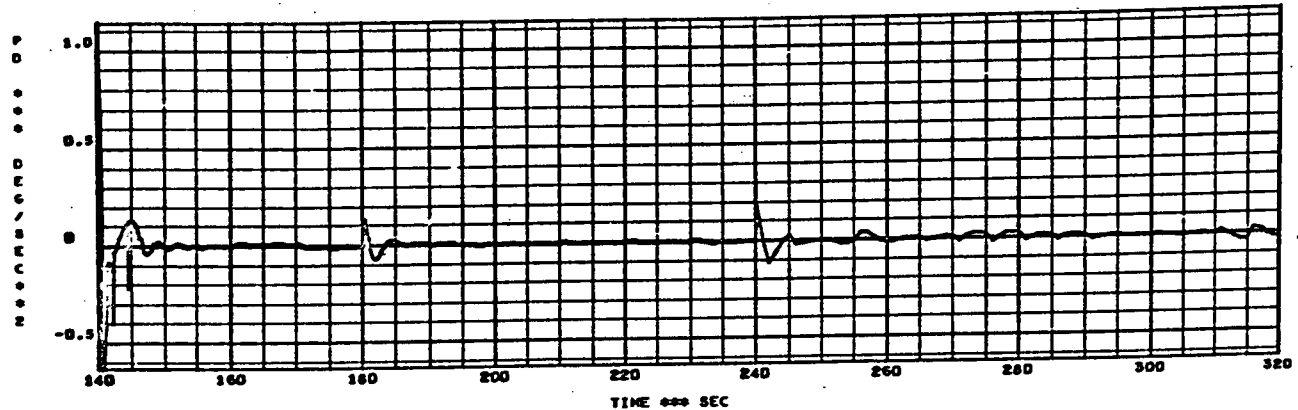


CDC BOOSTER 9U.



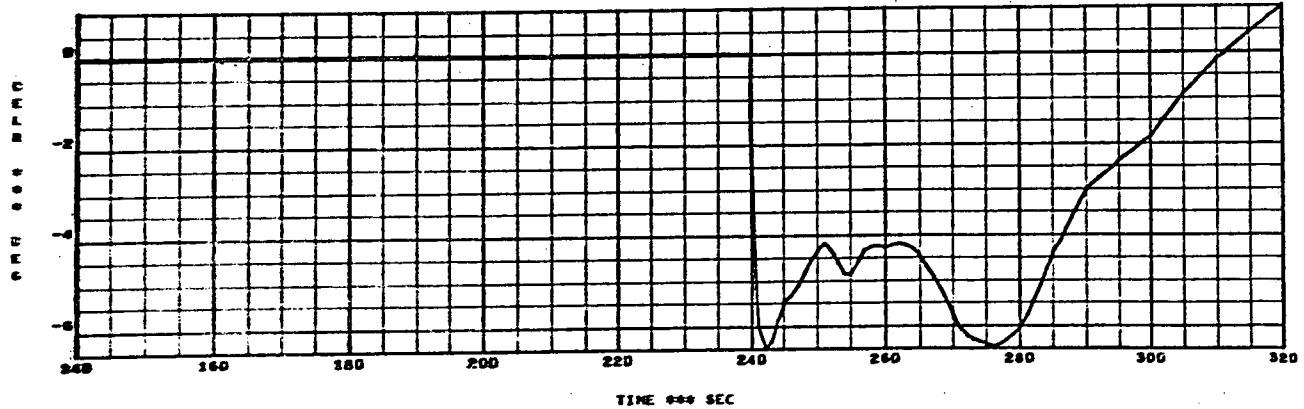
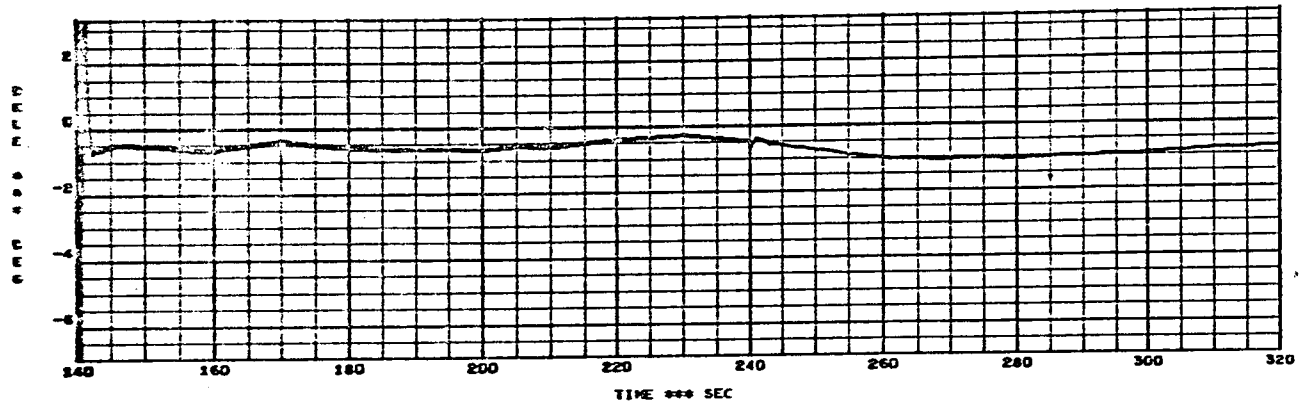
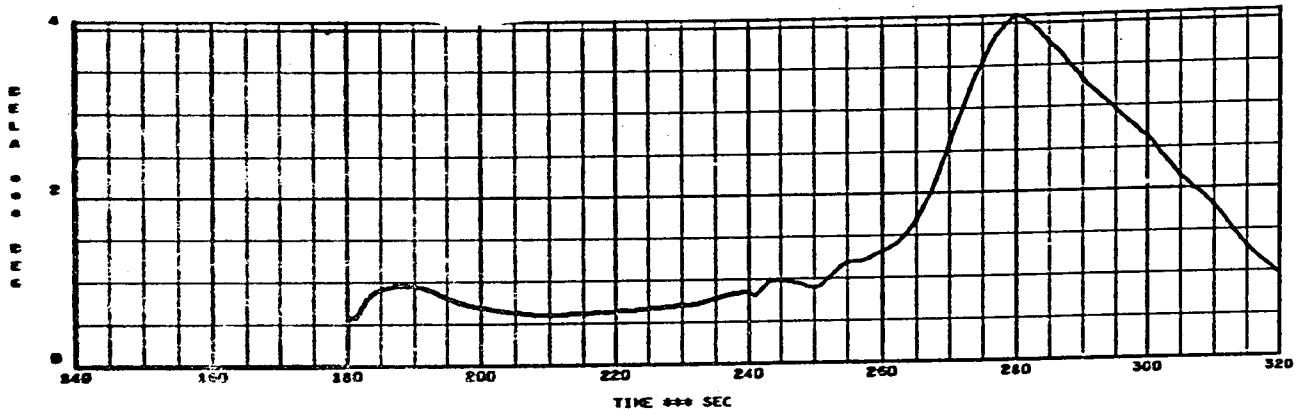


GCC BOOSTER SU.





GDC BOOSTER 9U.



Appendix I
SCOPE OF WORK

Appendix I

Task I - Boost

1. Analyze the ascent phase of the Shuttle mission to determine the requirements for blending aerodynamic surfaces and TVC system to achieve control of the composite launch vehicle. The studies will include the use of aerodynamic devices such as active canards for pitch control and differential movement of the aerodynamic surfaces to achieve roll control.
2. Determine the feasibility of such systems and develop the associated blending logic to achieve integrated control of the vehicle for the conditions where the blending of the control forces were determined to have application and merit. The analyses will also include such detrimental effects as buffeting, actuation limitations and transonic aerodynamics. Study emphasis will be on the identification of important trade-offs and parameters influential to configuration design.

Task II - Reentry

1. Determine the optimum automatic blending control concepts for transition from reaction jet control to aerodynamic surface control for the two types of reentry vehicles (manned control as backup only). The thruster magnitudes and locations may be varied in order to better optimize the control (vehicle and environmental constraints must be considered).
2. Define the control logic analytically and the sensors required to effect the control. The system should be designed for time-varying parameters.
3. Establish the "optimal" flight control system performance model; then vary system parameters (aerodynamic control coefficients, control gains, etc.) to determine controller sensitivity. Consider various malfunctions in the controller logic or control source and determine effect on control design.